15126

THE DECAY OF ^{124}Sb

by

JOHN R. JOHNSON

B.Sc. The University of British Columbia 1967

M.Sc. The University of British Columbia 1970

A THESIS SUBMITTED IN PARTIAL FULFILMENT OF

THE REQUIREMENTS FOR THE DEGREE OF

DOCTOR OF PHILOSOPHY

in the Department

of

PHYSICS

We accept this thesis as conforming to the

required standard

THE UNIVERSITY OF BRITISH COLUMBIA

April, 1973

In presenting this thesis in partial fulfilment of the requirements for an advanced degree at the University of British Columbia, I agree that the Library shall make it freely available for reference and study. I further agree that permission for extensive copying of this thesis for scholarly purposes may be granted by the Head of my Department or by his representatives. It is understood that copying or publication of this thesis for financial gain shall not be allowed without my written permission.

Department of Physics

The University of British Columbia
Vancouver 8, Canada

Date April 27, 1973

Abstract

The gamma-rays, beta rays and conversion electrons emitted in the beta decay of $^{124}Sb \rightarrow ^{124}Te$ have been observed using Ge(Li) and Si(Li) detectors both singly and in coincidence. The measured energies and intensities of the different transitions involved in this decay together with the coincidence results have allowed us to construct the decay scheme. The angular momentum of most of the states and the parity of all of the states of ^{124}Te populated in this decay have been deduced, some of them for the first time, and others as confirmations of previous assignments. We have also been able to assign collective parameters to many of these states, in terms of the vibrational model of nuclei, from the reduced branching ratios calculated from the gamma ray intensities.

Table of Contents

List of Tables

List of Tables (Cont.)

List of Figures

List of Figures (Cont.)

Acknowledgements

I wish to express my gratitude to Dr. K. C. Mann for guidance and encouragement throughout the course of this work.

I also thank the University of British Columbia Van de Graaff group for making some of their equipment available to me.

This project was supported, in part, by Grants-in-Aid of Research to Dr. K. C. Mann from the National Research Council of Canada. I also wish to acknowledge the assistance of the National Research Council through awards to me of N.R.C. Bursaries, and of the H.R. MacMillan Fellowship Foundation through a Fellowship Award.

Chapter I

Introduction

It has been known for a long time now that many low energy excitations of nuclei could be explained in terms of quantized motions of the nuclear matter.[1] These excitations, called collective states, are distinguished from other low energy excitations, called particle states, by their much larger transition rates. The mathematical description of these collective states, called the collective model of the nucleus, has been developed by Bohr,[2] and others.[3]

This collective model has been most successful in describing nuclei that have stable deformations from a spherical shape. The low energy collective excitations of these "deformed" nuclei can be adequately explained in terms of rotations and/or vibrations of the nucleus. However, there are many nuclei that do not have stable deformations but still have low energy collective excitations. There have been attempts[2,3,4] to describe these excitations in terms of vibrations about their spherical equilibrium shape. This "vibrational model" has not been nearly as successful as the so-called "rotational model" used to describe the deformed nuclei, although it does, in general, allow one to classify the different type of collective vibrations that can be assumed to take place in these spherical nuclei, as explained in Chapter II. There are a few spherical nuclei, however, (^{62}Ni, reference 5, and ^{114}Cd, reference 6) for which the vibrational model is almost as successful in describing the low energy excitations, as the rotational model is for deformed nuclei.

The rather limited success of the vibrational model led to the inclusion of features of the nuclear shell model into the description of collective motion.

Belyaev[7], Kisslinger and Sorensen[8] and others,[9] have shown that the collective features of nuclei can be accounted for by the coherent motion of many nucleons, where the individual nucleons are described by their shell model wave functions. This approach was successful in describing the mechanisms that caused stable deformed equilibrium shapes, "shell closure" effects, and many other features that could only by introduced in a phenomenological way into the collective model. However, detailed calculations using only the shell model become prohibitively difficult when the numbers of protons and neutrons are not close to one of their "magic numbers", the filled, or closed, major shells.[25] In this case the collective model can be used to describe the motion of the inner nucleons, or the core, while the shell model approach is used to describe the outermost nucleons. In general, there is no criterion that can be used to say which of the nucleons should be treated as the core, and which as shell model nucleons. This combined description is often called the unified model.[2]

The simplest nuclei to describe in this manner are the odd mass nuclei[2,8,26]. The collective model is used to describe all but the "un-paired" nucleon, and shell model wave function of the un-paired nucleon is coupled to the collective motion by the change in the shell model potential it causes. Again, the most successful calculations using this description of odd mass nuclei were for the deformed nuclei.[26]

Kisslinger and Sorensen[11] used this model to describe the odd-mass spherical nuclei, although they used a microscopic description of the core

rather than the collective vibrational model described in Chapter II. Their description of the core involved the "quasi-Boson" or "random phase" approximation.[10] In this approximation the even-even core is described in terms of the "correlated pairs."[7] That is, a nucleon close to the Fermi surface may spend part of the time in a shell model state $|j\ m\rangle$, where j and m are the shell model spin and spin projection. The rest of the time the nucleon is in a state $|j'm'\rangle$ which can be any of the nearby (in energy) shell model states. During the time that it is not in the state $|j\ m\rangle$, the "pairing force"[7] that coupled it to another nucleon in the state $|j\ -\ m\rangle$ to form a total spin of 0 is broken. The two nucleons, one in state $|j\ -\ m\rangle$ and the other in any of the states $|j\ m\rangle$ or $|j'm'\rangle$ therefore form a correlated pair. The collective motion is then described as coherent excitations of many pairs of $|j'm'\rangle$ and $|j\ -\ m\rangle$ shell model states. The extent to which these pairs can be treated as Bosons (integer spin particles) is the quasi-Boson approximation. This approximation is the same as assuming that the interaction between one member of a pair (a half-integer particle, or Fermion) with another member of any other pair, is not coherent for all the pairs that make up the collective motion, and that these interactions tend to cancel each other;[10] hence the term, random phase. The interaction that causes the pairs to move coherently is the "residual interaction"; that is, the part of the potential between the nucleons that remains after the shell model potential is subtracted. This interaction is introduced phenomenologically by requiring that it account for the systematic variations in the observed collective properties of nuclei as the number of protons and/or neutrons is varied within a major shell.

The quasi-Boson approximation was used by Kisslinger and Sorensen in an earlier work[8] to describe successfully the ground and first excited states of singly closed shell, even-even nuclei, in which the number of protons or neutrons corresponds to a closed major shell. More recently,[12] this quasi-Boson representation has been used to describe higher energy excitation of even-even spherical nuclei with neither the protons nor the neutrons having closed major shells. Detailed calculations for this type of nucleus quickly become as difficult as the simple shell model calculations, although the mathematical formalism of the quasi-Boson approximation allows one to extend the region for which one can do detailed calculations a little further away from closed shells.

One method[13] of circumventing this difficulty is to describe the motion of one type of nucleon, say the neutrons, by the vibrational model, and then describe the protons by the quasi-Boson formalism, where now the quasi-Bosons are acted upon by the residual potential that is perturbed by the collective motion. These types of calculations are often called semi-microscopic.

In order to deduce the effects of the collective motion on the quasi-Boson states, and vice versa, accurate measurements of energy levels and transition probabilities are required over the entire range of proton and neutron numbers for which this semi-microscopic model may possibly be valid. For this reason, we have decided to re-investigate the excited states of ^{124}Te populated in the beta decay of ^{124}Sb. ^{124}Te, with 52 protons and 72 neutrons is an even-even spherical nucleus and the ^{124}Sb beta decay populates states in this nucleus above 2 MeV excitation energy, the approximate energy at which the first particle states (or non-coherent quasi-boson states of the two extra core (Z=50) protons) are expected to be found.

After this investigation was begun, a theoretical semi-microscopic theory of ^{124}Te was published by Lopac.[14] This theory will be briefly described in Section II-4 and will be compared to the experimental results of this investigation in Section VI-5.

The ^{124}Sb beta decay has been investigated in the past using magnetic spectrometers;[15] and the gamma transitions depopulating the excited states of ^{124}Te, using NaI detectors.[40] More recently, the gamma transitions have been measured using good resolution Ge(Li) detectors[17,18,36]. The excited states of ^{124}Te populated by coulomb scattering[76,77,80] and by the reactions (n,γ)[75], (^{3}He,d) and (p,t)[74], have also been recently investigated. However, we felt that with the combined detection of gamma, beta and conversion electron transitions, and by using coincidence measurements, that we could make a useful contribution to our knowledge of the excited states of ^{124}Te.

The measurements of the gamma transitions' intensities and energies are reported in Chapter III. The coincidence measurements between the gamma transitions are reported in Chapter IV. The results of the investigations involving beta transitions and conversion electron transitions are summarized in Chapter V. It was possible, using all these data, to construct the decay scheme of ^{124}Sb $\rightarrow$ ^{124}Te, and to assign spin and parity and to establish the nature (whether mainly collective or particle) of the states of ^{124}Te populated in this decay. This will be described in Chapter VI. The ^{124}Sb sample that was used in our investigations was obtained from New England Nuclear, Inc., where it was prepared by the ^{123}Sb(n,γ)^{124}Sb reactions. The impurities expected to be found in the sample were the short lived ^{122}Sb(2.8 days) and the long lived ^{125}Sb (2.7 years). These impurities were less than 1%.[19] Individual sources

were prepared for our measurements from this sample in the usual way.[44,48]

Chapter II

The Vibrational Model of Even-Even Nuclei

II-1 The Collective Model

The starting point of the collective model is to describe the nuclear surface by[2,20]

$$R = R_0 \left(1 + \sum_{\lambda>1} \sum_{\mu=-\lambda}^{\lambda} \alpha_{\lambda\mu}(t)\, Y_{\lambda\mu}(\theta,\phi) \right) \qquad \text{II-1}$$

where R_0 is the radius of a sphere whose volume is equal to the nuclear volume, and the $Y_{\lambda\mu}$'s are the spherical harmonics. The $\alpha_{\lambda\mu}(t)$'s are expansion coefficients whose form depend on the equilibrium shape of the nucleus and the type of motion that is assumed to describe the excited states.

The Hamiltonian of the collective motion will be a function of the $\alpha_{\lambda\mu}$'s and their time derivatives, $\dot{\alpha}_{\lambda\mu}$. The form the Hamiltonian takes depends on the detailed assumptions made about the motion of the nuclear surface; that is, do we assume that the different motions are coupled or not, are the vibrations harmonic or anharmonic, are the rotations rigid or irrotational, is the fluid compressible, homogeneous, etc.

II-2 The Simple Vibrational Model

The assumptions used for the simple vibrational model are:

a) The nucleus has a spherical equilibrium shape.

b) The only collective motions are uncoupled harmonic vibrations about this shape.

c) The fluid is incompressible and homogeneous.

d) No particle states are involved.

The potential energy of the harmonic vibrations about the spherical equilibrium shape is

$$V = \tfrac{1}{2} \sum_{\lambda\mu} C_\lambda |\alpha_{\lambda\mu}|^2$$

where C_λ is the restoring force parameter and is the sum of surface tension and coulomb energy terms.[2]

The kinetic energy is

$$T = \tfrac{1}{2} \sum_{\lambda\mu} B_\lambda |\dot{\alpha}_{\lambda\mu}|^2$$

where B_λ is the mass transport parameter.[2] B_λ and C_λ do not depend on the orientation (μ), because spherical symmetry is assumed.

The momenta of the generalized coordinates $\alpha_{\lambda\mu}$ are[21]

$$\pi_{\lambda\mu} = \frac{\partial T}{\partial \dot{\alpha}_{\lambda\mu}}$$

and therefore the kinetic energy can be written as

$$T = \tfrac{1}{2} \sum_{\lambda\mu} \frac{1}{B_\lambda} |\pi_{\lambda\mu}|^2$$

The Hamiltonian can now be written as

$$H = \sum_\lambda H_\lambda \qquad \text{with}$$

$$H_\lambda = \sum_\mu \frac{1}{2B_\lambda} |\pi_{\lambda\mu}|^2 + \sum_\mu \frac{C_\lambda}{2} |\alpha_{\lambda\mu}|^2 \qquad \text{II-3}$$

This Hamiltonian describes a system of uncoupled harmonic oscillators whose frequencies are given by[2,20]

$$\omega_\lambda = \left(C_\lambda / B_\lambda\right)^{1/2} \qquad \text{II-4}$$

and, in general $\omega_i < \omega_j$ for $i < j$. This system can be quantized in the normal fashion by demanding that π and α obey the commutation relations.

$$[\pi_{\lambda\mu}, \alpha_{\lambda'\mu'}] = -i\hbar\, \delta_{\lambda\lambda'}\, \delta_{\mu\mu'}$$

$$[\pi_{\lambda\mu}, \alpha^\dagger_{\lambda'\mu'}] = [\pi^\dagger_{\lambda\mu}, \alpha_{\lambda'\mu'}] = 0 \qquad \text{II-5}$$

The Hermitian conjugates, $\alpha^\dagger$ and $\pi^\dagger$, can be derived from the fact that the nuclear surface must be real. i.e.,

$$\alpha_{\lambda\mu} Y_{\lambda\mu} = (\alpha_{\lambda\mu} Y_{\lambda\mu})^+$$

therefore

$$\alpha^\dagger_{\lambda\mu} = (-1)^\mu \alpha_{\lambda,-\mu} \qquad \text{II-6}$$

and

$$\pi^\dagger_{\lambda\mu} = (-1)^\mu \pi_{\lambda,-\mu}$$

Oscillations with $\lambda = 0$ would describe variations in the volume of the fluid while it retained its spherical shape. These vibrations, sometimes called breathing modes, are not allowed in this model as the fluid is assumed to be incompressible.

Oscillations with $\lambda = 1$ correspond to a vibration in the position of the centre of mass of the nucleus, without any variations in the nuclear shape. For high energy (10-20 MeV), collective dipole ($\lambda = 1$) oscillations are observed but these can be interpreted as oscillations of the proton fluid against the neutron fluid. These oscillations require that the protons and neutrons be treated separately, in contradiction to the assumption that the fluid is homogeneous.

Quadrupole ($\lambda = 2$), octupole ($\lambda = 3$) and higher modes of vibrations are allowed. These vibrations, if the model is applicable, will describe the excited states of the nucleus.

Each mode of vibration can be treated as a particle[20] of spin λ, parity $(-1)^{\lambda}$, and projection μ, onto the quantization axis. These particles are commonly called phonons. In the vibrational model, therefore, an excited state of the nucleus is described by the number and type of the phonon that make up the state. That is, states can be made up of, say, one quadrupole phonon, two quadrupole phonons, one octupole phonon, one octupole and one quadrupole phonon, etc.

The state functions for the low energy states involving only quadrupole and octupole vibrations are derived in Appendix A using the number representation.[21] The transitions that are allowed in this model, together with their reduced transition probabilities, are derived in Appendix B. The basic features of the simple vibrational model are

described below.

i) States in this model are characterized by the symbol $J^{\pi}_{n_\lambda}$, J being the angular momentum, π the parity, and n_λ the number of phonons of character λ. The first excited state is 2^+_1, a one quadrupole phonon state; that is, a 2^+ state with $n_2=1$. The symbol $E_{2^+_1}$ is used for the energy of this state.

A state with two or more phonons is degenerate. There are three states with two quadrupole phonons, each with energy $2E_{2^+_1}$. These states have $J^{\pi}_{n_2} = 4^+_2$, 2^+_2 and 0^+_2. Similarly, there are five degenerate three quadrupole phonon states with $J = 0^+, 2^+, 3^+, 4^+$, and 6^+, each with energy $3E_{2^+_1}$; five degenerate one quadrupole ($n_2=1$) one octupole ($n_3=1$) states with $J = 1^-, 2^-, 3^-, 4^-$ and 5^-, each with energy $E_{2^+_1} + E_{3^-_1}$, where $E_{3^-_1}$ is the energy of the one octupole phonon state, etc.

ii) Transitions can occur only between states that differ by one phonon, and, for the emission of a gamma ray of angular momentum L, a phonon with $\lambda = L$ must be created or destroyed. Also, since the parity of the phonons is $(-1)^\lambda$, the parity change of the transition must be $(-1)^\lambda = (-1)^L$, and therefore only electric transitions are allowed (see Appendix B).

Neither of these two restrictions are completely obeyed in real nuclei. One does find, however, that many even-even nuclei have a 2^+ first excited state, with a group of positive parity states at energies of approximately $2E_{2^+_1}$ and $3E_{2^+_1}$. Quite often, a single 3^- state is found in the energy region between $2E_{2^+_1}$ and $4E_{2^+_1}$, with a group of negative parity states at about $E_{2^+_1}$ above this state. Many of these states have the large reduced transition rates expected of collective states. These states are interpreted to be vibrational states and attempts[5,6,24] have

been made to explain them with the simple harmonic states derived in Appendix A as basis states. Anharmonic terms are added to the harmonic Hamiltonian as perturbations to account for the deviations from the simple harmonic vibrational states.

II-3 Anharmonic Corrections

There will be no attempt to derive these corrections here. The method is outlined in what follows, and a few attempts to use this method to describe vibrational nuclei are discussed briefly. The Hamiltonian in this case is

$$H = H_o + O(\alpha)^3 + O(\alpha)^4 + \ldots.$$

where H_o is the simple vibrational Hamiltonian of equation II-3. $O(\alpha)^3 + O(\alpha)^4$ .... stands for terms in the expansion parameters, $\alpha_{\lambda\mu}$ or $\pi_{\lambda\mu}$ of order 3, 4 .... . The allowed combinations of $\alpha_{\lambda\mu}$ and $\pi_{\lambda\mu}$ are restricted by the requirement that H must be Hermitian and scalar.[5]

The matrix of H is calculated[21] in the basis provided by the simple harmonic state functions (the eigenstates of H_o) and the eigenstates and eigenvalues obtained by diagonalizing this matrix. The coupling constants between the harmonic terms ($O(\alpha)^2$ terms) and the anharmonic terms can then be treated as free parameters whose values can be adjusted to fit the observed energies of the excited states of the nucleus under consideration. The transition rates are then calculated for these states, and hopefully, they will be in reasonably good agreement with those found experimentally.

Although the form of the perturbed eigenstates obtained with the above diagonalization will not be derived here, it is a simple matter to show which unperturbed eigenstates are coupled by anharmonic terms to

third, fourth, etc., order in the expansion parameters.

The expansion parameters are linear functions of the phonon creation and destruction operators, $a^+_{\lambda\mu}$ and $a_{\lambda\mu}$ (see Appendix A). Anharmonic terms to third order will therefore contain the number operators in the form

$$A = a_{\lambda\mu}\, a_{\lambda'\mu'}\, a_{\lambda''\mu''}$$

$$B = a^+_{\lambda\mu}\, a_{\lambda'\mu'}\, a_{\lambda''\mu''}$$

$$C = a^+_{\lambda\mu}\, a^+_{\lambda'\mu'}\, a_{\lambda''\mu''}$$

$$D = a^+_{\lambda\mu}\, a^+_{\lambda'\mu'}\, a^+_{\lambda''\mu''}$$

A and D will couple the simple phonon states that differ by three phonons and B and C will couple states that differ by one phonon.

Consider, for instance, that we wish to calculate the splitting of the two quadrupole phonon triplet to third order in $\alpha_{\lambda\mu}$ and $\pi_{\lambda\mu}$, where we only consider the coupling of quadrupole phonons (this is the simplest anharmonic correction available). We must consider as our basis set of states all quadrupole phonon states up to $n_2=5$.

Karmen and Shakin[5] have used this simplest coupling to derive the eigenvalues of the first 9 quadrupole vibrational states. Their results required that the energy of the 4^+ member of the two quadrupole phonon triplet, $E_{4^+_2}$, had to be less than twice the energy of the one quadrupole state $E_{2^+_1}$, and that the 0^+ member had to be below the 4^+ member. Since this ordering has only been observed in a very limited number of vibrational nuclei, these third order corrections do not, in general, describe spherical nuclei adequately.

Sorensen[24] extended the basis states for the quadrupole case up to $n_2=7$ (72 states) and included anharmonic coupling to fourth order in the quadrupole expansion parameters. The result was that the restriction $E_{4^+_2}$

$\leq 2E_{2_1^+}$ was removed, but that the restriction $E_{0_2^+} \leq E_{4_2^+}$, remained. The number of free parameters that must be fitted to the experimental data in Sorensen's expressions are greater than the number of known quadrupole vibrational states in any one nucleus.

Lipas[23] has derived expressions for the splitting of the one quadrupole-one octupole quintet ($J = 1^-, 2^-, 3^-, 4^-$ and 5^-) using this method. The basis he used consisted of the quadrupole states up to $n_2=4$ and the octupole states up to $n_3 = 3$. He considered anharmonic terms in H up to fourth order in the quadrupole and octupole expansion parameters. Any ordering of the 5 states could be achieved by different variations of the coupling constants, and, in order to get estimates of their relative strengths, at least one complete set of the five states must be observed. There is no nucleus for which such a group of states has been identified.

This type of phenomenological description cannot be considered to be too successful, and has indicated the need to include other types of coupling in the collective description of spherical nuclei. That is, the observed energies of the collective states can not be achieved by varying the coupling constants, as indicated above, between realistic limits. It is therefore assumed that another coupling of the vibrational states, presumably via particle states,[27] is required to achieve these results. Particle coupling is taken into account automatically in the microscopic description of these nuclei.[8] The semi-microscopic description, while it does not consider particle states of one type of nucleon at all, does handle the particle states of the other type automatically.

II-4 Semi-Microscopic Description of ^{124}Te

^{124}Te has 2 protons and 22 neutrons outside the closed major shell of 50 protons and 50 neutrons. The semi-microscopic description of this

nucleus, as outlined by Lopac,[14] is

i) The coherent motion of the 22 neutrons, and the polarization of the core by this motion, is given by the vibrational Hamiltonian H_V (with or without anharmonic terms).

ii) The excitations of the two protons are described by a quasi-Boson Hamiltonian, H_p.

iii) The eigenvalues and eigenstates of the excited states of ^{124}Te are obtained by diagonalizing the matrix of the Hamiltonian

$$H = H_V + H_p + H_{int}$$

obtained in the basis formed by the eigenstates of the Hamiltonian $H_V + H_p$.

The form of H_{int}, the interaction Hamiltonian between H_V and H_p, is taken to be

$$H_{int} = -\sum_{i=1}^{2} k(r_i) \sum_{\lambda\mu} Y_{\lambda\mu}(\theta_i, \phi_i)\, \alpha_{\lambda\mu}$$

where r_i θ_i, ϕ_i are the coordinates of the protons in the coordinate system used to describe the collective motion. The $Y_{\lambda\mu}$'s are spherical harmonics. The $\alpha_{\lambda\mu}$'s are the surface expansion parameters and can be written as

$$\alpha_{\lambda\mu} = \left(\frac{\hbar}{2\omega_\lambda B_\lambda}\right)^{1/2} (a_{\lambda\mu} + (-1)^{\mu} a^{+}_{\lambda-\mu})$$

as shown in A ppendix A. The $k(r_i)$'s are the proton radial wave functions whose matrix elements are treated as a free parameter that can be adjusted to give the best agreement with the observed energy levels. This type of interaction couples vibrational states that differ by one phonon.

Lopac[14] has chosen the harmonic quadrupole vibrations, including up to the three quadrupole phonon states to represent the collective motion. He has not considered octupole states. The shell model states chosen to describe the proton excitations were the $1g_{7/2}$, $2d_{5/2}$, $2d_{3/2}$, $3S_{1/2}$ and

$1h_{11/2}$ states; in other words, all the shell model states above the Fermi energy at Z=52 and below the next closed major shell at Z=82. All these states were used as Lopac[28] and others[29] have shown they are required in a similar description of the odd mass Sb isotopes, which have one proton outside the major shell. He was able to obtain reasonable agreement (as shown in section VI-5) with the experimental energy levels up to the two quadrupole phonon states. To achieve this agreement, he used a value of 0.7 MeV for the free coupling parameter, given by

$$a = \frac{\langle k \rangle}{\sqrt{4\pi}} \left(\frac{\hbar}{2\omega_2 B_2} \right)^{\frac{1}{2}}$$

where <k> is the radial matrix element.

Using this value of the coupling constant, he was able to calculate reduced E2 transition rates. The form of the electric quadrupole operator used was

$$m^E_{2\mu} = e^p_{eff} \sum_{i=1}^{2} r_i^2 Y_{2\mu}(\theta_i, \phi_i) + \frac{3}{4\pi} R_0^2 \left(\frac{\hbar}{2\omega_2 B_2} \right)^{1/2} (a_{2\mu} + (-1)^{\mu} a^{\dagger}_{2,-\mu})$$

He sets $e^p_{eff} = 2e$ (e = proton charge) to account for the polarization of the core by the proton. He then calls

$$e^V_{eff} = Ze \left(\frac{\hbar}{2\omega_2 B_2} \right)^{\frac{1}{2}}$$

the effective charge of the vibrator and varies it so that $m^E_{2\mu}$ will give the observed reduced transition rate of the first 2^+ excited state. The best fit was obtained using $e^V_{eff} = 2.63e$. Using this value he calculates the reduced E2 transition rates of the higher energy states. Some of these will be compared to the experimental values found in our investigation in Chapter VI.

Chapter III

Gamma-Ray Singles Spectroscopy

The energies and intensities of the gamma rays emitted in the decay of ^{124}Sb were measured with two different germanium lithium-drifted (Ge(Li)) detectors. When this investigation was begun, the best Ge(Li) detector available to this laboratory was a 30 cc. trapezodal detector with an energy resolution of 4.5 KeV at 1332 KeV. The largest multi-channel analyser (MCA) available was a 512 channel Northern Scientific, Model 600. In order to obtain suitable peak definition, eight different spectra were required to cover the energy range, 0→3000 KeV, involved in this decay. Shortly after these spectra had been analysed, a much larger (45cc.) Ge(Li) detector with a resolution of 3.0 KeV at 1332 KeV, together with a 4096 channel MCA were purchased by the U.B.C. Van de Graaff. The gamma spectrum of ^{124}Sb was re-analysed using this detector and the larger MCA. Although the energies and intensities of all gamma transitions found with both detectors agreed within experimental error, twenty-seven weak transitions were found with the large detector that were not found with the smaller one.

Since the results obtained with the large detector were far superior, only the method of peak fitting, and energy and efficiency calibration, used for it will be discussed here. The method of analysis was essentially the same for spectra obtained with either detector.

The preamplifier used was a Tennelec, Model 135M, and the amplifier used was a Tennelec 203BLR, an active filter amplifier with baseline restoration.

III-1 Peak Fitting

The energies and intensities of unknown gamma transitions are usually found by comparison of their spectra to those of known gamma transitions. An accurate comparison requires that the areas and positions of the peaks in a spectrum can be consistently estimated. Good estimates can be made without any function to describe the peak shape if the height of the peak is much greater than the height of the background and if the peaks do not overlap. In general, this is not the case, and so a function that describes the peak shape must be found and this function fitted to the experimental data.

The peak shape obtained with a Ge(Li) detector is a distorted Gaussian, an example of which is the "total function" curve shown in figure III-1. There have been many attempts in the past[30] to describe these peak shapes in terms of combinations of different functions, usually energy dependent. A number of different functions were tried in this investigation, and finally a combination of three gaussians and a "step function" (see figure III-1) , superimposed on a linear background, was chosen.

The function chosen had the form:

$$y = P_1 + P_2X + E_1 + E_2 + E_3 + S$$

with

$$E_1 = P_4 \exp[- (X-P_5)^2/2P_6^2]$$

$$E_2 = P_7 \exp[- (X-P_8)^2/2P_9^2]$$

$$E_3 = P_{10} \exp[- (X-P_{11})^2/2P_{12}^2]$$

$$S = P_3 (\pi/2 - \text{Arctan}[(X-P_{14})P_{13}]$$

E_1 is the main gaussian with height P_4, position P_5, and standard deviation P_6. E_2 and E_3 are the satellite gaussians with heights P_7 and P_{10}, positions

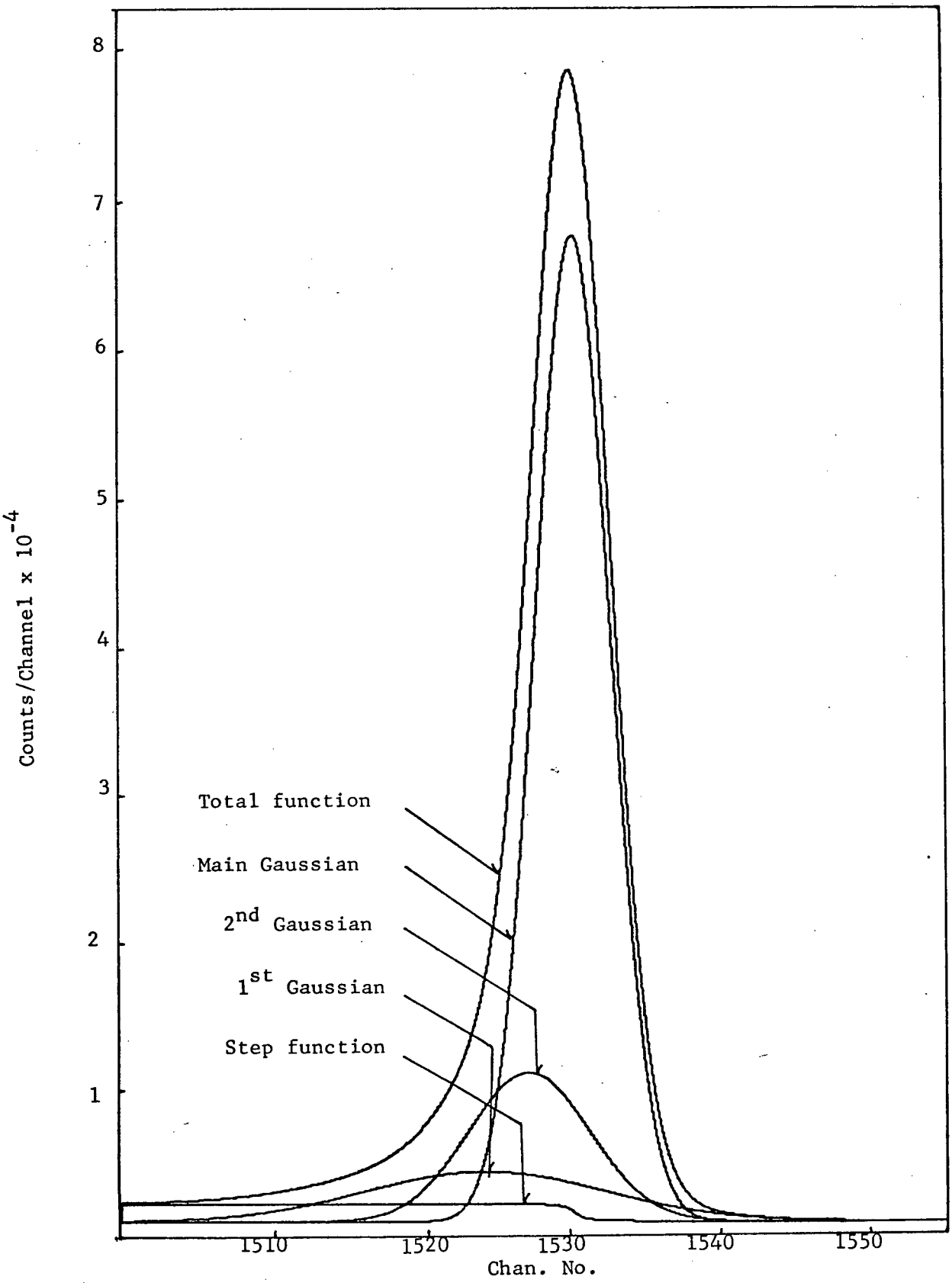

Components of the peak fitting function (for 1274 KeV)

P_8 and P_{11}, and standard deviations P_9 and P_{12}, respectively. S is the step-function, with height P_3, step position P_{14} and "steepness" P_{13}. $P_1 + P_2X$ is the linear background. The individual components of this function are plotted (by computer) in figure III-1. The 14 parameters used to generate the plot data were those found by fitting the function to the peak at 1274 KeV in a spectrum of ^{22}Na.

This function was least-square fitted to known peaks in the energy region 120 → 2600 KeV. The relationship of the satellite gaussians' parameters to the main gaussian's parameter were found as a function of energy to be

Height (See figure III-2)

$P_7/P_4 = .126 + 5.0 \times 10^{-5} \times E(KeV)$

$P_{10}/P_4 = .022 + 2.2 \times 10^{-5} \times E(KeV)$

Resolution (See figure III-3)

$P_9/P_6 = 1.5$

$P_{12}/P_6 = 3.2$

Position (See figure III-4)

$P_8 = P_5 - (3.3 + .0026 \times E(KeV))/P_6$

$P_{11} = P_5 - (8.6 + .005 \times E(KeV))/P_6$

The best position for the step, P_{14}, was found to be the centre of the main gaussian (P_4). The steepness of the step, related to P_{13}, was not critical as long as S reached its maximum (P_3) and its minimum (0) under the region of the peak. The value chosen was $P_{13} = 2.0$.

There are therefore only 2 + 4 x m independent parameters needed to fit a region of a gamma spectrum containing m peaks superimposed on a linear background; the step height for each peak, and the height, resolution, and position of the main gaussian of each peak. In special cases the back-

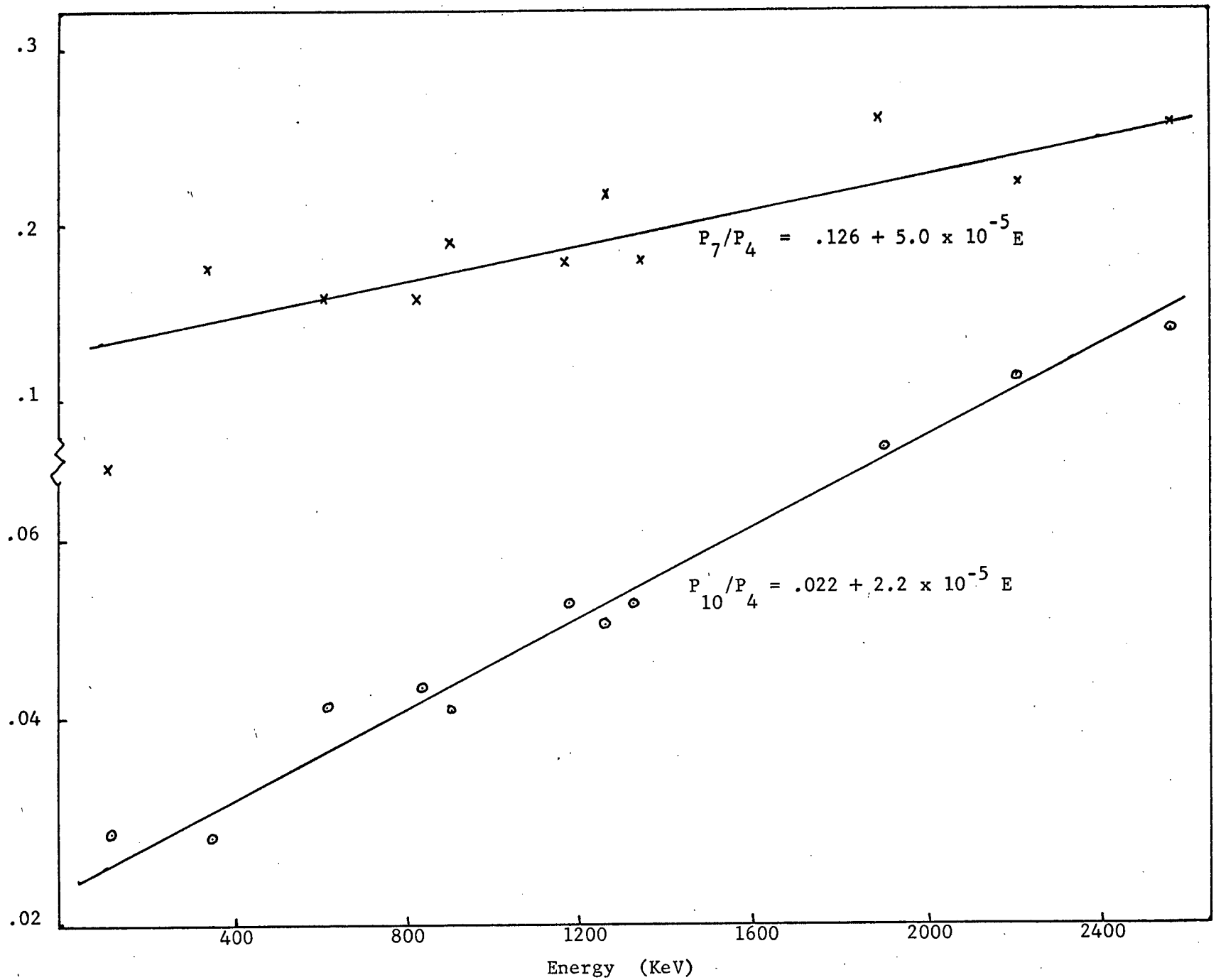
.3
.2
.1
.06
.04
.02
400
800
1200
1600
2000
2400
Energy (KeV)
Ratios of Heights
$P_7/P_4 = .126 + 5.0 \times 10^{-5} E$
$P_{10}/P_4 = .022 + 2.2 \times 10^{-5} E$

Figure III-2

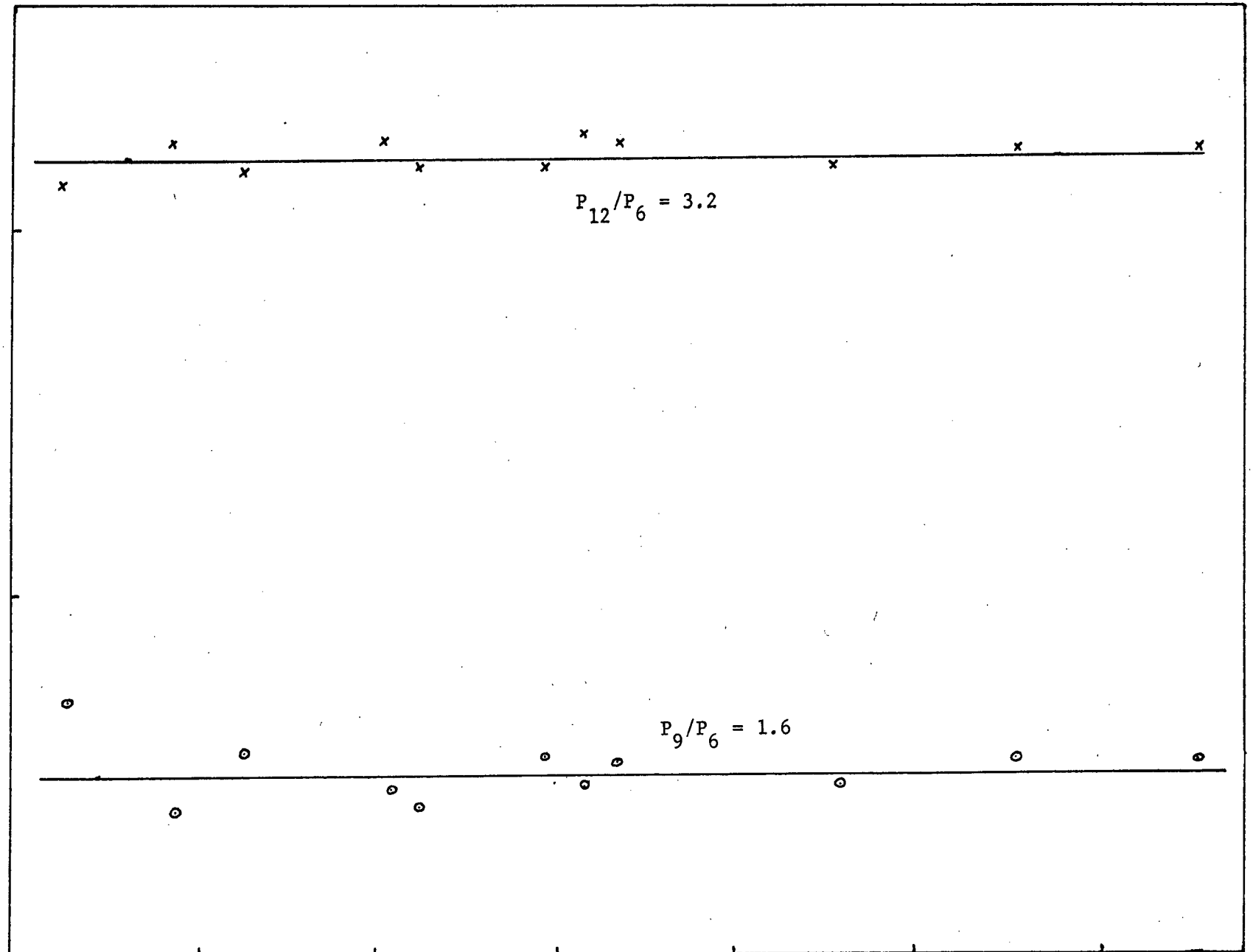
Ratios of Widths
3
2
1
$P_{12}/P_6 = 3.2$
$P_9/P_6 = 1.6$
400
800
1200
1600
2000
2400
Energy (KeV)

Figure III-3

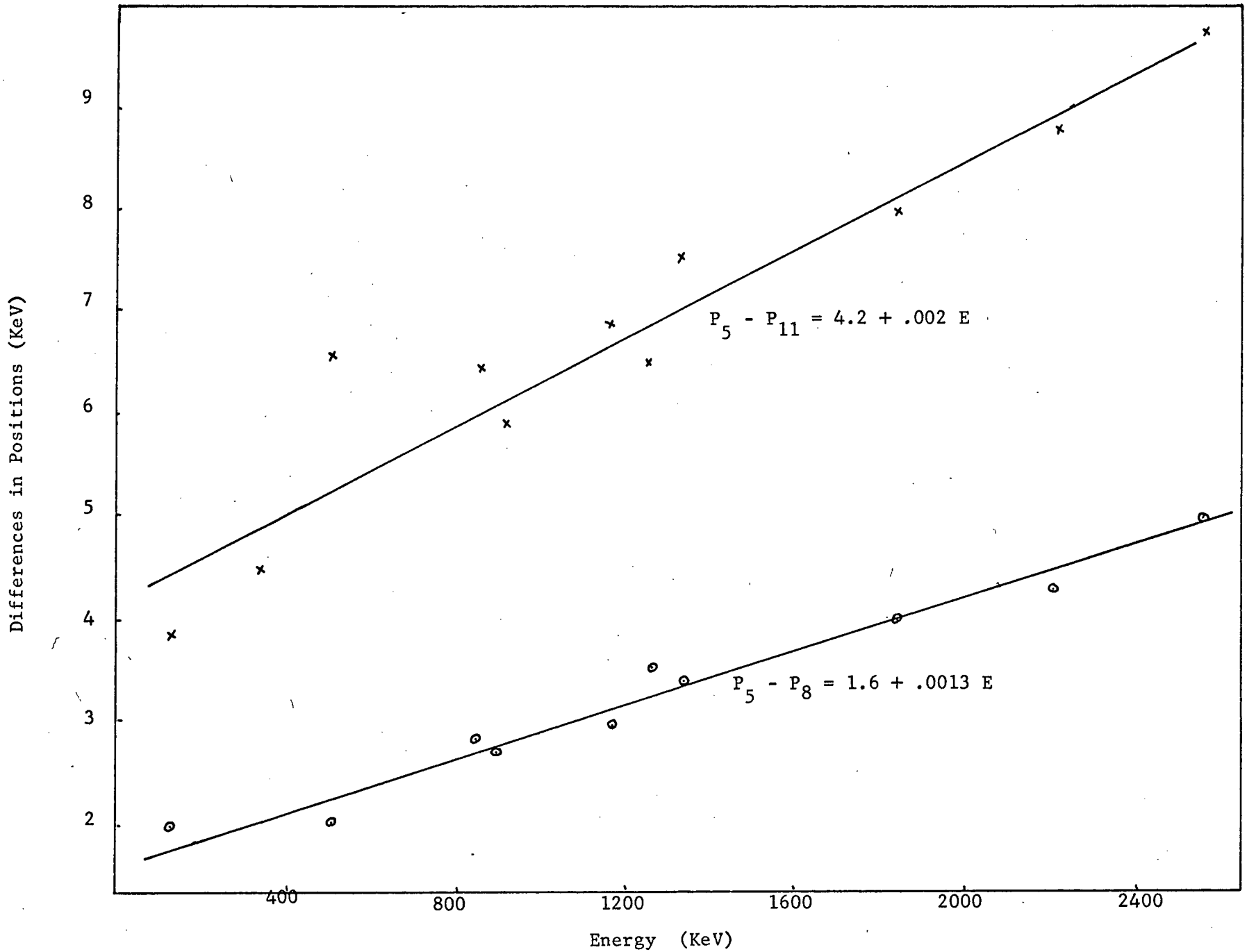
Differences in Positions (KeV)
9
8
7
6
5
4
3
2
400
800
1200
1600
2000
2400
Energy (KeV)
$P_5 - P_{11} = 4.2 + .002\ E$
$P_5 - P_8 = 1.6 + .0013\ E$

Figure III-4

ground could not be approximated by a straight line. Therefore, in the final fitting program an X^2 term in the background was allowed for, although in most cases the coefficient of this term was set equal to zero. The actual least-square fitting was done using the U.B.C. Computer Centre Library Subroutine RLQF[31] (Restricted-Least-Square fit).

The areas of the peaks were taken as the sum of the areas of the three gaussians. The position of the peak was taken as the centre of the main gaussian. The error in peak areas and positions were calculated from the errors returned from this subroutine.

The consistency of this fitting program was checked by fitting the peaks due to six different gamma transitons in the energy range 100 → 2600 KeV. Different spectra were obtained for each peak by allowing the MCA to accumulate for different lengths of time. The positions and the normalized intensities found for each energy agreed to within the calculated error.

A check on the ability of the program to unfold overlapping peaks was performed in the following way. Two spectra of a single gamma transition were taken and the peak parameters for each spectrum found. One spectrum was shifted relative to the other by a few channels by a shift of the spectrum origin and the two spectra added. The composite spectrum was then fitted and the parameters for each peak compared to those found from the individual spectra. The relative intensities of the two peaks were also varied. It was found, as expected, that the ability of the program to unfold peaks depended on their relative intensities and their separation. If the peaks were of about the same intensity a peak separation of about $P_6/10$ was required for the program to

unfold the peaks. If one peak was 10 times more intense than the other, a separation of about P_6 was required. These requirements are only approximate as the ability of the program to unfold peaks depends on the height and shape of the background, as well as on the total intensity of the peaks.

III - 2 Efficiency Calibration

The sources used to measure the gamma-ray efficiency of the Ge(Li) detector are listed in table III-1. The total efficiency (the product of solid angle and intrinsic efficiency) was calculated from the ratio of the total gamma ray intensity, I_o, to the measured intensity, I , at each energy. The total intensity was calculated from the data given in table III-1. The source-detector distance was 10 centimeters.

The standard sources were obtained from the International Atomic Energy Agency (IAEA), Vienna. They are encapsulated in plastic disks which are, in turn, cold welded into aluminum disks. A dummy disk is supplied with the sources.

The standard sources were used to determine the efficiency of the detector over the energy range 120 → 1350 KeV. The intensities of the secondary standards were found using this calibration and published relative intensities of the secondary standards' gamma-rays. In this manner, the efficiency was extended up to 2750 KeV. ^{88}Y and ^{228}Th were used as secondary standards as they both have transitions in the energy range of the calibration sources whose relative intensities to higher energy transitions is well known.

The uncertainty in the efficiency of the Ge(Li) detector for each calibration energy is the combination of the following uncertainties.

Table III-1

Efficiency Calibration Standards

Source	Strength(curies) at Jan.1 1970	Half-life	Transition Energy(KeV)	Relative Int.(%)
^{57}Co	11.43±.7%	271.6±.5days	122	85.0±1.7
^{203}Hg	20.25±1.%	46.8±.2days	279	81.55±.15
^{113}Sn	$4.22X10^{5}$ gamma/sec	115.0±.5days	393	-
^{22}Na	9.16±1.0%	2.602±.005years	511	181.1±.2
			1275	99.95±.02
^{137}Cs	10.35±1.8%	30.5±.3years	662	85.1±.4
^{54}Mn	10.96±.7%	312.6±.3days	835	100.0
^{60}Co	10.57±.6%	5.28±.01years	1173	99.87±.05
			1332	99.999±.001

Secondary Standards

^{88}Y	Reference 32	898*	91.4±.7
		1836	99.4±.1
		2734	.62±.04
^{228}Th	Reference 33	583*	100.0
		2614	117.4±1.0

*Used to calibrate secondary standards

a Error in I due to uncertainty in the data used to calculate it; i.e., the uncertainties in the standards decay schemes, half-lives, and initial source strengths at t=0. The uncertainties listed in table III-1 are for a quoted 95% confidence interval.[32]

b Random counting error: The MCA was run until at least 10^6 counts had accumulated in each calibration peak, except for the 279 KeV transition of ^{203}Hg and the 2734 KeV transition of ^{88}Y, where fewer counts were taken because of low intensity. The error is therefore less than 0.1%,except for the 279 and 2734 KeV transitions which had an uncertainty of 1.0%.

c Peak fitting error: The error in the peak area (found with the fitting routine) was typically 0.1 → 0.5%.

d Error in the source-detector distance: Each source disk was placed in a holder fixed at 10 cm. from the detector. A spectrum of each source was taken, the source disk reversed, and the spectrum re-taken. The measured intensities were averaged, thereby cancelling any error due to the source material not being at an equal distance from the faces of the source disk. The individual disks could be replaced with less than .01 cm. difference in the source-detector distance. The error in the measured intensity is therefore approximately 0.2%.

e Absorption in the disk: The gamma ray absorption in the source disk was found by inserting the dummy disk between the sources and the detector and finding the decrease in measured intensity. The absorption ranged from (2.4 ± .1)% for

122 KeV to ($.85 \pm .10$)% for 1332 KeV.

f Analyser dead time: Once a pulse is applied to the input of a MCA, the input is blocked to all subsequent pulses until the first pulse has been analyzed. In general, large pulses take longer to analyse than small pulses.[34] Therefore the time that the input is blocked, or the dead time, is a function of the pulse height. The time that the input is blocked per unit time is

$$\sum_i^N \tau_i m_i$$

where m_i is the measured counts per channel, τ_i the dead time for each channel, and N the total number of channels. Since the pulses arrive at the input randomly in time, the number of pulses lost for each channel is

$$n_i - m_i = n_i \sum_i^N m_i \tau_i$$

where n_i is the true counts per channel. The correction for any channel in a given spectrum is

$$f = n_i/m_i = \frac{1}{1 - \sum m_i \tau_i}$$

f will, in general, be different for different spectra.

The correction can be found by analysing the pulses from a pulser at the same time the spectrum is analysed. f is then just the ratio of the true pulse rate (as measured with a scaler)to the measured pulser rate, which can be found by fitting the pulser peak. The pulser pulses will not be random in time with respect to each other, but they will be random with respect to the true pulses. This will not affect

the result if the time between pulser pulses is long compared to the analyser dead time. The pulse rate used was 1000/sec. Typical dead times are about 10^{-5} sec.

This method of dead time correction has the advantage of correcting for pulse summing at the same time. Pulse summing occurs when two individual pulses are separated by a time which is less than the time required by the amplifying system to respond to each individually. The pulses are then analysed as a single pulse. Since the pulser is applied to the input of the preamplifier, its pulses have the same probability as true pulses of being lost from the corresponding peak in the spectrum.

The error in this method of dead time and pulse summing correction is the error in the measured intensity of the pulser peak, which is the combination of the random counting error and the error in fitting the peak. The random counting error can be calculated if the probability distribution for the number of pulses lost is assumed to be Poisson.[35] This assumption is reasonable as the total number of pulses is large and the probability that any one is lost is small. This error is then just the square-root of the number of pulser pulses lost. The error in fitting the pulser peak can be minimized by insuring that the pulser peak is situated on a low background region of the spectrum.

The total error in the efficiency, I_o/I, was calculated from the proper combinations of the above errors for each calibration energy.

Fig.III-5

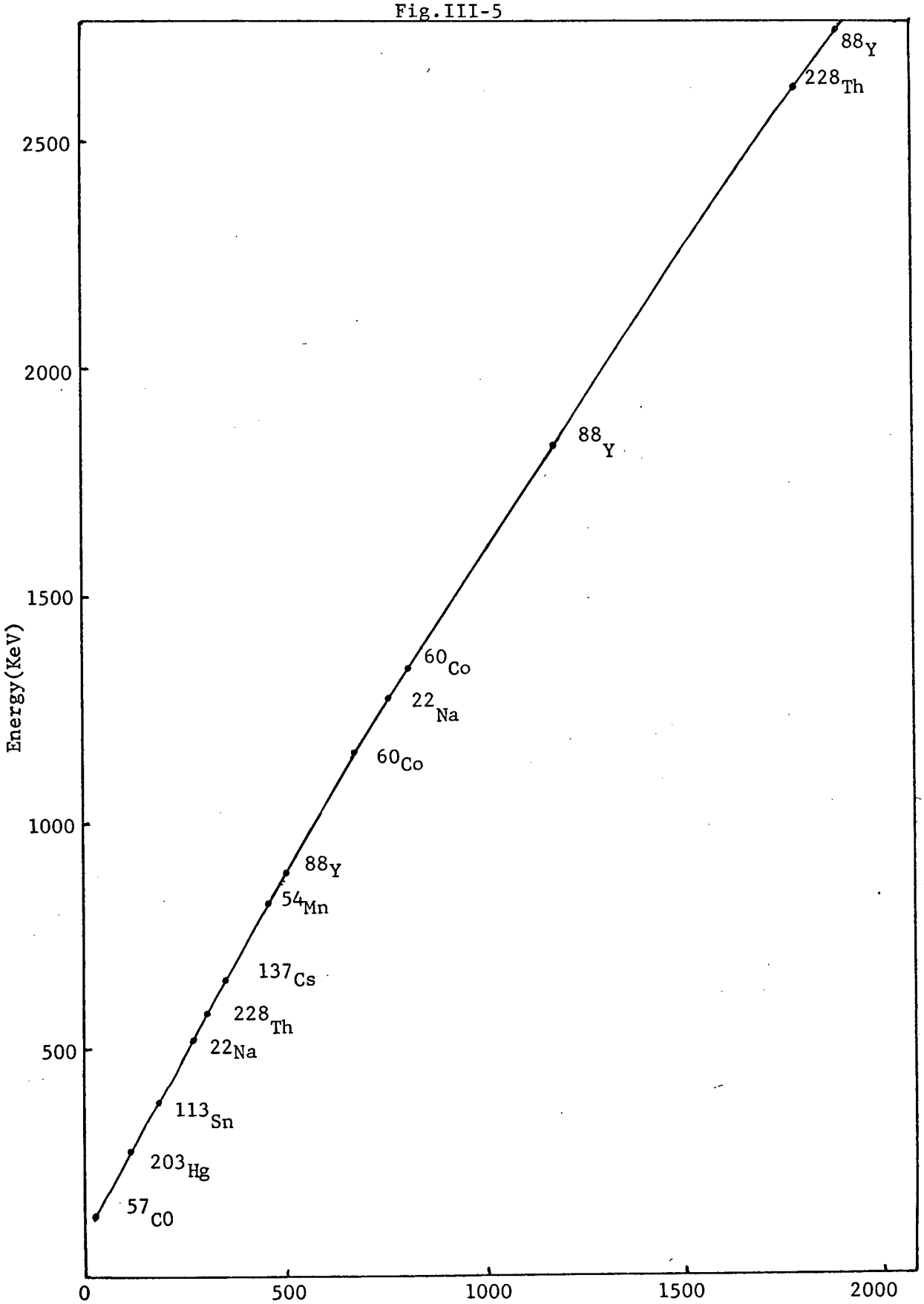

Efficiency of the 45cc. Ge(Li) Detector

This error was used to weight the least square fitting[31] of the I_o/I data to a function of the form

$$I_o/I = a + b\,E - c\,E^2 \qquad E < 550$$

$$I_o/I = a' + b'(E - 500) - C'(E-500)^2 \qquad E > 500$$

The results of the fits were:

$$a = 19.5 \pm 1.0$$

$$a' = 290.7 \pm 3.5$$

$$b = .46 \pm .03\ (KeV)^{-1}$$

$$b' = .656 \pm .008\ (KeV)^{-1}$$

$$c = (2.2 \pm .4) \times 10^{-4}\ (KeV)^{-2}$$

$$c' = (2.19 \pm .04) \times 10^{-5}\ (KeV)^{-2}$$

The large uncertainty in the paramters of the low energy fit is a result of the large uncertainties in the calculation of I_o, and of the relatively large curvature of the efficiency function in this region. These functions are plotted in figure III-5.

III-3 Energy Calibration

The energy calibration of the gamma spectrum of ^{124}Sb was done in two steps. The first consisted of measuring the energies of the intense gamma transitions in the decay of ^{124}Sb found in four hours of analysing, using the standard sources listed in table III-2. The second step used these transitions as secondary energy standards for a much longer analysing period (sixty hours) required to identify weak gamma transitions.

The standard sources were used to calibrate the analysing system before and after the four hour run. The position of the peaks of the standard sources were found using the peak fitting routine described in section III-1. These positions were least-square fitted to a function of

Table III-2

Energy Standards[32,40]

Source	Energy(KeV)	Source	Energy(KeV)
^{57}Co	121.97(.03)	^{207}Bi	1063.58(.06)
^{57}Co	136.33(.03)	^{60}Co	1173.23(.04)
^{226}Ra	241.92(.03)	^{22}Na	1274.55(.04)
^{203}Hg	279.191(.008)	^{60}Co	1332.49(.04)
^{226}Ra	351.99(.06)	^{228}Th	1592.46(.10)
^{113}Sn	391.70(.05)	^{226}Ra	1764.45(.22)
^{22}Na	511.006(.002)	^{88}Y	1836.13(.04)
^{228}Th	583.14(.02)	^{228}Th	2103.47(.10)
^{137}Cs	661.64(.08)	^{226}Ra	2204.25(.48)
^{54}Mn	834.81(.03)	^{228}Th	2614.47(.10)
^{88}Y	898.04(.04)	^{88}Y	2734.14(.08)

Table III-3

Secondary Energy Standards

Energy(KeV)	Energy(KeV)
602.80(.06)	1045.17(.09)
646.02(.07)	1325.56(.11)
722.90(.07)	1691.05(.09)
790.78(.08)	2091.0(.2)
968.20(.09)	2614.47(.10)*

* ^{228}Th peak in background

the form

$$E(KeV) = a + b \times (Chan)$$

The results of the fits were:

Before a= 51.26 ± .03 KeV

b= .71506 ± .00003 KeV/Chan

After a= 51.30 ± .04 KeV

b= .71504 ± .00003 KeV/Chan

Figure III-6 shows the distribution of the energies of the standard sources over the calibration range. The width of the line drawn through the points is much larger than the error associated with any point.

The energies of the transitions found in the four hour run were calculated from the average of "before" and "after" parameters. The width of the peaks in this run were the same as the width of peaks found in much shorter runs (10 min.), indicating that no appreciable fluctuations in the gain of the system had occurred during this period.

The energies of ^{124}Sb transitions used to calibrate the sixty hour run are given in table III-3. The positions of the peaks corresponding to these transitions for the sixty hour run were fitted to a straight line with the results

a = 51.34 ± .07 KeV

b = .7150 ± .0001 KeV/Chan.

The full widths-at-half-maximum (FWHM) of the peaks in the sixty hour run were larger than the peaks in the four hour run by approximately 2×10^{-4} KeV/Chan. This peak broadening corresponds to a gain instability of the total analysing system of .02%. The energy cali-

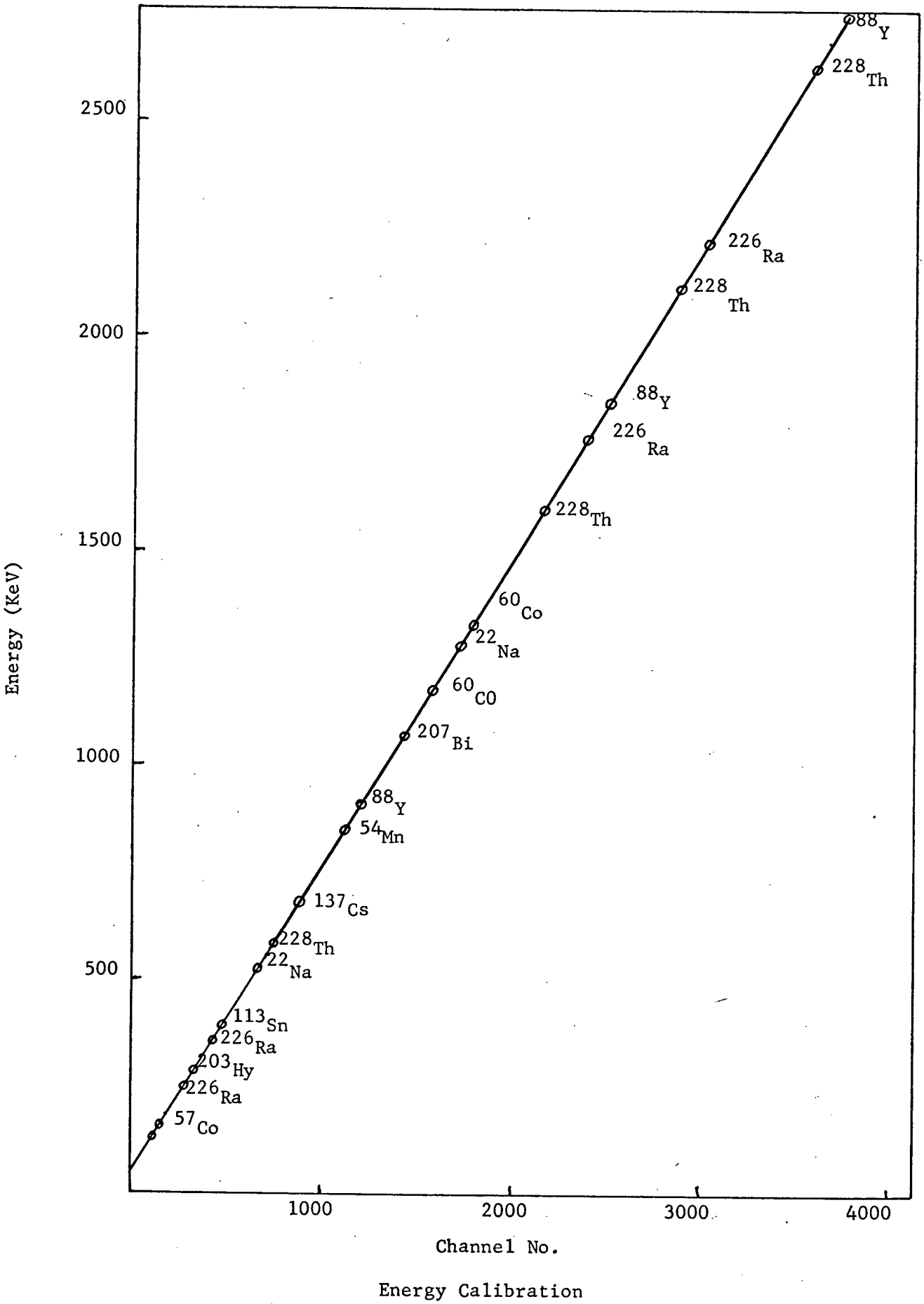

Energy Calibration

bration of the sixty hour run was not affected appreciably by this instability as it was obtained from the secondary standards whose positions were, of course, subjected to the same fluctuations.

III-4 ^{124}Sb Gamma Spectrum

The gamma spectrum of the decay of ^{124}Sb to ^{124}Te obtained in sixty hours of analysing is shown in figures III-7 (a-h). The positions and areas of the peaks of this spectrum were found using the fitting program described in section III-2. The energies and intensities of the gamma transitions corresponding to these peaks were calculated using the appropriate calibration functions described in sections III-3 and III-4. Table III-4 gives the results of these calculations. Included for comparison are the results of another recent investigation of this decay by Meyer.[36]

The gamma spectrum contains single and double escape peaks, sum peaks, along with the full energy peaks resulting from the gamma transitions in the decay, and in addition, peaks resulting from radioactivity in the laboratory other than ^{124}Sb. These "background" peaks were identified by removing the source and taking a background run for the same length of time as for the total spectrum. Only one background peak (444 KeV) overlapped a true peak.

The peaks resulting from single and double escape of the positron annihilation radiation were identified by taking spectra of ^{60}Co, ^{88}Y, Bi^{207}, ^{226}Ra and ^{228}Th sources. The ratios of the areas of the escape peaks to the full energy peaks were found. These ratios were plotted as a function of energy (see figure III-8) and this graph used to identify escape peaks in the total spectrum.

Fig. III-7(a)

Gamma spectrum of ^{124}Sb

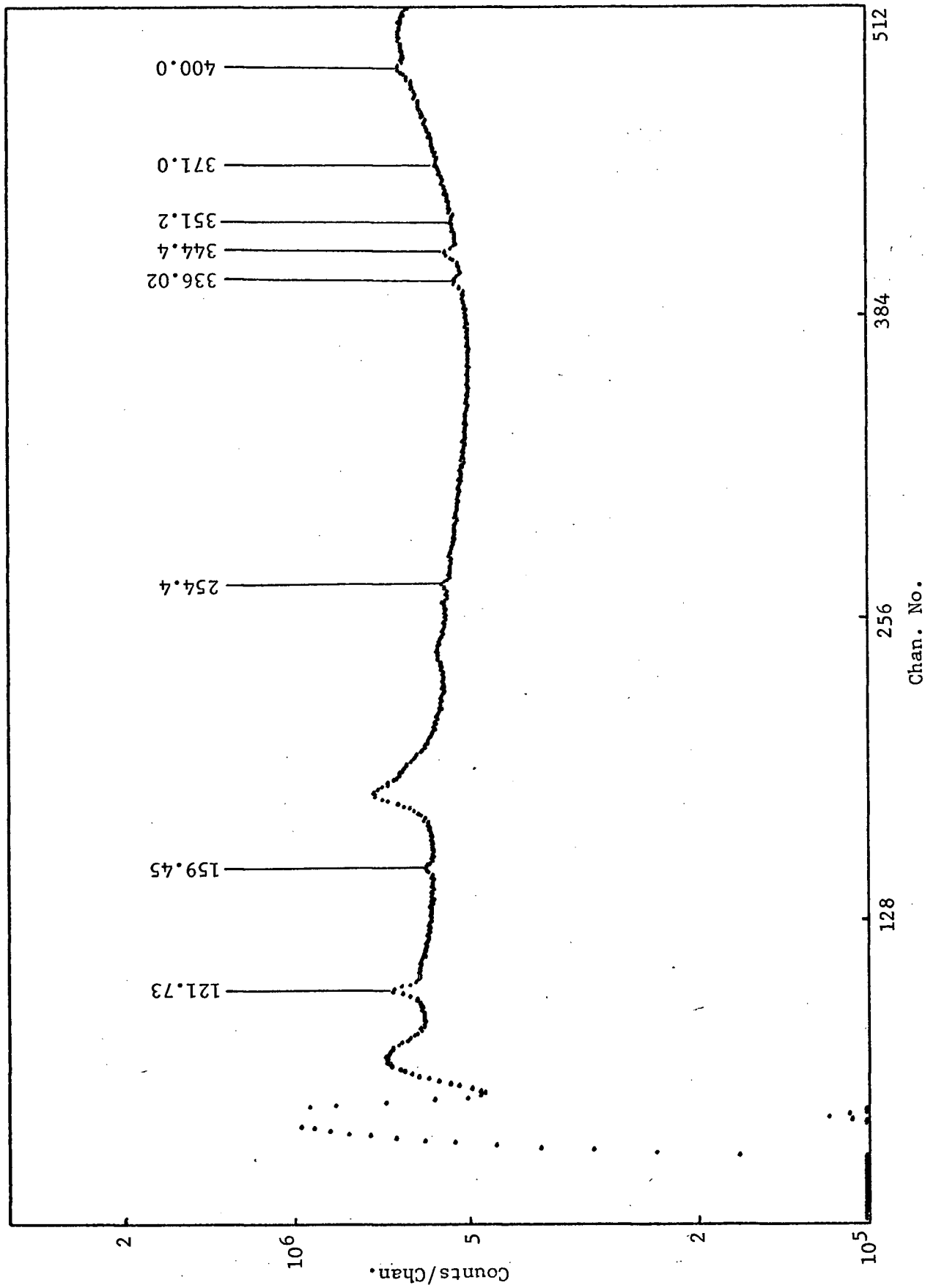

Counts/Chan.
5
10^5
2
5
10^6
2
5
10^7
Chan. No.
640
768
896
444.18
468.8
481.4
525.4
602.80
632.4
646.02
662.7
669.2
709.4
713.9
722.9
735.4
765.4

Fig. III-7(b)

Counts/Chan.
5
10^5
2
3
5
10^6
790.78
816.9
856.9
867.6
900.0
911.5
968.2
976.0
1014.7
1045.19
1054.4
1069.1
1086.2
1112.2
1120.3
1152
1280
1408
1536
Chan. No.

Fig. III-7(c)

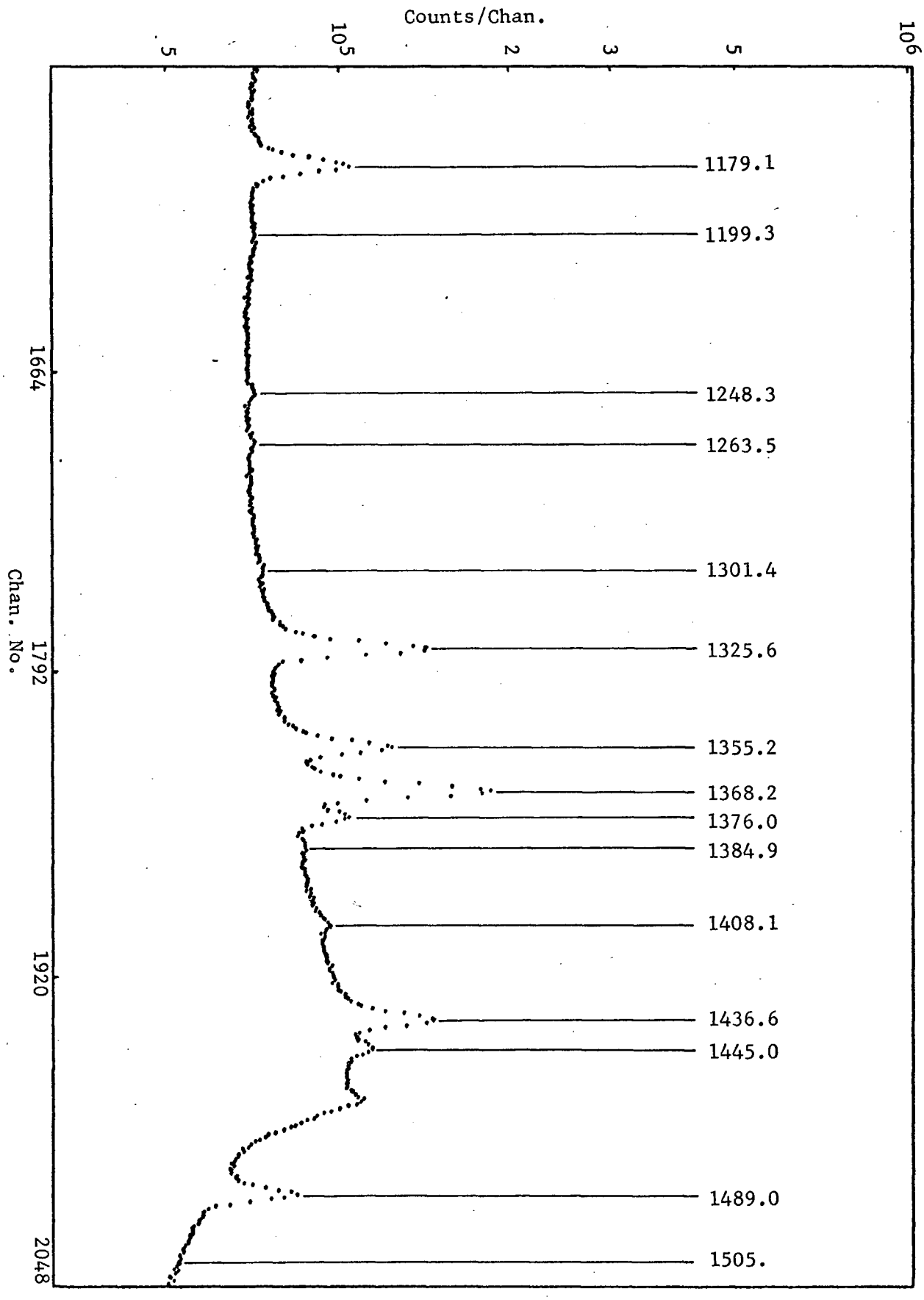
Counts/Chan.
5
10^5
2
3
5
10^6
1179.1
1199.3
1248.3
1263.5
1301.4
1325.6
1355.2
1368.2
1376.0
1384.9
1408.1
1436.6
1445.0
1489.0
1505.
1664
1792
1920
2048
Chan. No.

Fig. III-7(d)

Counts/Chan.
5
10^4
2
5
10^5
2
5
10^6
2
1526.3
1579.9
1622.4
1691.05
1720.3
1732.1
1764.7
2176
2304
2432
2560
Chan. No.

Fig. III-7(e)

Counts/Chan.
5
10^3
2
5
10^4
2
5
10^5
2
Chan. No.
2668
2816
2944
3072
1918.6
1941.4
1957.7
1971.1
2016.2
2039.3
2091.0
2098.7
2107.5
2172.
2182.6
2204.7

Fig. III-7(E)

Counts/Chan.
2
5
10^3
2
5
10^4
2
5
2283.3
2293.7
2323.4
2450.2
2454.4
2614.5
3200
3328
3456
3584
Chan. No.

Fig. III-7(g)

Fig. III-7(h)

Table III-4

Energies and Intensities of Gamma Transitions in ^{124}Sb Decay

Energy(KeV)		Intensity		
This Work	Meyer[36]	This Work	Meyer[36]	Comment
121.73(.15)	-	205(40)	-	a
159.4(.2)	-	140(40)	-	
-	185.4	-	400	c
239.4(.2)	-	200(40)	-	b
244.6(.2)	-	230(60)	-	a
254.4(.3)	254.4	120(20)	100	
336.0(.2)	335.8	560(100)	790	
344.4(.2)	-	1000(130)	-	a
351.2(.6)	-	500(200)	-	b
371.0(.2)	370.4	290(100)	200	
380-390	385.9	100	800	j
400.0(.2)	400.0	1300(150)	5300	
444.2(.1)	444.0	1700(150)	3500	d
468.8(.3)	468.6	300(100)	300	
473-479	476.5	100	350	j
481.4(.2)	481.	200(100)	650	
498.6(.3)	498.4	200(100)	500	
525.4(.2)	525.5	1300(100)	3100	
550-555	553.8	<100	≤ 200	j
602.80(.06)	602.72	10^6	10^6	e
632.4(.7)	632.4	1200(300)	1100	
646.02(.07)	645.82	74000(1600)	72300	
662.7(.5)	662.5	150(30)	250	
669.2(.1)	-	5770(100)	-	f

Table III-4(cont.)

This Work	Meyer	This Work	Meyer	Comment
709.4(.1)	709.3	13600(900)	14300	
713.9(.1)	713.8	23900(1000)	24000	
722.90(.07)	722.78	109700(2000)	113000	
745.4(.2)	735.9	1400(300)	1300	
765.4(.5)	765.3	90(30)	280	
771-777	775.	<50	90	
779.1(.2)	-	660(80)	-	b
790.78(.08)	790.77	7500(150)	7200	
816.9(.1)	816.8	640(60)	790	
856.9(.4)	856.9	220(60)	230	
867.6(.4)	-	180(50)	-	b
900.0(.2)	899.8	110(40)	140	
911.5(.4)	-	140(50)	-	b
935-942	937.9	< 50	65	j
968.20	968.25	20000(400)	18400	
976.0(.3)	796.6	1000(200)	850	
995-1000	997.0	< 50	60	j
1012-1019	1014.5	<50	85	j
1045.19(.09)	1045.24	18900(400)	18500	
1054.4(.5)	1054.8	100(50)	85	
1069.1(.1)	-	2300(120)	-	f
1086.2(.2)	1086.3	300(50)	340	
1112.2(.2)	-	730(100)	-	a
1120.3(.6)	-	120(70)	-	b
1160-1165	1163.2	< 50	190	j
1179.9(.1)	-	8800(250)	-	g
1199.3(1.0)	1198.	80(60)	60	
1238.0(1.0)	1235?	60(30)	60	b

Table III-4(cont.)

This Work	Meyer	This Work	Meyer	Comment
1248.3(.3)	-	50(100)	-	i
1250-1260	1253.4	<50	80	j
1263.4(.4)	1263.1	440(100)	300	
1267-1273	1269.	<50	120	j
1325.6(.1)	1325.5	16400(400)	14200	i
1355.2(.1)	1355.2	11200(350)	9300	
1368.2(.1)	1368.2	27100(600)	23600	
1376.0(.2)	1376.1	5300(250)	4300	
1384.9(.9)	1385.2	310(70)	530	
1385-1390	1388.7	<100	≤100	j
1408.1(.3)	-	1300(200)	-	a
1436.6(.1)	1436.7	13600(400)	10200	
1445.0(.2)	1445.3	2900(250)	2100	
1450-1457	1453.2	<100	180	j
1462.2(.5)	-	3000(500)	-	b
1489.0(.2)	1489.0	6900(250)	5490	
1505.(1.)	1505.6	50(40)	50	
1526.3(.2)	1526.3	4400(200)	3900	
1553-1560	1557.	<50	230	j
1579.9(.8)	1579.7	1500(500)	2000	h
1622.4(.3)	1622.4	300(50)	240	
1691.05(.09)	1691.02	504000(10000)	490000	
1720.3(.2)	1720.4	940(70)	850	
1732.1(.2)	-	100(50)	-	
1764.7(.4)	-	240(50)	-	b
1845-1855	1851.5	<25	20	j

Table III-4(cont.)

This Work	Meyer	This Work	Meyer	Comment
1918.6(.2)	1918.7	570(40)	530	
1941.4(1.0)	-	28(20)	-	g
1945-1952	1950.4	<20	30	j
1957.7(1.0)	-	45(15)	-	
1971.1(.4)	-	20(20)	-	i
2016.2(.4)	2015.	70(20)	90	
2039.3(.2)	2039.2	660(40)	610	
2079.(2.)	2078.5	≤800	110	
2091.0(.2)	2091.0	57600(1400)	56100	
2098.7(.3)	2099.0	500(200)	400	
2107.5(.3)	2108.0	550(100)	420	
2145-2155	2151.5	<5	8	j
2172.(1.)	2172.	12(4)	10	
2182.6(.2)	2182.6	400(30)	410	
2204.7(.4)	2203.?	80(20)	8	b
2283.3(.5)	2283.2	70(20)	80	
2293.7(.3)	2293.7	250(50)	300	i
2323.4(.8)	2323.1	10(4)	24	
2450.2(.7)	-	24(4)	-	b
2454.6(1.0)	2454.4	9(4)	7	
2614.6(.2)	-	780(20)	-	b
2681.3(.5)	2681.4	20(5)	16	
2693.1(.6)	2693.9	24(5)	26	i

Comments

a)Background from ^{152}Eu

b)Natural radioactivity background

Table III-4(cont.)

c)Backscatter peaks from 603,646,709,714, and 723 KeV transitions have energies from 179-189KeV.

d)Background from ^{152}Eu subtracted.

e)Data normalized to this peak.

f)Double excape peak from gammas with energy = $E+2m_oc^2$.

g)Single excape peak from gammas with energy = $E+m_oc^2$.

h) Intensity of single excape peak from 2091KeV transition subtracted.

i)Corrected for one-detector-coin.-sum events.

j)Maximum intensity for transitions found by Meyer[36].

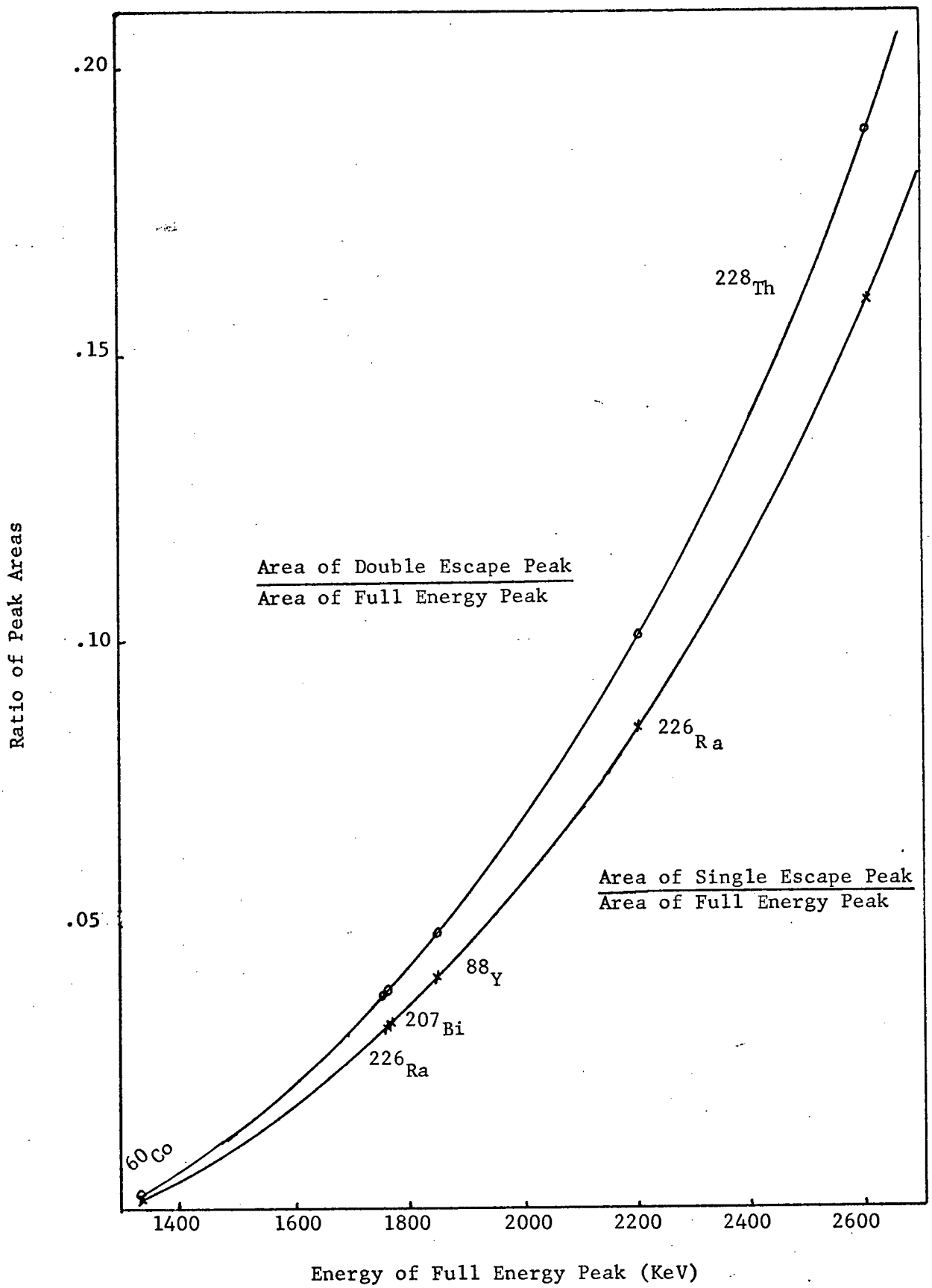
.20
.15
.10
.05
Ratio of Peak Areas
Area of Double Escape Peak
Area of Full Energy Peak
Area of Single Escape Peak
Area of Full Energy Peak
228Th
226Ra
88Y
207Bi
226Ra
60Co
1400
1600
1800
2000
2200
2400
2600
Energy of Full Energy Peak (KeV)

Sum peaks can be divided into two groups, those which result from random coincidences of pulses, and those which result from true coincidences between cascading gamma transitions.

The rate of random sums between two peaks with energy E_1, E_2 and count rates R_1, R_2 that sum to a peak at energy $E_1 + E_2$ is[37]

$$R_{1+2} = 2 \tau R_1 R_2$$

where τ is the maximum time between pulses 1 and 2 for them still to be analysed as a single pulse of energy $E_1 + E_2$. τ can be found by measuring the random sum rate of a transition with itself. The 603 KeV transition was used for this calculation with the rates found from the sixty hour run.

$$R_{603} = 6.43 \times 10^7 / 60 \text{ hrs.}$$

$$R_{603 + 603} < 2000 \quad \text{(No peak was found at 1206 KeV)}$$

The result was $\tau < 5 \times 10^{-7}$ sec. The maximum area of random sum peaks for any two transitions in the decay were calculated using this value. In every case the area was too small to be distinguishable above the background.

Sum pulses that result from cascading gamma transitions will always have an energy equal to the sum of the transition energies if the lifetime of the intermediate state is short compared to τ. The summing rate will be

$$R_{1+2} = K_1^2 \; R_1 \; R_2$$

where K_1^2 is a constant depending on the details of the decay scheme. In general, a peak at energy $E_1 + E_2$ can be the result of a cross-over transition or coincidence sum pulses, or both. A plot of

$$\left(\frac{N_2}{N_{1+2}} \right)^{\frac{1}{2}} \quad \text{or} \quad \left(\frac{N_1}{N_{1+2}} \right)^{\frac{1}{2}}$$

against source-detector distance

where N_1, N_2 and N_{1+2} are peak areas at energy E_1, E_2 and $E_1 + E_2$ respectively, will reveal the nature of the peak at $E_1 + E_2$. A straight line with zero slope indicates that the peak is entirely due to a cross-over transition. A straight line with positive slope indicates that it is a sum peak, and a curve indicates that it is a combination of the two.

Plots such as these are shown in figure III-9 for the cascades 603 - 1691 KeV and 603 - 2091 KeV. The true and sum nature of the peaks at 2293 and 2693 KeV is immediately apparent. The asymptotic values of these curves were found from much larger graphs and the intensities of the 2293 and 2693 KeV transitions calculated.

The constant K_1^2 in the above equation can be estimated for these cascade transitions from the slope of these graphs in the region where the sum term dominates (small source-detector distance). This constant will be, in general, different for different cascade transitions. Once the decay scheme is known, however, the ratio of K_2^1 to K_k^j for any other two transitions j and k, can be calculated (see chapter IV), and therefore the contribution to any peak at energy $E_j + E_k$ due to coincidence summing of transitions j and k can be estimated.

The usual method of identifying sum peaks is to place an absorber between the source and the detector.[38] The absorber will reduce the measured intensity of the low energy transitions much more than high energy ones. The sum peak will therefore be greatly reduced, while any contribution to the peak from a cross-over transition will be only slightly reduced. Figure III-10 is a high energy spectrum of ^{124}Sb with 7.5 cm. of lead between the source and detector. The peaks at 2293 and 2693 KeV have been reduced much more than the other peaks in this energy region. (See figures III-7(g) and (h) for comparison.) This spectrum

Figure III-9

Sum Peak Identifacation

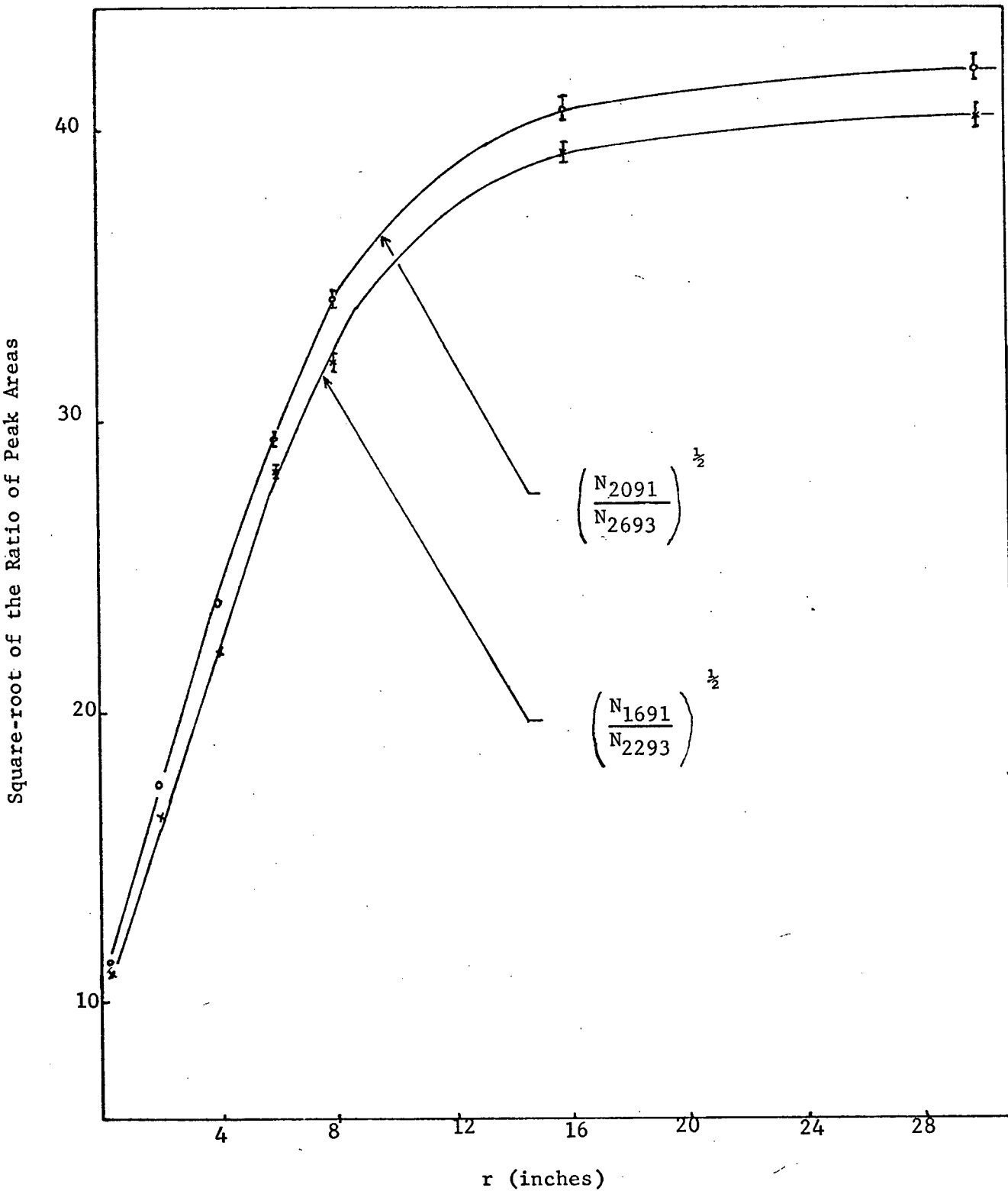

Source-Detector Distance

Fig.III-10

High energy spectrum taken with a lead absorber.

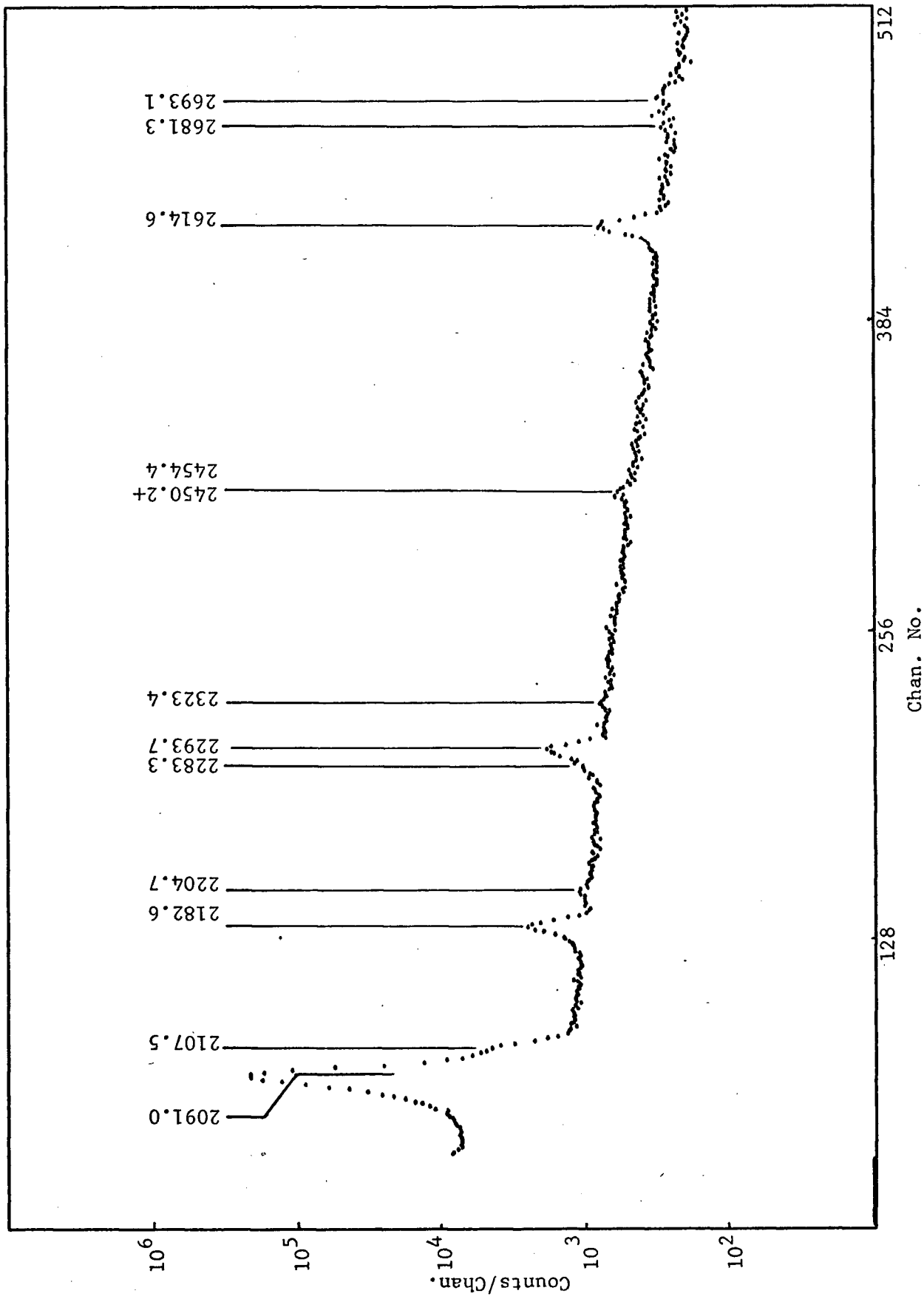

was taken with the 30 cc. Ge(Li) detector and therefore the peaks are much wider than those in figure III-7.

Chapter IV

Gamma-Gamma Coincidence Measurements

IV-1 Experimental Arrangement

The gamma-gamma coincidence spectra were taken using the coincidence arrangement shown in figure IV-1. This type of coincidence arrangement is called fast-slow coincidence.

The fast coincidence is performed on the fast negative logic pulses obtained from each detector using the constant-fraction timing discriminators (C.F.T.D.). These logic pulses are used as start and stop pulses for a time-to-amplitude converter (TAC). The TAC output produces an output pulse whose voltage is proportional to the time difference between the start and stop pulses. The time spectrum of the TAC will contain a peak situated on a flat background, as shown in figure IV-2. The peak represents coincidence events between the two detectors and the background represents random events.

The slow coincidence is performed on the outputs of the three single channel analysers (SCA). SCA#1 was set on a single peak in the energy spectrum obtained from detector #1, commonly called the gate detector. SCA#2 was set on the coincidence peak in the time spectrum produced by the TAC. SCA#3 was set to accept all pulses from detector #2 above a given lower level. This lower level discrimination is required to reject pulses that are too small to give a proper fast logic pulse from CFTD#2.[39] The three coincidence output was used to gate the amplified output of detector #2, commonly called the analog detector.

The gated spectrum from detector #2 will contain the peaks resulting from gamma transitions that are in coincidence with the gamma transition

Figure IV-1

Electronic Arrangement used for Coincidence Measurements

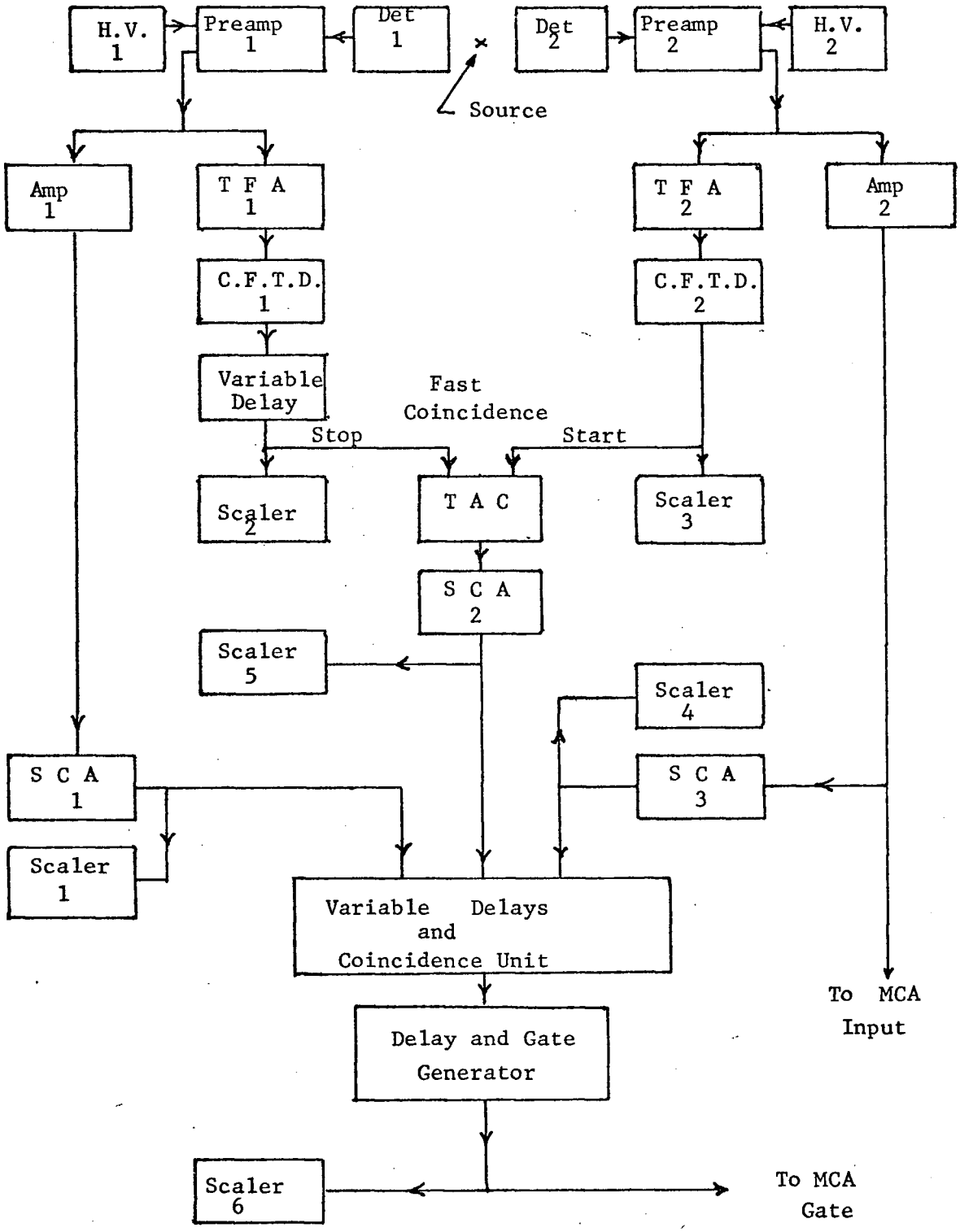

Table IV-1

Description of the Electronics used for the Coincidence Measurements

Detector#1: A 7cc. planer Ge(Li) detector frabricated by P.Taminga at the University of B.C.

Detector#2: A 30 trapezodal Ge(Li) detector obtained from Nuclear Diodes.

Preamp#1&2: Tennelec 125 FET preamplifiers

TFA#1&2 : Ortec 454 Timing Filter Amplifiers

CFTD#1&2 : Ortec 453 Constant-Fraction Timing Discriminators

Variable delay: Coaxial Cable

TAC :Ortec 437A Time-to-Amplitude Converter

SCA#1,2&3 :Ortec 420A Single Channel Analysers

Amp#1 : Tennelec Active Filter Amplifier

Amp#2 : Tennelec 203BLR Active Filter Amplifier with Baseline Restoration

Variable Delays : Nuclear Chicago 27351 Coincidence Unit &Coin. Unit

Delay and Gate Generator : Ortec 416

Scalers :Tennelec 562; Only 2 scalers were available. The scalers 1-6 are points in the curcuit where the count rates were monitored.

MCA :Either; Nuclear Diodes 110 (128Chan)
Nuclear Diodes 160 (1024Chan)
Northern Scientific 600 (512Chan)
The best MCA available at any time was used.

Fig IV-2

Typical output of the TAC.

Illustrating the coincidence and random gates

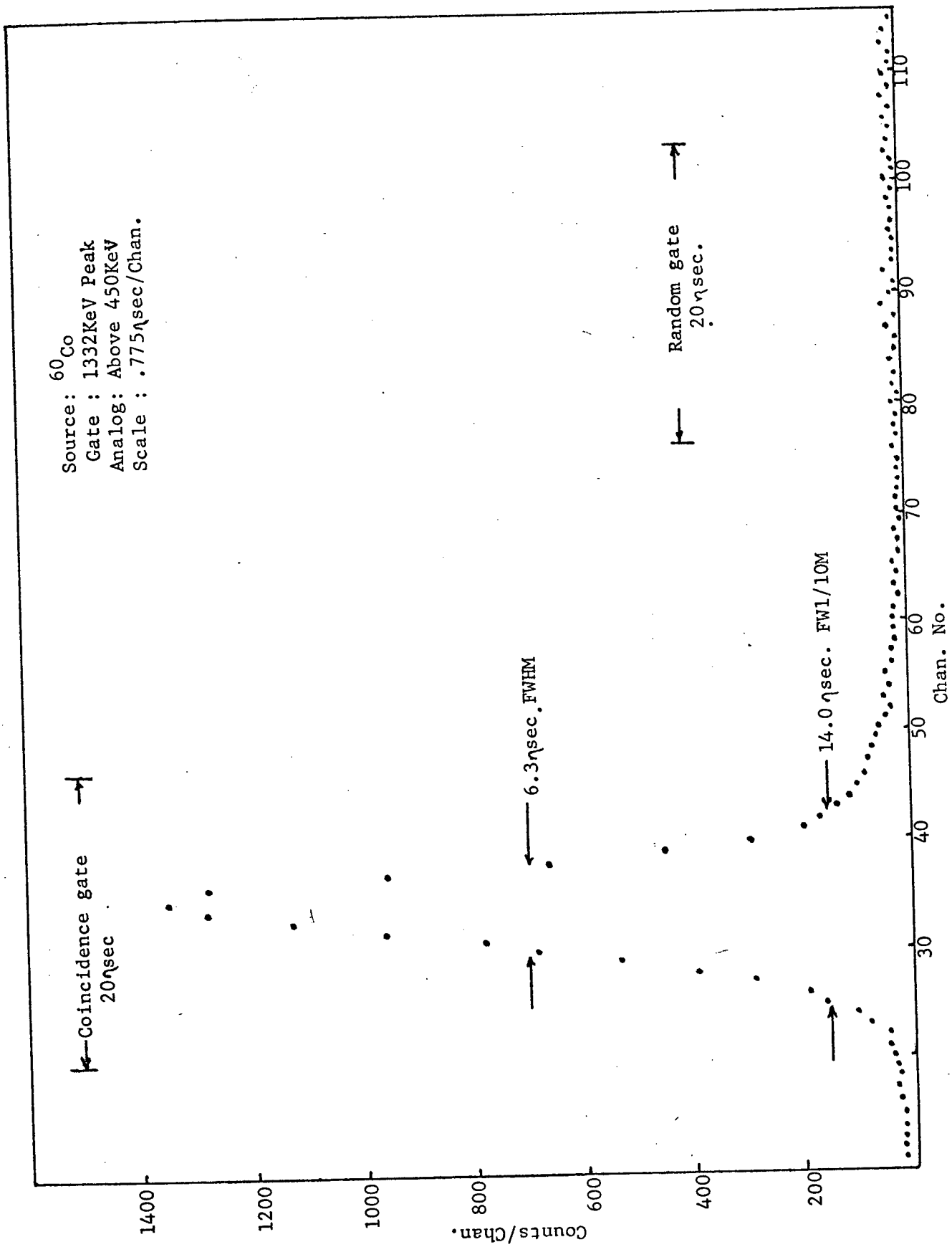

selected with the gate detector. It will also contain events that are in coincidence with the background under the gate peak and random coincidence events.

IV-2 Random Coincidences

The rate of random coincidences in the output of the TAC can be found from the usual formula,[37]

$$N_R^f = 2\tau N_2 N_3 \qquad \text{IV-1}$$

where N_3 is the start rate, N_2 the stop rate, N_R^f the fast random rate and 2τ the width of the gate set on SCA#2. Not all of these random coincidences will meet the energy requirements set by SCA#1 and SCA#3. The random rate in the actual gate pulses will therefore be reduced by the factors N_1/N_2 and N_4/N_3, where N_1 and N_4 are the count rates measured by scalers 1 and 4 respectively. The random rate for the coincidence spectrum is therefore just

$$N_R^S = 2\tau N_1 N_4 \qquad \text{IV-2}$$

where N_R^S is the slow random rate. The validity of these equations was checked using a ^{60}Co source. A gate corresponding to $2\tau = 20 \pm .1$ nsec. was set on the level background of the output of the TAC. The gate detector SCA was set on the 1332 KeV peak of the ^{60}Co spectrum[40] and the analog SCA was set to accept all pulses above 500 KeV. The measured results were

$$N_1 = 5.30 \times 10^2 \text{ counts/sec.}$$

$$N_2 = 6.82 \times 10^3 \text{ counts/sec.}$$

$$N_3 = 3.12 \times 10^4 \text{ counts/sec.}$$

$$N_4 = 2.08 \times 10^4 \text{ counts/sec.}$$

$$N_R^f = 4.2 \pm .1 \text{ counts/sec.}$$

$N_R^s = (2.3 \pm .5) \times 10^{-2}$ counts/sec.

The calculated results were, $N_R^f = 4.25 \pm .01$ counts/sec., and $N_R^s = (2.2 \pm .1) \times 10^{-2}$ counts/sec., both in agreement with the measured values.

A ^{22}Na source was substituted for the ^{60}Co source and the measured random rates again were found to agree with the calculated ones. In addition, a coincidence spectrum was taken with the gate set on the 1275 KeV peak. The resulting single and coincidence spectra are shown in figure IV-3. The singles spectrum has a peak corresponding to the 511 KeV positron annihilation radiation and a peak corresponding to the 1275 KeV gamma transition[40] that follows the positron decay of ^{22}Na to the excited state of ^{22}Ne. The coincidence spectrum contains only the 511 KeV peak except for a small peak at 1275 KeV due to random coincidences. The expected number of counts in this random peak was calculated by replacing N_4 in equation IV-2 by the count rate for this peak obtained from the singles spectrum. The calculated and measured random rates were again in good agreement. i.e.

N_1 = Gate Rate = 340/sec.

N_4 = 1274 KeV peak rate = 1.1×10^5/hr.

$2\tau = 20$ n sec.

Expected random rate = 1.5/hr.

Measured random rate = 13 ± 4 / 10 hrs.

Random rates were calculated in this way for every coincidence spectrum taken, and the contribution to peak intensities, if appreciable, subtracted.

IV-3 Corrections to Coincidence Spectra for Background Events

The contribution to a coincidence spectrum from the background under

Fig. IV-3

^{22}Na spectra

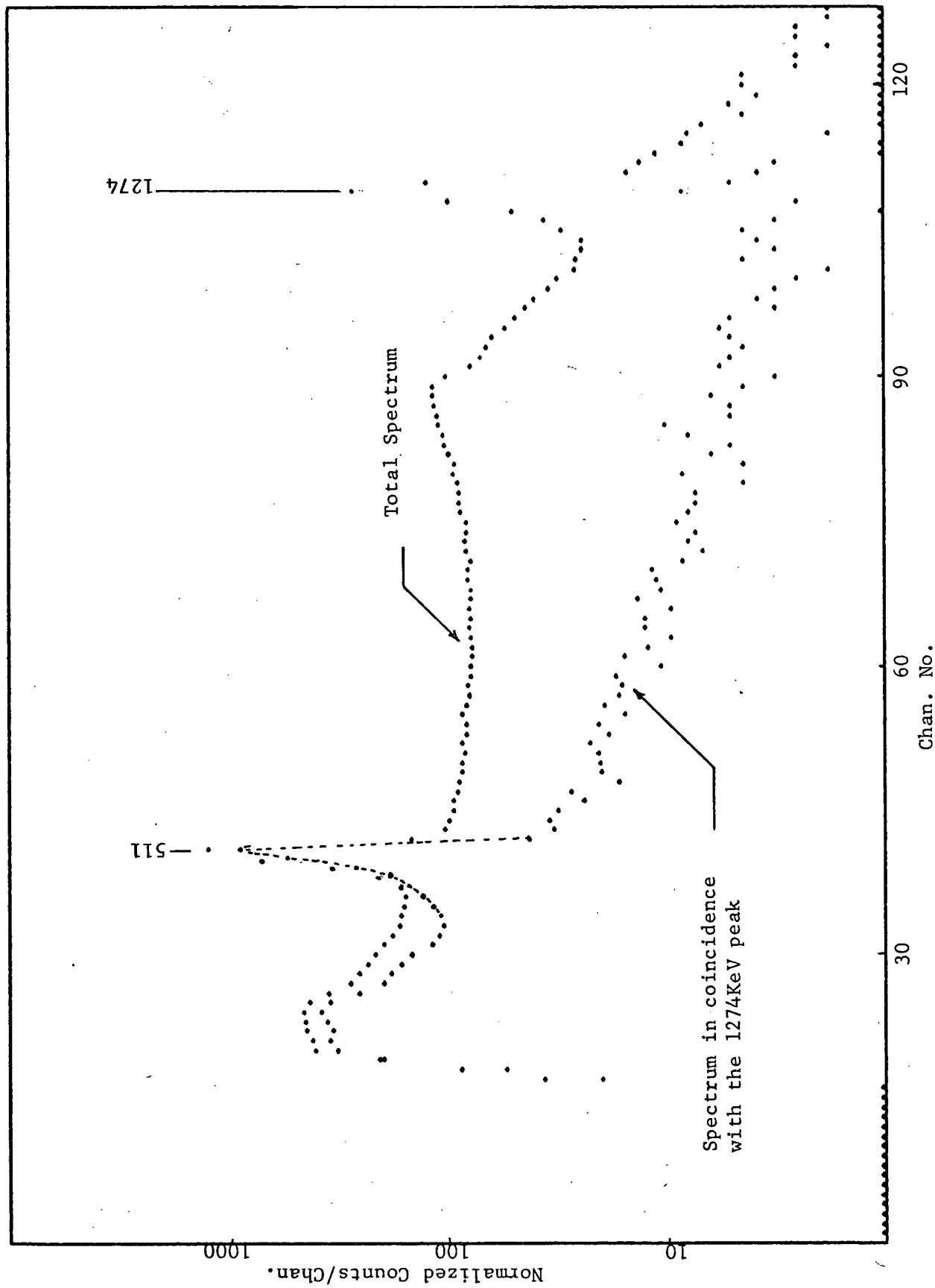

the gate peak can be found by taking on-peak and off-peak coincidence spectra. Typical on-peak and off-peak gates are shown in figure IV-4 The peak areas in the off-peak coincidence spectra must be corrected for any difference in accumulation time from the on-peak spectrum, for the difference in height of the background, and for the difference in source intensity if the half-life of the source is not large compared to the accumulation time. The difference in random coincidence rates, if appreciable, must also be taken into account.

Suppose that the gate peak shown in figure IV-4 was due to transition 1 in the general decay scheme

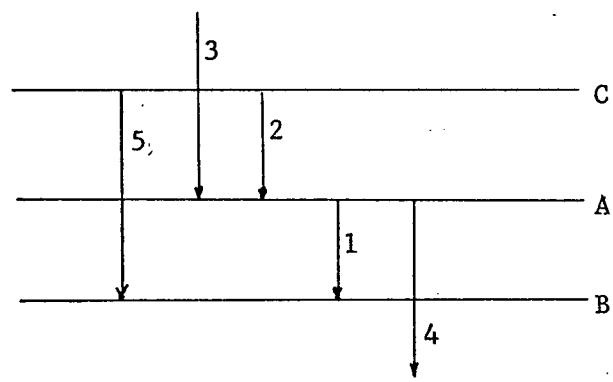

Then the gate would contain pulses due to transition 1 plus the background resulting from transitions 2, 3, 4 and 5.

The rate of coincidences detected between the on-peak gate and transition 2 would be

$$N^{on}_{1\text{-}2}(t) = \epsilon_1\epsilon_2 f_A^2 b_A^1 I_A(t) + N_B(t)K_2 \qquad \text{IV-3}$$

The first term represents the coincidence rate for transitions 1 and 2, and the second the coincidence rate for the background and 2. ϵ_1 and ϵ_2 are the

Fig.IV-4

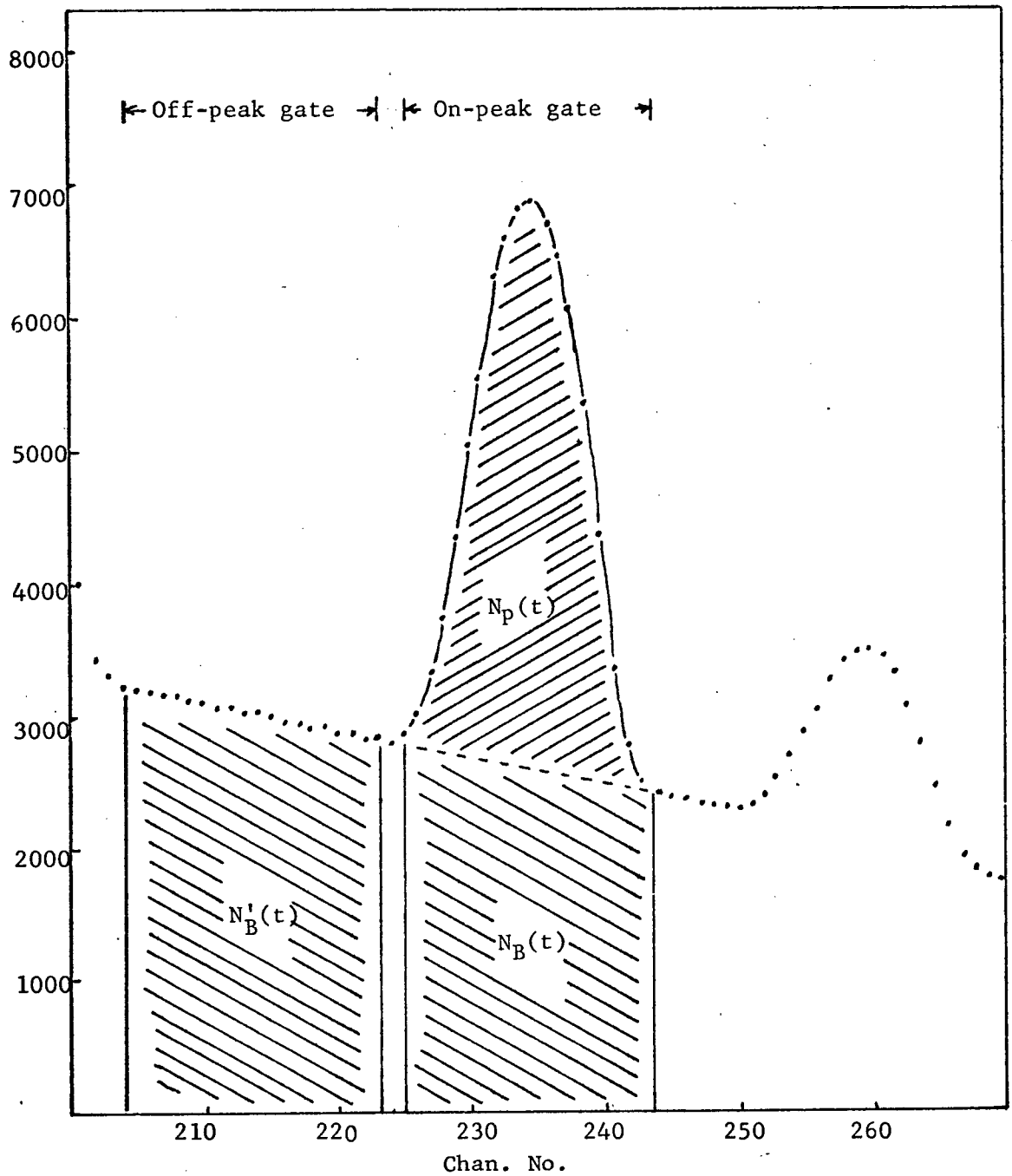

Typical on-peak and off-peak gates. The peak in this figure is the 646KeV peak in the spectrum of ^{124}Sb

efficiencies (intrinsic and solid angle) for gamma 1 in the gate detector and gamma 2 in the analog detector respectively. $f_A^2 = I_2/I_A$ is called the feeding ratio, and is the relative probability that level A is populated by transition 2. $b_A^1 = I_1/I_A$ is called the branching ratio and is the relative probability that level A decays via transition 1. $I_A(t)$ is the rate at which level A is populated, which of course decreases with time by the factor $e^{-t/\tau}$, where τ is the lifetime of the source. $N_B(t)$ is the background rate under the peak which also decreases as $e^{-t/\tau}$. K_2 is a constant.

The rate of coincidences between the off-peak gate and transition 2 will be

$$N_{1-2}^{off} = N_B'(t)K_2' \qquad \text{IV-4}$$

If the on-peak coincidence spectrum is allowed to accumulate from times t_o to t_1 and the off-peak from t_2 to t_3, the number of counts in the peak due to transition 2 will be

On-peak

$$C_{on} = \int_{t_o}^{t_1} N_{1-2}^{on}(t)dt \qquad \text{IV-5}$$

$$= \tau[\epsilon_1\epsilon_2 f_A^2 b_A^1 I_A(o) + N_B(o)K_2](e^{-to/\tau} - e^{-t_1/\tau})$$

Off-peak

$$C_{off} = \int_{t_2}^{t_3} N_B'(t)dt = \tau K_2' N_B'(o)\ (e^{-t_2/\tau} - e^{-t_3/\tau}) \qquad \text{IV-6}$$

The number of true coincidences between transition 1 and 2 will be

$$C^{true} = C_{on} - \frac{K_2\ N_B(o)}{K_2'\ N_B'(o)}\ X\ T(t)C_{off} \qquad \text{IV-7}$$

with $T(t) = (e^{-t_o/\tau} - e^{-t_1/\tau}) / (e^{-t_2/\tau} - e^{-t_3/\tau})$

putting $t_1 - t_o = t_3 - t_o - \Delta t = t_R$

and $t_2 - t_o = t_D$, and if $\Delta t \ll \tau$ and $t_R^2 \ll \tau^2$, then

$$T(t) = e^{t_D/\tau} \frac{t_R}{t_R + \Delta t} \qquad \text{IV-8}$$

The ratio N_B/N'_B can be estimated from the shape of the gate detector spectrum in the region of the gate peak. The ratio K_2/K'_2 is unity if the backgrounds for the on-peak and off-peaks have exactly the same origins. This will only be true if no Compton scattering events from a higher energy transition contribute to one gate but not the other.

IV-4 Coincidence Gamma Spectra of ^{124}Sb

Gamma coincidence measurements of the nucleus ^{124}Sb were taken with three different gates. They were the 603 and 646 KeV transitions, and the energy region 700 - 730 KeV, which contains the 709, 714 and 723 KeV transitions. On-peak and off-peak spectra were taken for all three gates. After analysing these spectra it was felt that no more information could be obtained with the equipment used by selecting other gates.

The coincidence spectra for the 603 KeV gate were taken in three parts. The energy regions 100 - 750 KeV and 700 - 1700 KeV were analysed with the 512 channel MCA. The energy region 1600 - 2750 KeV was analysed with the 1024 channel analyser. The on-peak and off-peak spectra for the first two regions are shown in figure IV-5(a) and (b) respectively. A portion of the on-peak spectrum of the high energy region is shown in figure IV-5(c). The portion of the spectrum above 2120 KeV did not contain any peaks and is therefore not shown.

The on-peak coincidence spectra for the 646 and 700 - 730 KeV gates are shown in figure IV-6 and IV-7 respectively. The high energy regions of each spectrum that did not contain any peaks is again omitted. These spectra were analysed with the 1024 channel MCA.

The area of the peaks in the on-peak and off-peak spectra for each gate were found and the number of true coincidences calculated using equation IV-7. The data used for these calculations and the results are tabulated in table IV 2(a-e).

The true coincidence results can be categorized in the following way. Consider the decay scheme

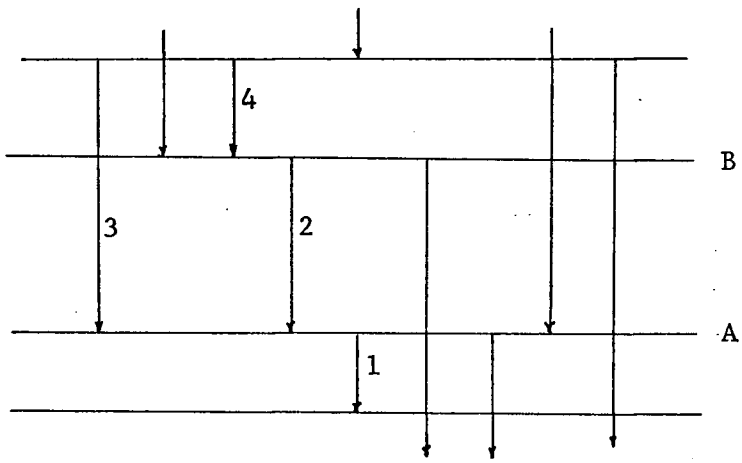

If the gate is set on transition 1, the number of detected true coincidences for transitions 2, 3 and 4 will be

$$C_{1\text{-}2} = \epsilon_1 \epsilon_2 f_A^2 b_A^1 I_A$$

$$C_{1\text{-}3} = \epsilon_1 \epsilon_3 f_A^3 b_A^1 I_A$$

$$C_{1\text{-}4} = \epsilon_1 \epsilon_4 f_A^2 b_A^1 f_B^4 b_B^2 I_A$$

Other coincidence rates can be written in a similar manner. Using the

Fig.IV-5(a)

Low energy region of ^{124}Sb gamma spectrum in coincidence with the 603KeV transition.

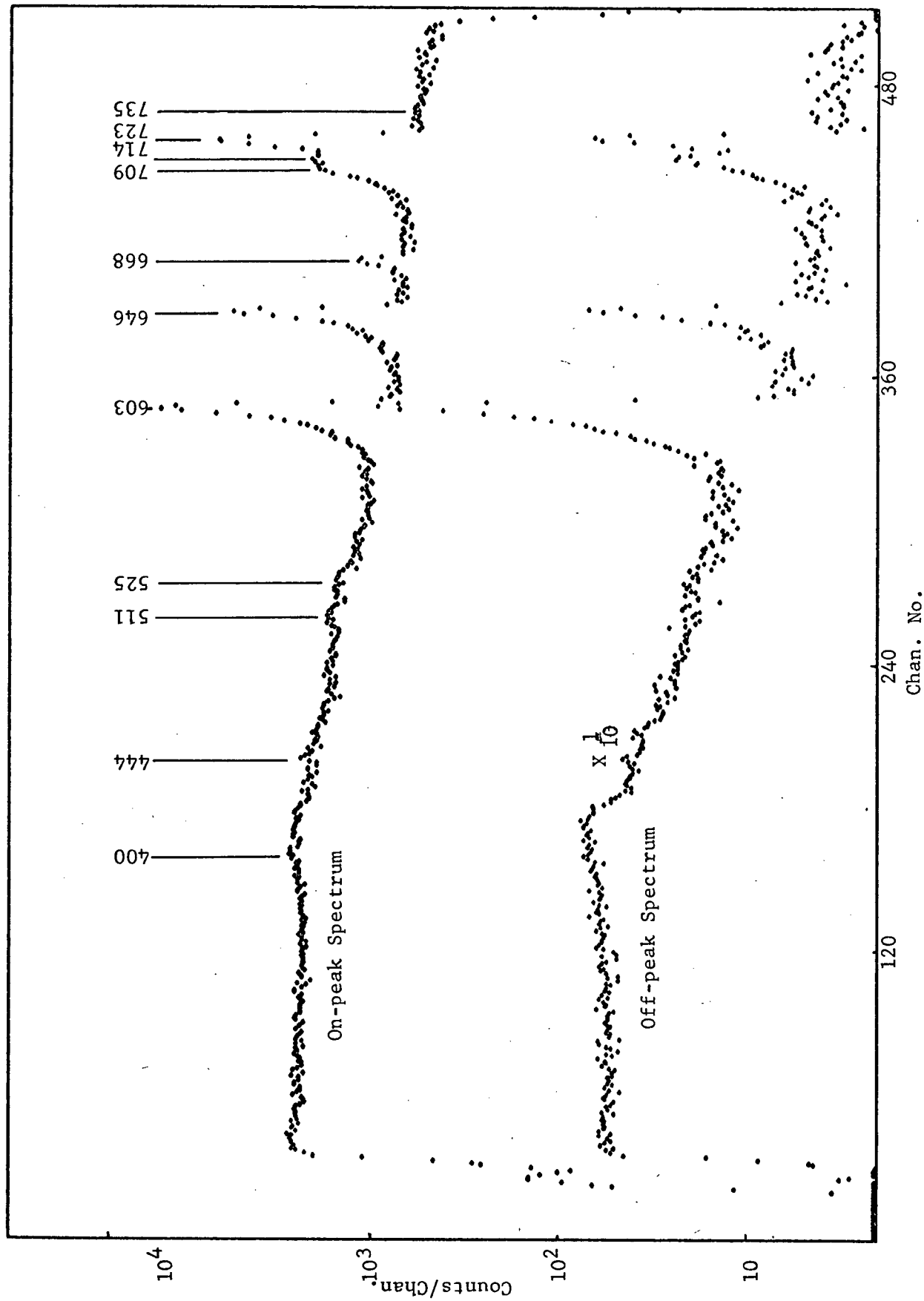

Fig.IV-5(b)

Medium energy region of the ^{124}Sb spectrum in coincidence with the 603Kev transition

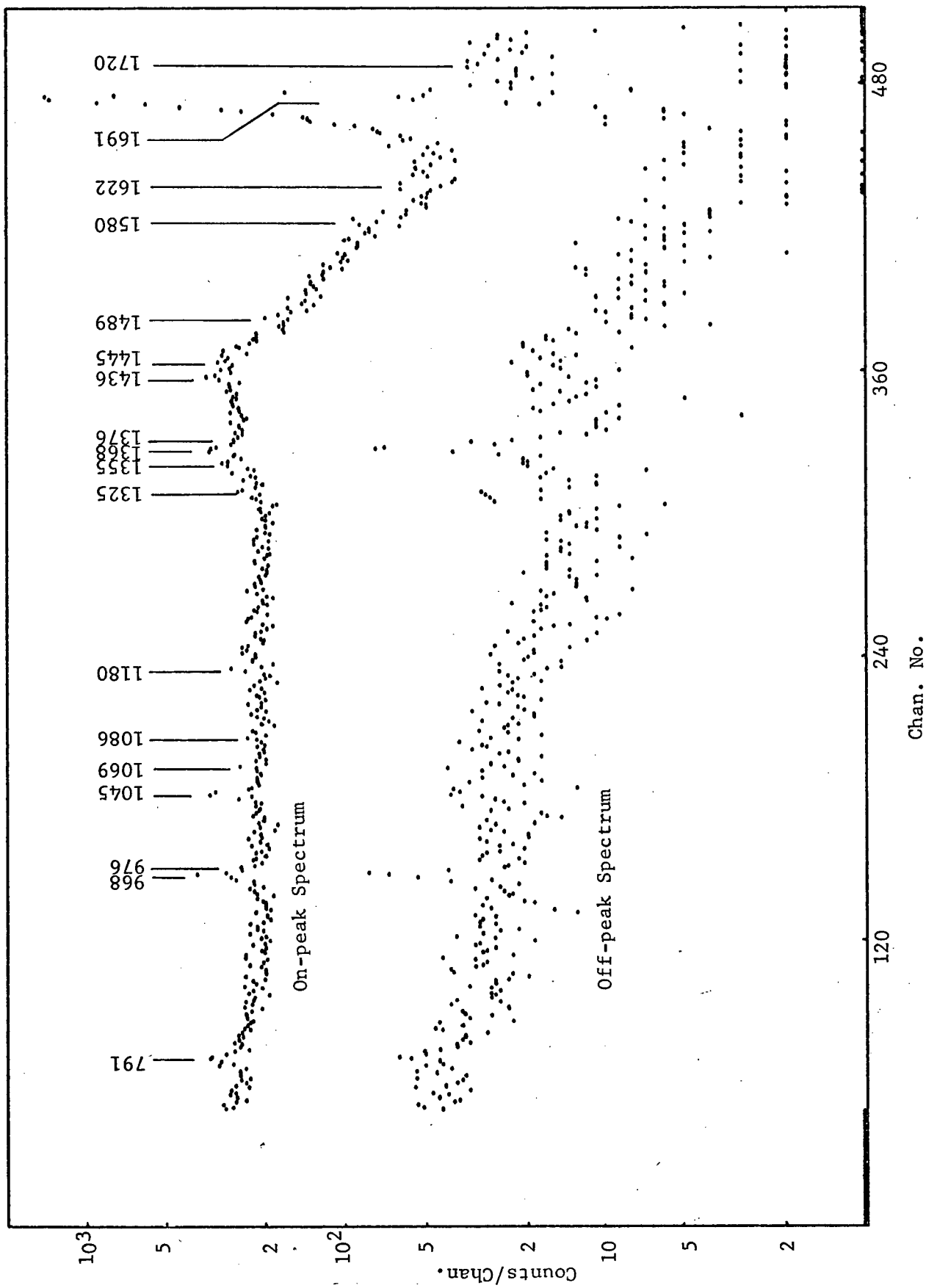

Fig.IV-5(c)

High energy region of ^{124}Sb in coincidence with the 603KeV transition.

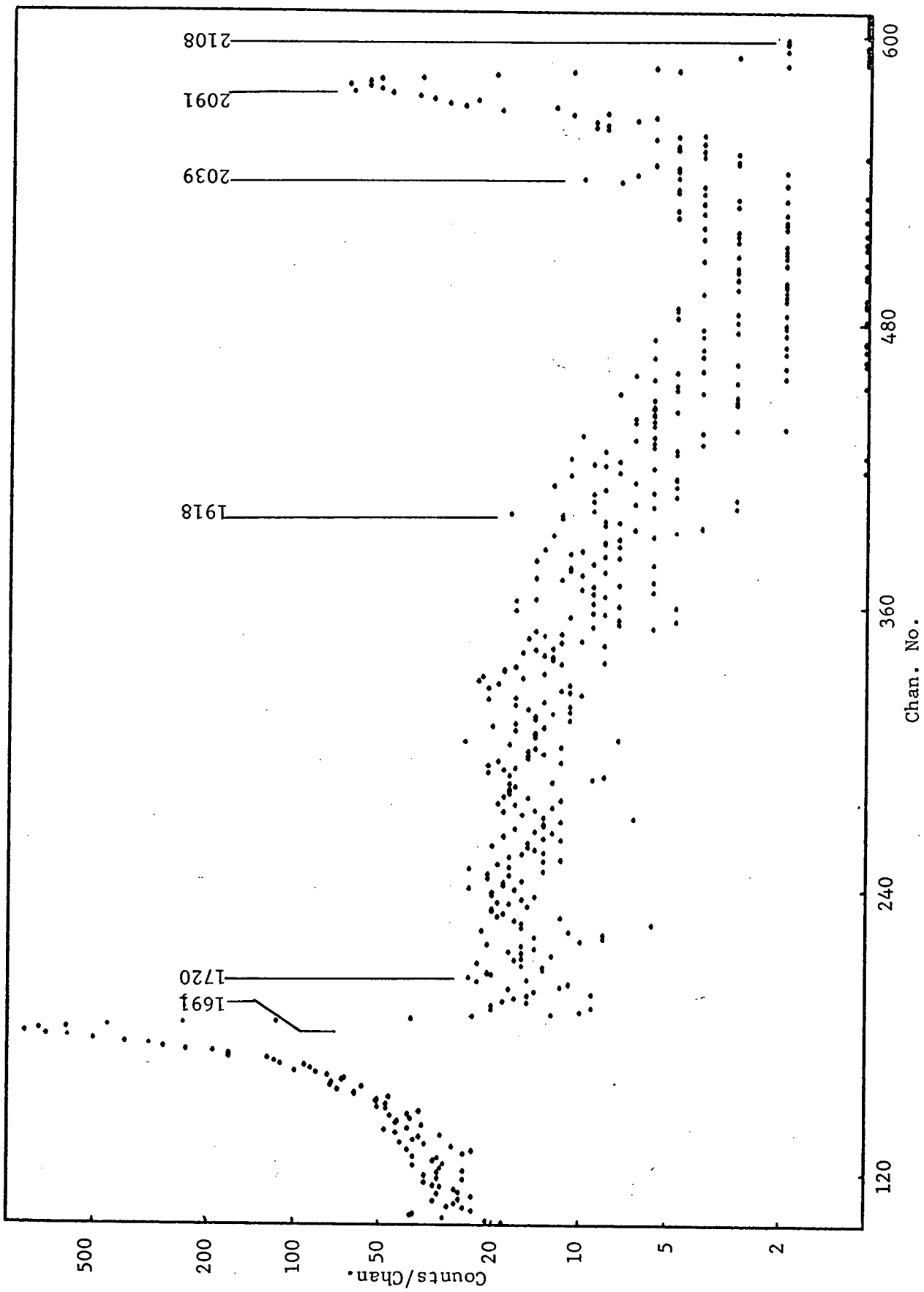

Fig. IV-6(a)

Low energy portion of the 646KeV on-peak coincidence spectrum

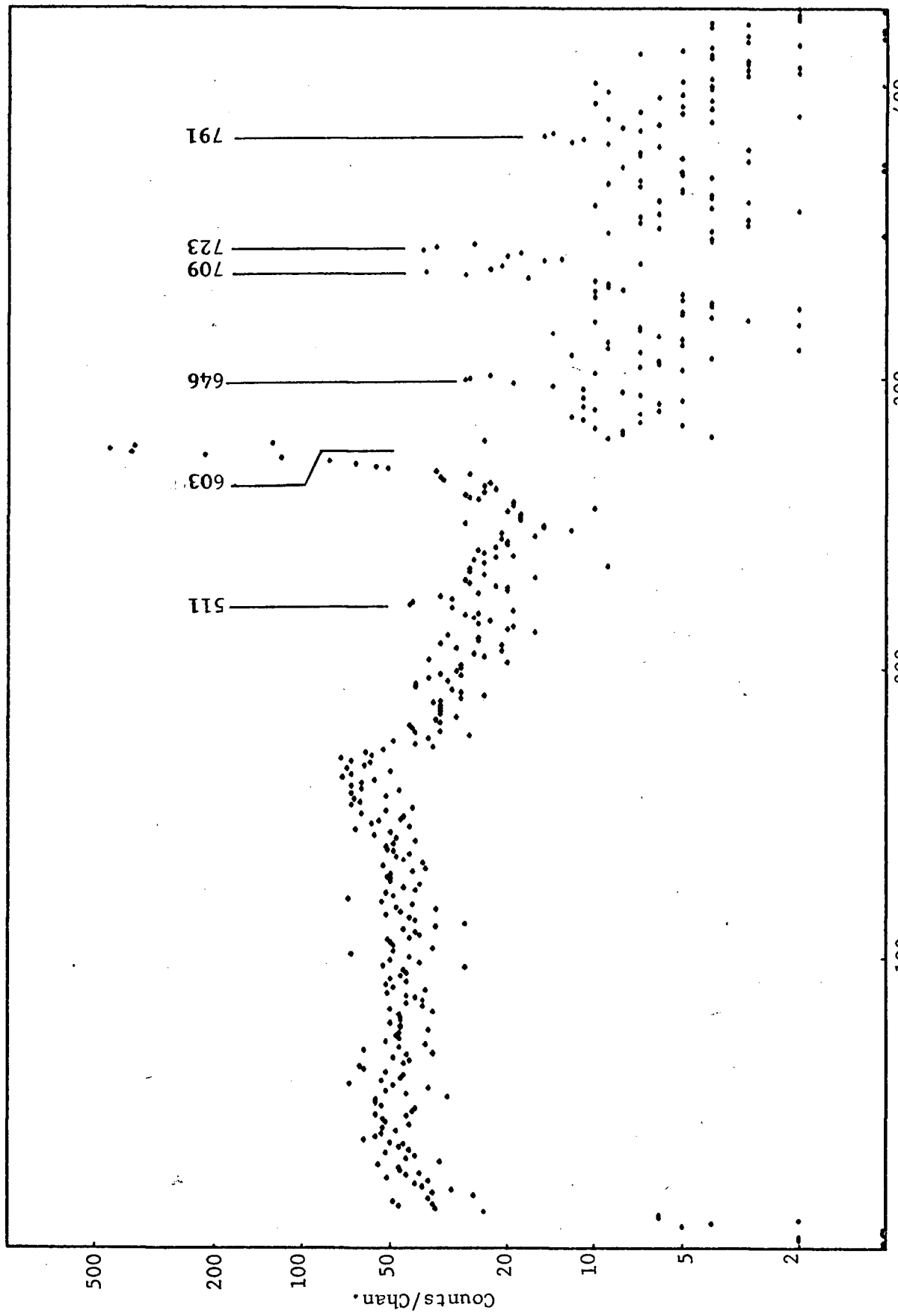

Fig. IV-6(b)

High energy portion of the 646KeV on-peak coincidence spectrum.

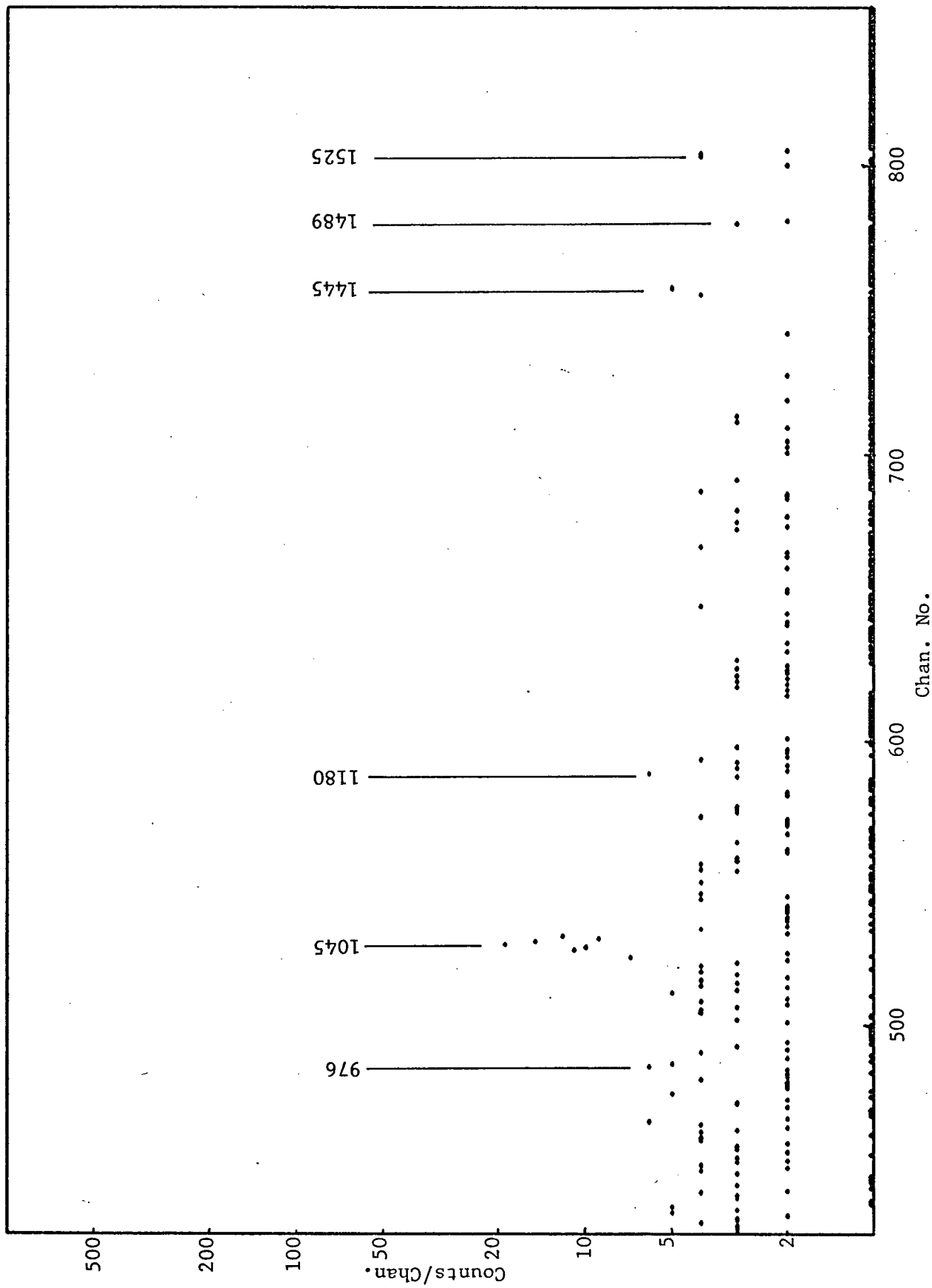

Fig. IV-7(a)

Low energy portion of the 700-730KeV on-peak coincidence spectrum

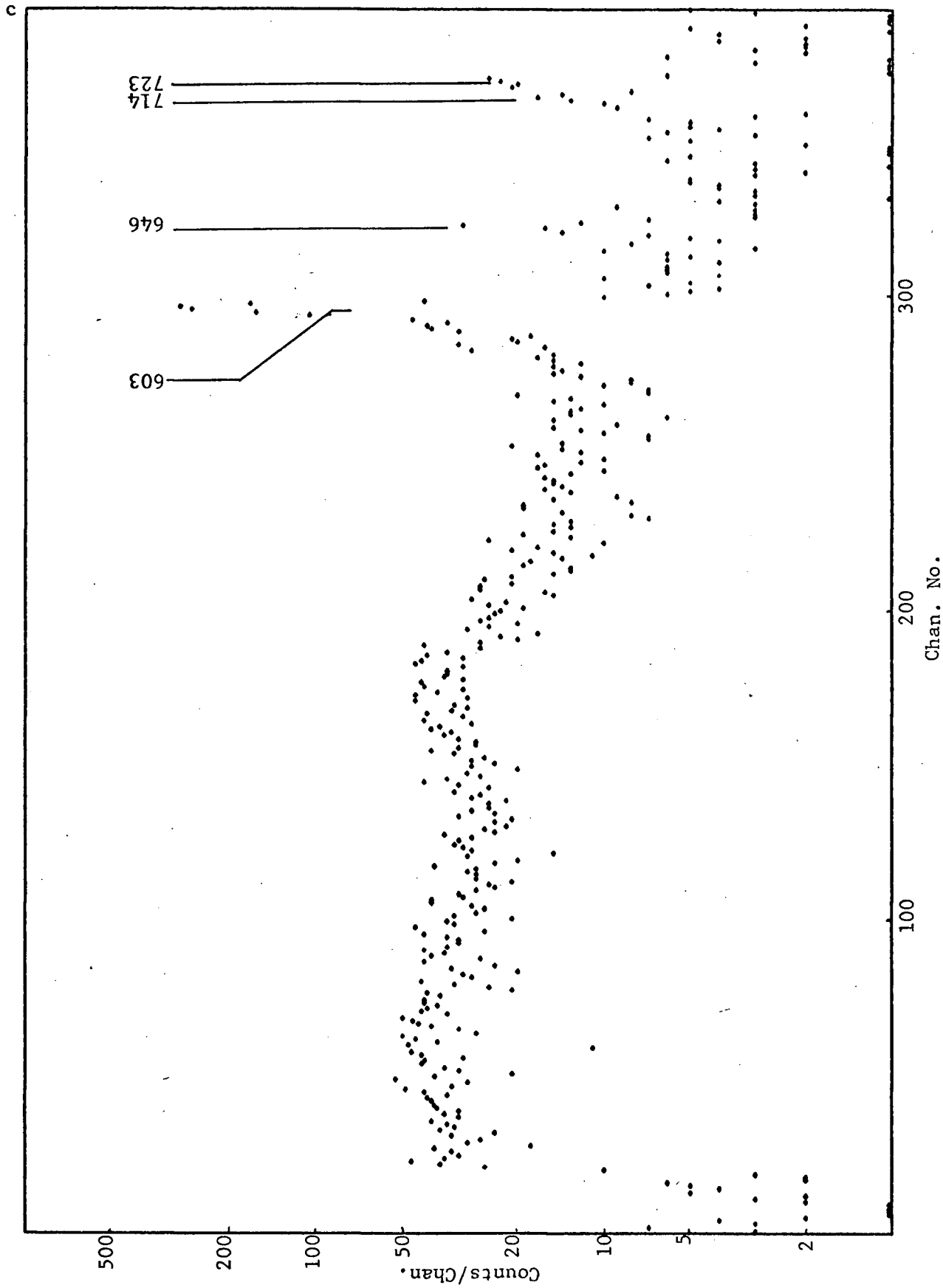

Fig. IV-7(b)

High energy portion of the 700-730KeV on-peak coincidence spectrum

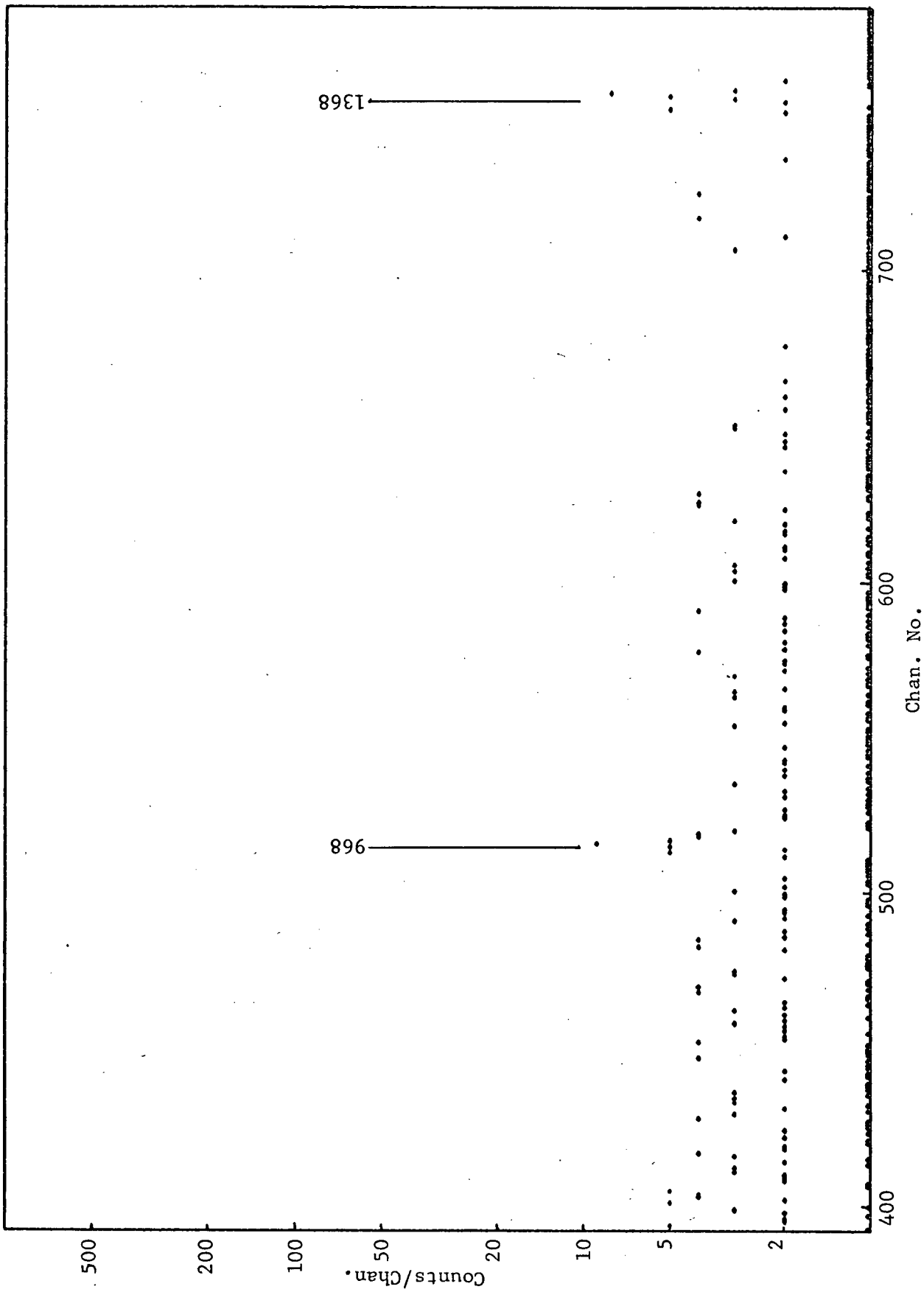

Table IV-2(a)

Energy region 100-750KeV in coincidence with 603KeV transition

$t_R=2X10^5$sec. $t_D=2.01X10^5$sec. $\Delta t=0$ $N_B/N'_B=.76$

Peak Energy(KeV)	C_{on}	C_{off}	C_{true}
400	170	30	135±100
440	180	20	165±100
525	200	20	180±100
603	24700	27900	-400±1000
646	11000	2700	8400±300
668	1150	24	1130±50
709	2800	800	2200±500
714	2600	100	2500±500
723	12900	2400	11000±700
735	25	-	25±20

TableIV-2(b)

Energy region 700-1700KeV in coincidence with 603KeV transition

$t_R=2X10^5$sec. $t_D=2.01X10^5$sec. $\Delta t=0$ $N_B/N'_B=.76$

791	280	60	230±50
968	400	140	290±50
1045	350	40	320±30
1086	40	15	28±20
1325	80	90	10±20
1355	210	15	200±30
1368	350	200	200±100
1376	40	-	40±30
1436	190	25	170±40

Table IV-2(b) (cont.)

Energy(KeV)	C_{on}	C_{off}	C_{true}
1445	22	15	10±20
1489	40	-	40±30
1526	46	-	46±30
1580	38	-	38±30
1622	30	-	30±25
1691	6730	230	6550±100

Table IV-2(c)

Energy region 1500-2700KeV in coincidence with 603KeV transition

t_R=117hrs t_d=120hrs Δt=+5hrs N_B/N_B'=.76

1720	5	-	5±4
1918	5	-	5±4
2039	16	-	16±10
2091	740	20	725±100
2108	5	-	5±4

Table IV-2(d)

Energy region 100-2000KeV in coincidence with 646KeV transition

t_R=116hrs t_D= 504hrs Δt= 46hrs N_B/N_B'=.9

603	3300	200	3100±200
646	45	40	5±15
709	65	25	40±20
723	80	70	10±20
791	20	-	20±10
976	4	-	4±3
1045	62	20	40±15
1180	3	2	1±2
1445	11	3	8±4
1489	3	2	1±2
1525	10	2	8±4

Table IV-2(e)

Energy region 100-2000KeV in coincidence with 700-730KeV gate

t_R=167hrs t_D=120hrs Δt=1hr N_B/N'_B=.9

Energy(KeV)	C_{on}	C_{off}	C_{true}
603	4600	400	4200±500
646	35	15	20±10
714+723	120	20	100±15
968	14	2	12±4
1368	15	5	10±4

definition of f and b one can write

$$\frac{C_{1-2}}{C_{1-3}} = \frac{\epsilon_2}{\epsilon_3} \times \frac{I_2}{I_3}$$

$$\frac{C_{1-2}}{C_{1-4}} = \frac{\epsilon_2}{\epsilon_4} \times \frac{I_2}{I_4 f_B^4 b_B^2}$$

where the I's are the total intensities found from the singles spectrum. Now, if the true coincidence results are normalized such that

$$\frac{C_{1-2}}{\epsilon_2} = I_2$$

where transitions 1 and 2 are known to be in coincidence, then, if for a general transition k

$$\frac{C_{1-k}}{\epsilon_k} = I_k, \text{ transitions 1 and k are in total coincidence.}$$

If

$$0 < \frac{C_{1-k}}{\epsilon_k} < I_k \quad \text{then transition 1 and k are in partial}$$

coincidence. Knowledge of whether two transitions are directly, or indirectly, in coincidence is often useful in deducing the decay scheme of the isotope being studied. It should be noted that if the levels have an appreciable probability of decaying by the electron conversion process, then these transitions must be taken into account in the feeding and branching ratios.

The true coincidence data for the 603 and 646 KeV gates were normalized and compared to the singles data. The 1691 KeV transition was used to

normalize the 603 KeV gate data. The comparison of the singles and coincidence intensities is given in table IV-3. The 603 KeV transition was used to normalize the 646 KeV gata data; the comparisons are given in table IV-4. In these tables, a cross (x) under the coincidence column means that that transition is judged to be in either total or partial coincidence. A question mark is used when there is some doubt about the correct assignment.

The coincidence data for the 700-730 KeV gate were not analysed in the above manner as the three transitions in this gate make exact analysis impossible. The transitions found to be in coincidence with this gate are the 602, 646, 714, 723, 968 and 1368 KeV transitions.

Table IV-3

Transitions in coincidence with 603KeV transition

Energy(KeV)	Normalized Coin. Data	Error %	Singles Intensity	Coincidence Total	Coincidence Partial
400	900	60	1300		x
440	1000	60	1690		x
525	1200	60	1300	x	
646	69300	13	74000	x	
709	14000	20	13600	x	
714	16000	20	23900		x
723	105000	5	109700	x	
735	750	80	1400	?	x
791	7500	40	7500	x	
968	11700	20	20000		x
1045	14800	10	18900		x
1086	500	80	300	x	
1355	11600	7	11200	x	
1368	17600	25	27100		x
1376	4000	75	5300	x	?
1436	14000	10	13600	x	
1445	500	100	3800		?
1489	3300	75	6900		x
1526	4000	70	4400	x	?
1580	2800	75	3200	x	?
1622	2000	75	300	x	
1691	$5.04X10^5$		$5.04X10^5$	x	

Table IV-3(cont.)

1720	300	80	935	?	?
1918	320	80	520	?	?
2039	800	60	660	x	?
2091	59500	15	57600	x	
2108	440	80	550	?	?

Table IV-4

Transitions in coincidence with 646KeV transition

Energy(KeV)	Normalized Coin. Data	Error %	Singles Intensity	Coincidence Total	Partial
603	10^6		10^6	x	
709	15000	25	13600	x	
791	8500	50	7500	x	
976	1500	50	1000	x	
1045	24000	35	18900	x	
1445	4500	50	3800	x	
1525	4000	60	4400	x	

Chapter V

Electron Spectra Using Si(Li) Detectors

V-1 Beta Spectra

a) General Considerations

The $\beta^{\pm}$ (electrons (-), positrons (+)) particles emitted in the decay of a nucleus have an energy distribution given by [41]

$$N(W)_{\pm}dW = pW(W_o-W)^2 F(\mp Z,W) S_{th}(p,q) \qquad V\text{-}1$$

$N(W)_{\pm}$ = the number of $\beta^{\pm}$ particles emitted in the energy interval dW

P = electron's momentum

W = electron's total energy = $E + M_oC^2$

W_o = energy difference between initial and final nuclear states, called the end-point energy

$F(\mp Z,W)$ = Fermi function; which corrects the $\beta^{\pm}$ spectrum for the distortion due to the Coulomb interaction with the nucleus.

$S_{th}(p,q)$ = Shape factor. In general, S is a function of the electron's (p) and associated neutrino's (q) momenta. The form of the function depends on the angular momentum (J) and parity (π) changes, or the degree of forbiddenness, involved in the decay under consideration.

Theoretical shape factors have been calculated by Kotani and Ross.[42] For instance, allowed spectra, with $\Delta J=0,1$; $\Delta\pi$ = No, have $S_{th}=1$, while first-forbidden transitions ($\Delta J = 0,1,2$; $\Delta\pi$ = Yes) and second-forbidden transitions

($\Delta J=2,3; \Delta\pi$ = No) have a shape factor of the approximate form,

$$S_{th} = \lambda p^2 + q^2 + C,$$

the values of λ and C varying with the atomic number of the daughter nucleus, and with the order of forbiddenness and total energy of the decay.

A comparison of the experimental shape factor, given by[43]

$$S_{exp} = \frac{N(W)dW}{pW(W_o-W)^2F} \qquad V\text{-}3$$

to different theoretical values will define the forbiddenness of the transition, if the experimental shape of the spectrum, N(W)dW, is known accurately enough. Both S_{exp} and S_{th} depend on W_o, which is not usually known beforehand. However, since W_o appears in both formulae in the form $(W_o - W)^2$, a small error in W_o will not affect the comparison if the comparison is not extended too close to W_o.

Once the shape factor is known, the function

$$\left(\frac{N(W)dW}{pWFS}\right)^{\frac{1}{2}}$$

can be plotted as a function of total energy. This plot, called a Kurie plot,[41] will be a straight line with energy intercept W_o. This value of W_o, if different from the one used in the original calculation of S, can be used to re-calculate S, and a new W_o found from the energy intercept of a Kurie plot. This iterative procedure can be continued until a consistent estimate of W_o is found.

b) Beta Spectra taken with a Si(Li) detector

The Si(Li) detectors used in this investigation have been described in detail elsewhere.[44] They are a 3 mm. planar detector with a .2 micron SiO_2 window and a 5 mm. planar detector with a 2 micron Au window. Both Si(Li) detectors were calibrated for the backscatter fraction, resolution,

and efficiency, as described below.

A beta spectrum taken with a silicon lithium-drifted detector Si(Li) will not have the shape given by equation V-1. Electrons that are scattered into, or out of, the detector and lose only part of their energy in the detector, will distort the spectrum.

The distortion can be corrected for if the spectra of mono-energetic electrons at different energies are taken, and the distribution of scattered electrons found. This distribution varies with the source-detector geometry, source thickness, source backing, etc. It is therefore impossible to measure this distribution using an electron gun, magnetic spectrometer, or any other artificial source for the mono-energetic electrons.

The mono-energetic electrons used in this investigation were the K-conversion electrons emitted in the decays of ^{137}Cs, ^{109}Cd and ^{207}Bi. These sources were deposited on thin (170 $\mu g/cm^2$) aluminum backings using the sublimation technique described in reference 44. This method of source preparation results in very little scattering from the source backing or the source itself. (All electron sources used in this investigation were prepared in this way.)

These sources also emit gamma rays and L, M,... conversion electrons along with the K-conversion electrons. ^{137}Cs also has two β^- groups associated with its decay (see figure V-1). An attempt was made to reduce the background due to these other transitions by only analysing those events in one Si(Li) detector that were in coincidence with the K-X-rays detected in the other Si(Li) detector. (See figure V-2 for the arrangement of the Si(Li)'s detectors. The electronics used for these coincidence measurements are shown in figure IV-1.) Unfortunately, the K-electrons are not the only particles in coincidence with the K-X-rays. In ^{137}Cs,

Fig. V-1

Isotopes used to measure the backscatter fraction

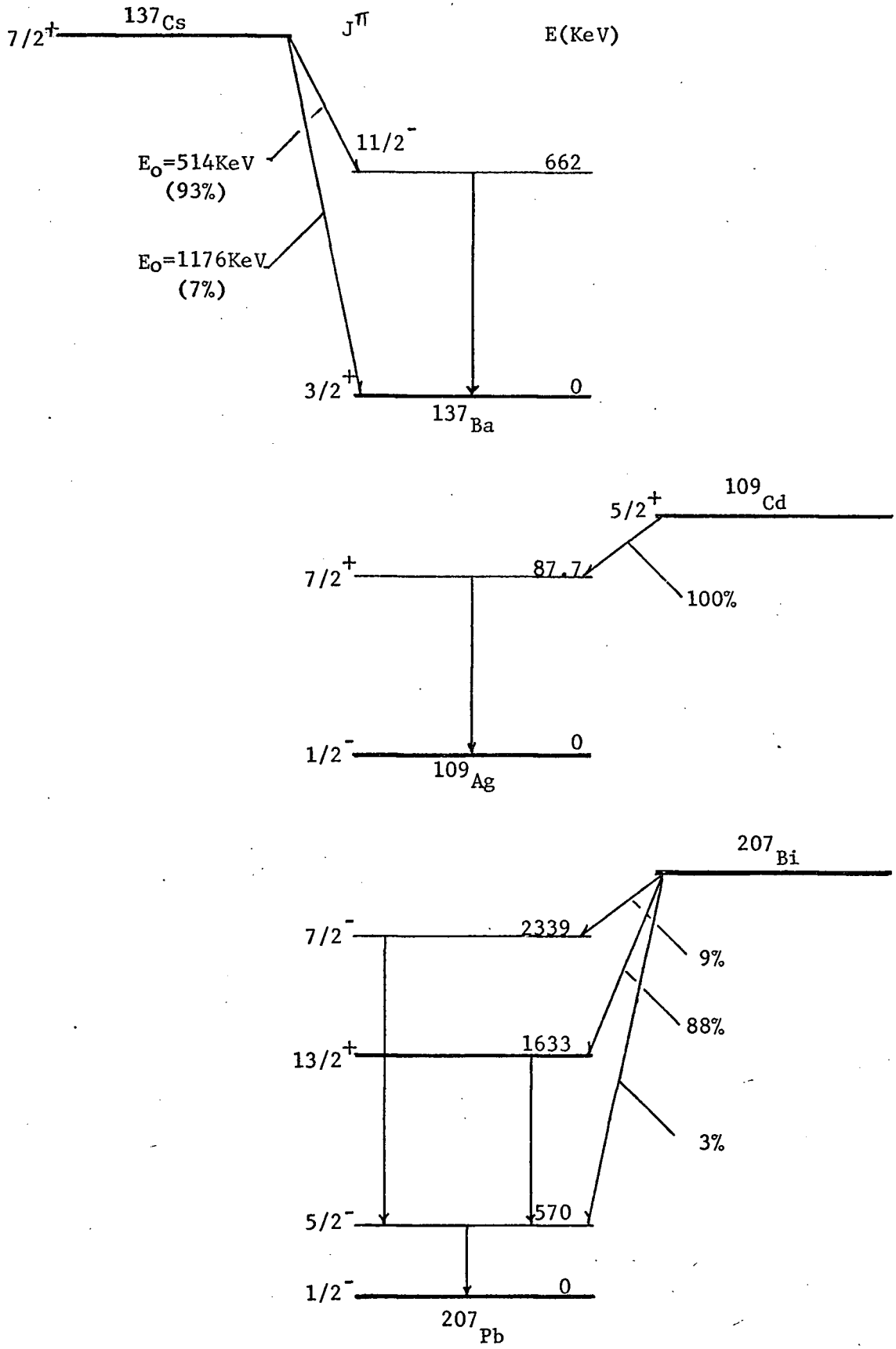

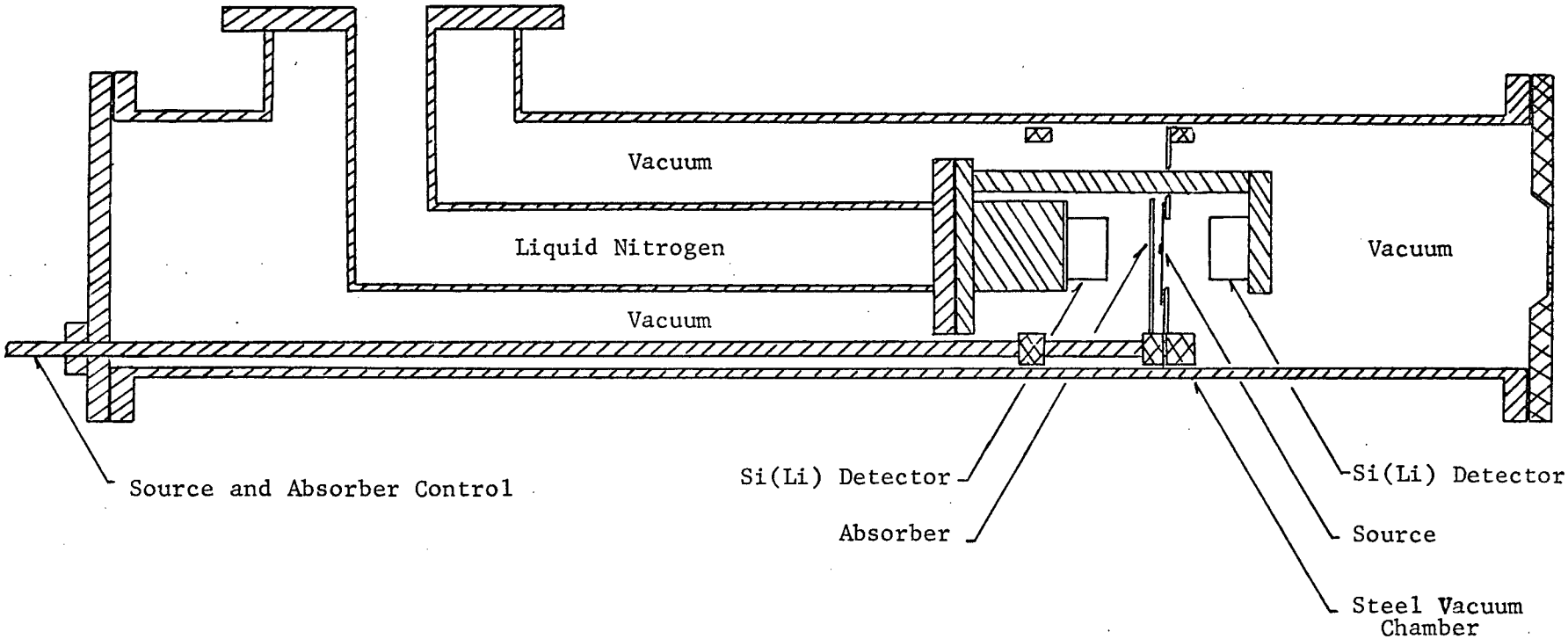

Fig. V-2
Si(Li) Detector Chamber

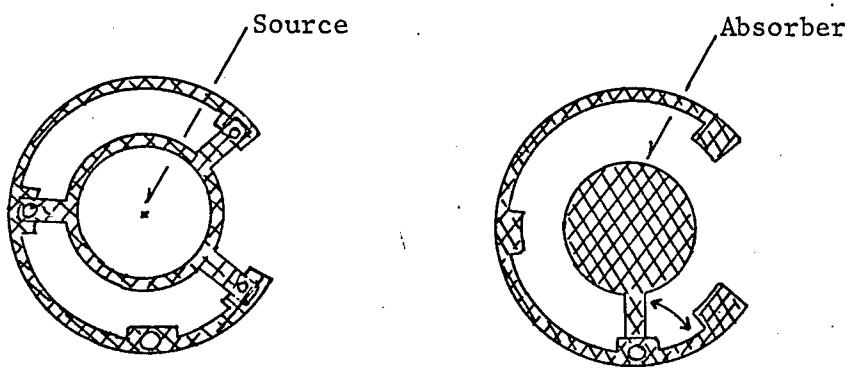

Source and Absorber Arrangement

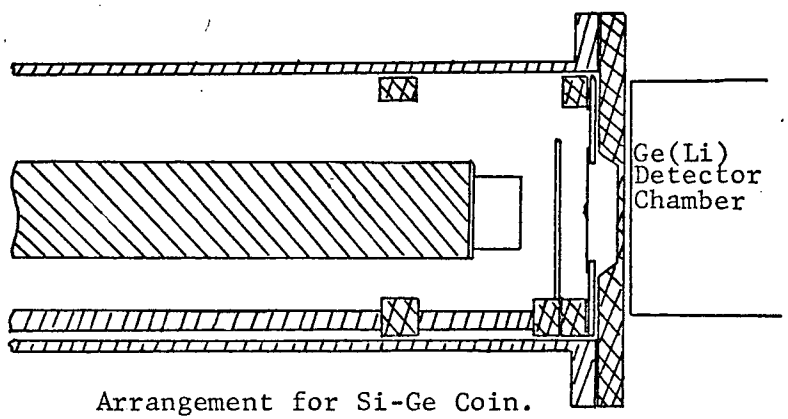

Arrangement for Si-Ge Coin.

the beta transitions populating the 662 KeV level are also in coincidence. In the two electron capture isotopes, ^{109}Cd and ^{207}Bi, the K-X-rays resulting from the electron capture decays, cannot, of course, be distinguished from the K-X-rays following the electron conversion process, and therefore some contribution to the background from the gamma transitions and the L, M,... conversion processes is to be expected. The ^{207}Bi decay has an added complexity in that the X-rays resulting from a K-conversion process for one transition will be in coincidence with the gammas, etc., of the other transitions.

Figure V-3 is the coincidence spectrum for ^{137}Cs. The flat region of the spectrum between the K-conversion peak for the 662 KeV transition and the start of the β^- group with endpoint energy equal to 514 KeV was used to estimate the number of scattered electrons detected. Coincidence spectra of ^{109}Cd and ^{207}Bi were also taken and the number of scattered electrons estimated from the flat portions of those spectra also.

The "backscatter" fraction, defined by

$$f(E) = N_b / N_t,$$

where N_b is the number of scattered electrons detected and N_t the total number detected, was estimated by extrapolating these flat regions to zero energy. The results were

Isotope	E(KeV)	f(E) (3mm. det.)	f(E) (5mm. det.)
^{109}Cd	620	.454	.561
^{137}Cs	624	.521	.634
^{207}Bi	482	.528	.621
^{207}Bi	972	.589	.690

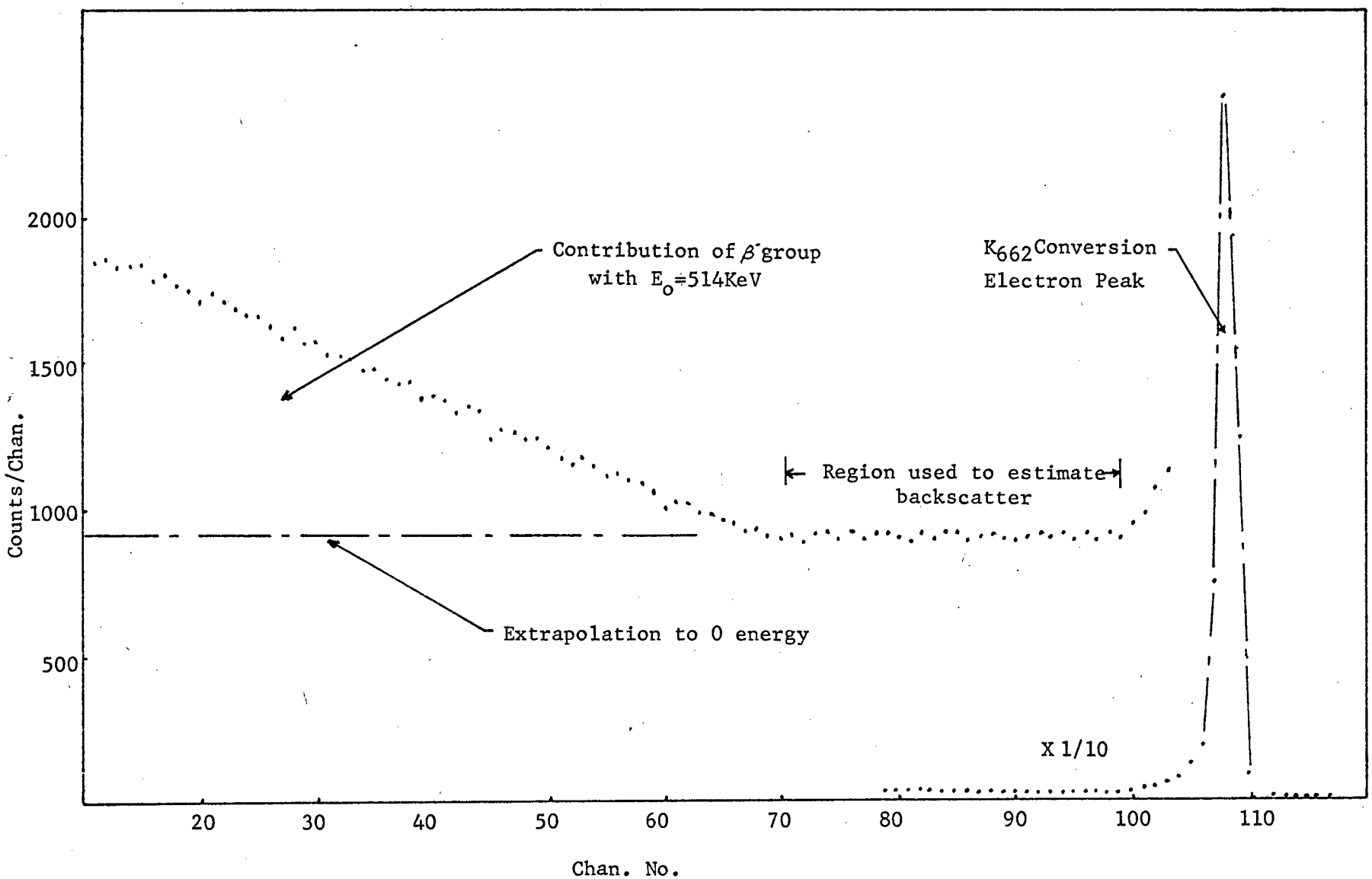
2000
1500
1000
500
Counts/Chan.
Contribution of β⁻ group
with E_o=514KeV
K_{662} Conversion
Electron Peak
← Region used to estimate→
backscatter
Extrapolation to 0 energy
X 1/10
20
30
40
50
60
70
80
90
100
110
Chan. No.

Fig. V-3

The best straight line through these points was

$$f(E) = .0015 \times E(KeV) + .45 \quad \text{(3mm det.)} \qquad \text{V-4}$$

$$f(E) = .0016 \times E(KeV) + .54 \quad \text{(5mm det.)}$$

As well as the correction for scattered electrons, the spectrum must be corrected for the change in the resolution of the system as a function of energy. The efficiency of the detector, if it varies with energy, must also be taken into account.

The relative efficiency for electrons that lose all their energy in the detector was calculated by measuring the intensities of conversion electron transitions in ^{152}Eu. These intensities were compared to those measured with a magnetic spectrometer by Malmsten et al.[45] (See table V-1.) The ratios of the intensities using the 3mm detector are plotted as a function of energy in figure V-4. No variation of efficiency with energy is evident. This result was also found for the 5mm detector.

The resolution of the system as a function of energy was also found from the conversion peaks of ^{152}Eu. The result was

$$\text{for 3mm det.} \quad D(E)\ (FWHM) = (7.2 + .0082\ E(KeV))^{\frac{1}{2}} \qquad \text{V-5}$$

$$\text{for 5mm det.} \quad D(E)\ (FWHM) = (7.9 + .0087\ E(KeV))^{\frac{1}{2}}$$

The correction to a beta spectrum taken with the Si(Li) detector can now be calculated. The correction to be subtracted from the first N-1 channels due to electrons scattering out of the energy region associated with the last (the N^{th}) channel is[46]

$$A_N = \frac{f(E_N)}{1-f(E_N)} \Delta D_N Cc(N) \qquad \text{V-6(a)}$$

where $f(E_N)$ is given by equation V-4

$$\Delta D_N = \frac{D(E_N)\ \Delta E}{D(0)E_N}$$

Table V-1

Relative Intensities of Conversion Electron from ^{152}Eu

Peak Identity	This Work(I_1)	Malmsten[45](I_2)	I_1/I_2 ±%
K-122	34500. ±3%	1570. ±4%	22.0±7%
L-122	17100. ±3%	725. ±10%	23.6±13%
K-244	1140. ±3%	53. ±4%	21.6±7%
L-244	360. ±3%	13.2±12%	27.2±15%
K-344	1370. ±3%	72. ±7%	19.0±10%
L-344	416. ±3%	17.3±12%	24.0±15%
K-411	78. ±5%	3.5±10%	22.2±15%
K-586	17.3±5%	1.1±20%	15.7±25%
K-615	17.3±5%	.8±10%	21.6±15%
K-656	17.4±5%	.6±17%	29.0±22%
K-675	3.5±20%	.2±25%	17.7±45%
K-689	62.9±5%	2.6±10%	24.2±15%
K-779	42.0±5%	1.9±10%	22.1±15%
K-867	21.5±5%	1.0±10%	21.5±15%
K-964	69.5±5%	2.9±8%	24.0±13%
K-1086	37.0±5%	1.7±17%	21.8±22%
K-1112	38.2±5%	2.0±10%	19.1±15%
K-1408	19.0±3%	.8±12%	23.2±15%

Fig. V-4

Relative Efficiency of the 3mm. Si(Li) Detector

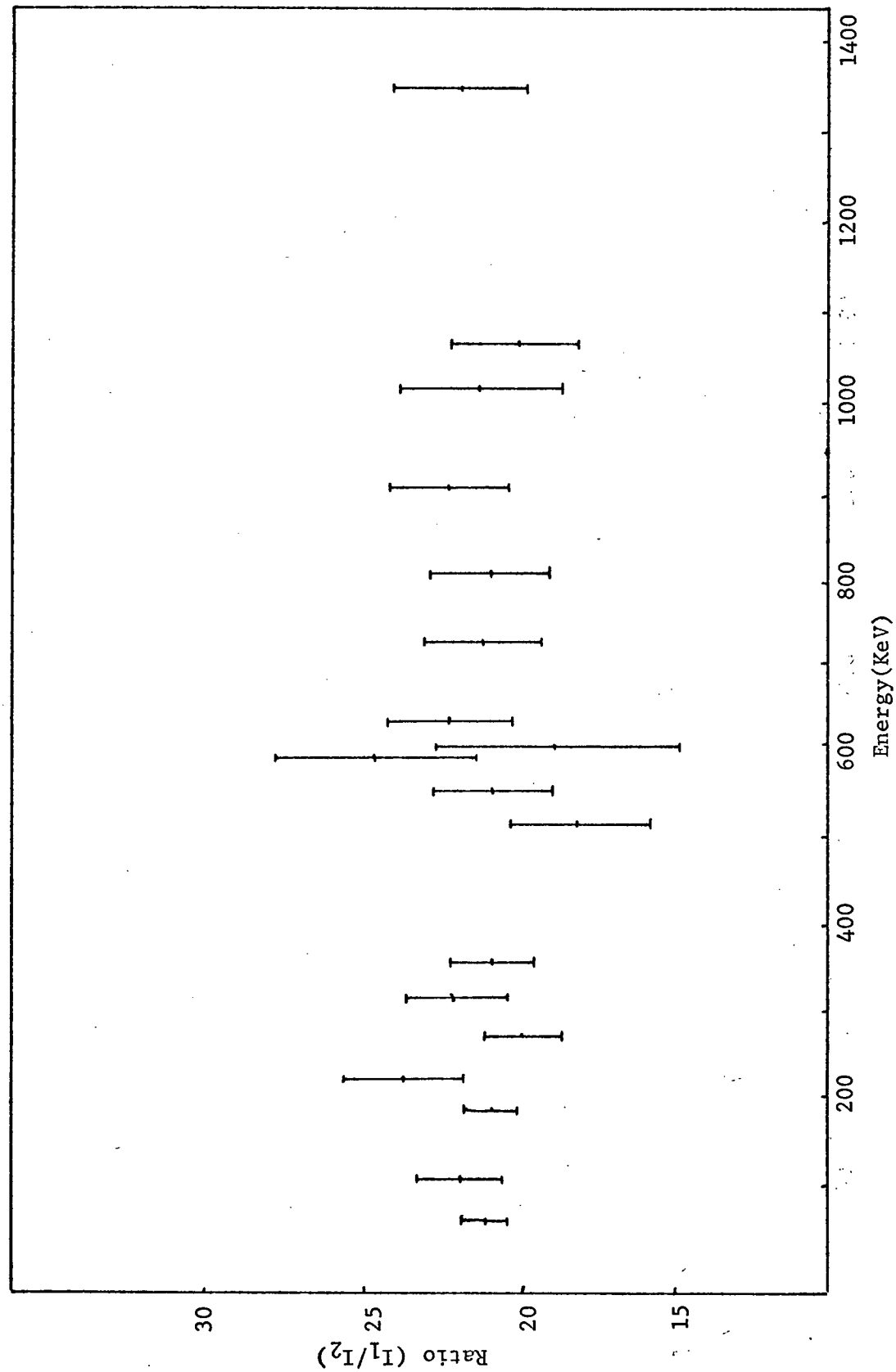

with D(E) obtained from equation V-5. $C_c(N) = C(N)$ = counts in channel N. E_N is the energy corresponding to channel N. ΔE is the energy per channel of the spectrum.

The correction to the first N-2 channels due to the counts in the second to last, or $(N-1)^{th}$ channel, is

$$A_{n-1} = \frac{f(E_{N-1})}{1-f(E_{N-1})} \Delta D_{N-1} \quad C_c(N-1) \qquad \text{V-6(b)}$$

where $C_c(N-1) = C(N-1) - A_N$

The correction to the first N-j channels is

$$A_{N-j} = \frac{f(E_{N-j})}{1-f(E_{N-j})} \Delta D_{N-j} \quad C_c(N-j)$$

where

$$C_c(N-j) = C(N-j) - \sum_{k=N-j+1}^{N} Ak \qquad \text{V-6(c)}$$

The corrected spectra, given by the C_c's, should have the shape given by equation V-1. To check that this was so, a spectrum of the high energy β^- group in the decay of ^{137}Cs was taken, the correction applied, and the shape factor and end-point energy calculated. The total and the corrected high energy spectrum of ^{137}Cs is shown in figure V-5.

The theoretical shape factor[47] for this β^- transition is $S_{th} = \lambda p^2 + q^2$ with $\lambda = .03$. The endpoint energy has been measured to be 1174 KeV.[40] A plot of $(S_{exp} - S_{th})/S_{exp}$ using these values is shown in figure V-6. If values of $\lambda = .02$ or $\lambda = .04$ were used, the function $(S_{exp} - S_{th})/S_{exp}$ did not fluctuate about zero. A least square fit of the data in the form

$$\left(\frac{C_c(K)}{pWFS_{th}}\right)^{\frac{1}{2}}$$

Fig. V-5

High energy electron spectrum of ^{137}Cs

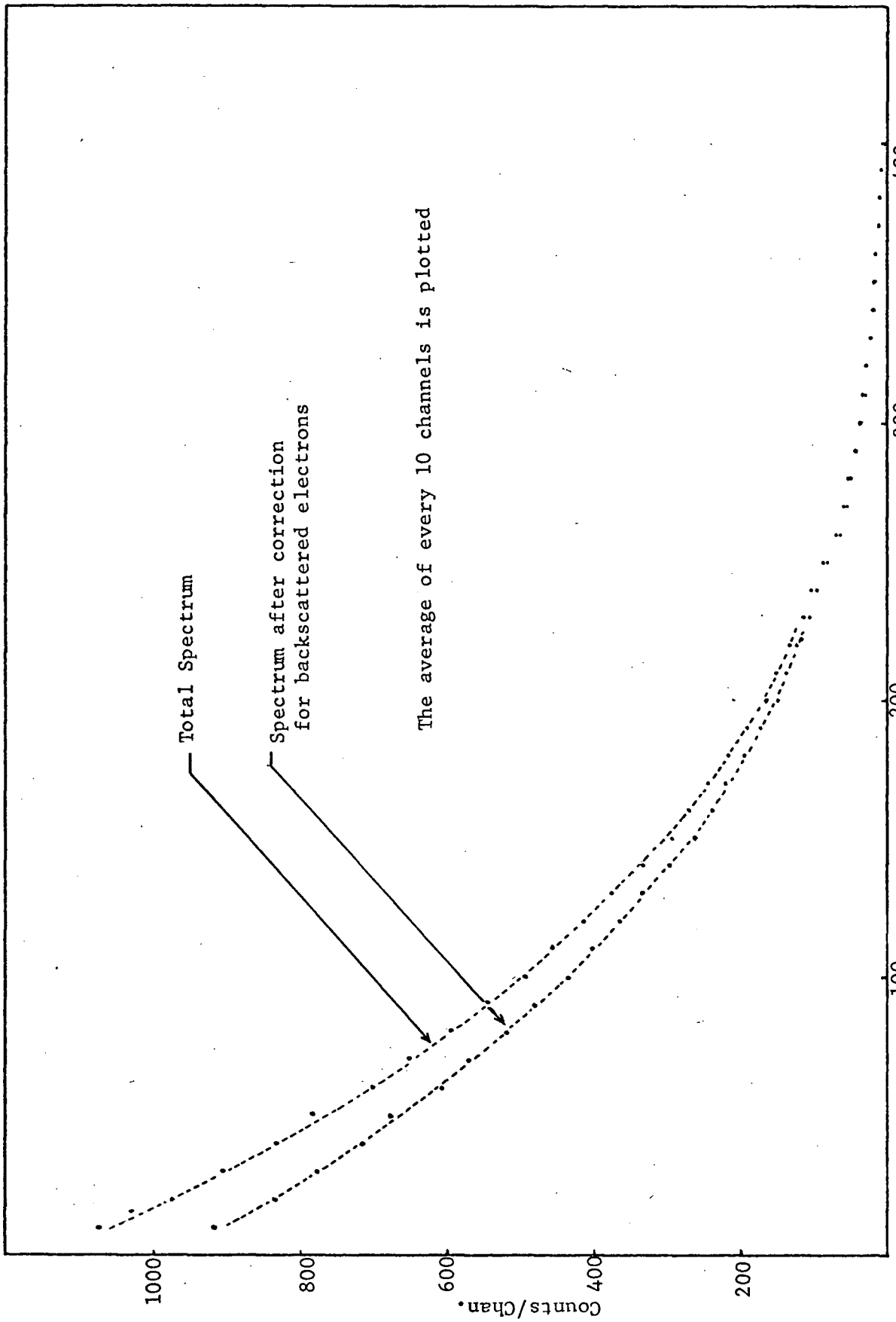

Fig. V-6

Shape factor for the high energy β^- group of ^{137}Cs

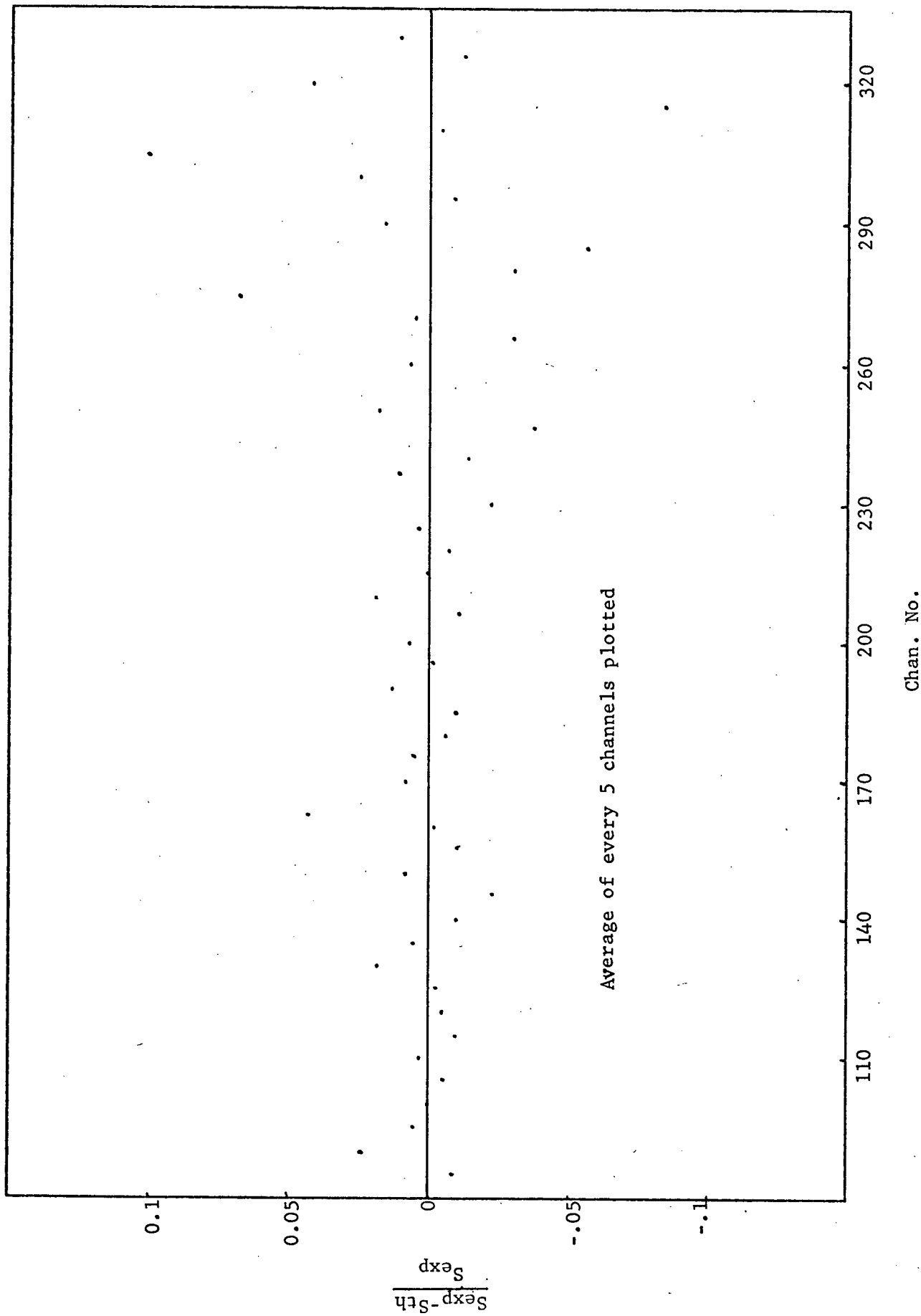

Fig. V-7

Kurie plots for the high energy β^- group of ^{137}Cs

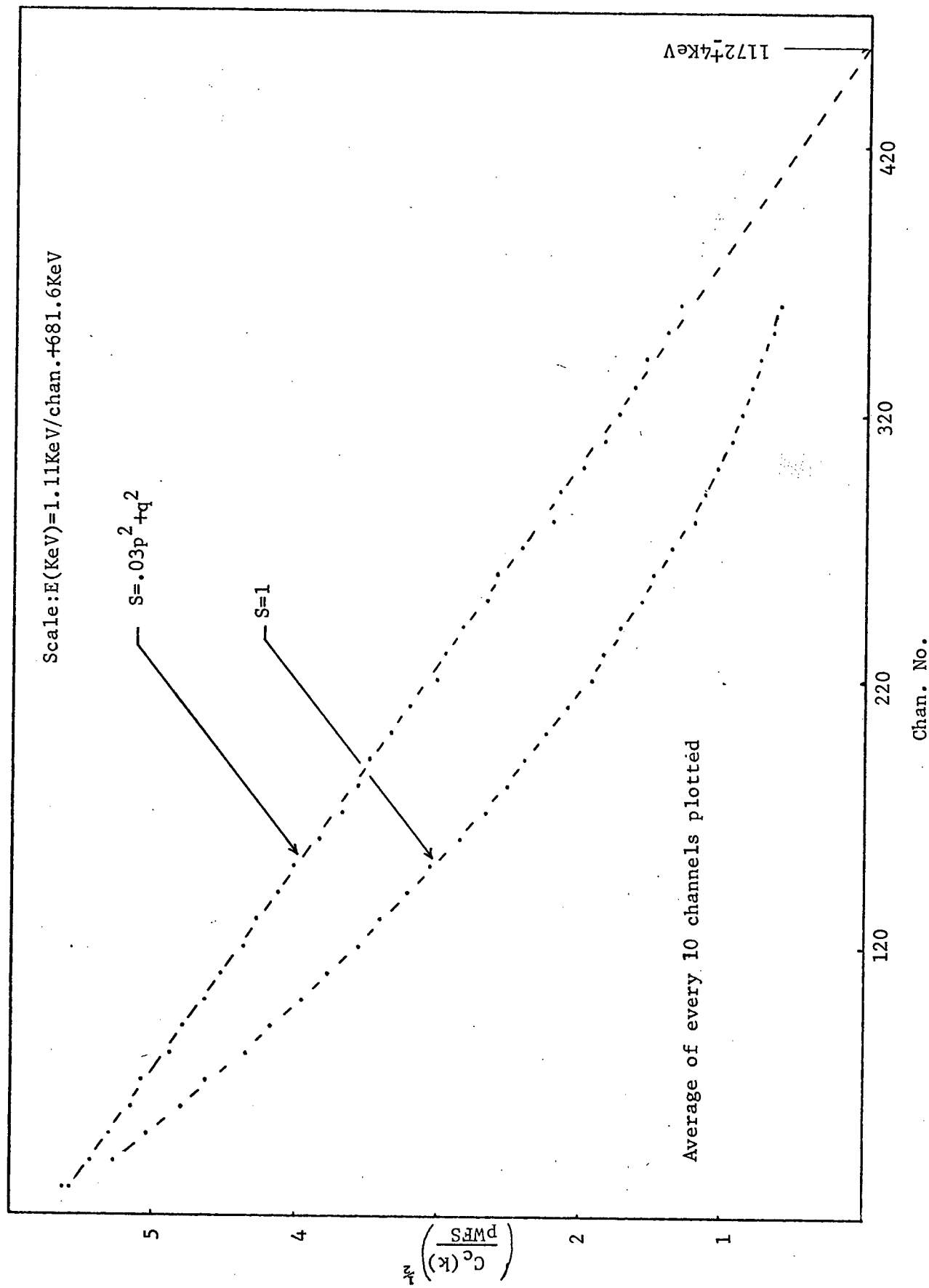

yielded an end-point energy of 1172 $\pm$ 4 KeV, as shown in figure V-7. Since these experimental values are in excellent agreement with the accepted ones, the correction technique described above was assumed to be valid.

Since Si(Li) detectors are also sensitive to gamma radiation, mainly by the Compton process, the background due to gamma transitions will often interfere with the electron spectrum analyses. Much of this background can be removed by taking coincidence spectra of the electrons in coincidence with the gamma transition depopulating the level fed by the β decay. These coincidence measurements can also be used to establish the decay scheme and to measure the individual β spectra when there are two or more competing β transitions involved in the decay. Of course, background due to other gamma transitions also in coincidence with the gamma transition used as a gate will remain. An estimate of this remaining background can be obtained by inserting a thin absorber between the source and detector, and the coincidence spectrum re-taken. The absorber should be chosen, if possible, such that all the electrons in coincidence with the gate are absorbed, while the gamma intensity is not appreciably affected.

The β^- decay of ^{152}Eu was investigated using these coincidence techniques. A short summary of the procedure used and the results obtained is reported in Appendix C.

c) Beta Spectra of ^{124}Sb

An attempt was made to analyse the β^- transitions in the decay of ^{124}Sb in the manner described above. The gamma transitions chosen as gates were the 603, 645, 709 + 714, 723, 1691 and 2091 KeV transitions. These are the most intense transitions in the decay, and are essentially the only gate possibilities. Only the coincidence spectra taken with the

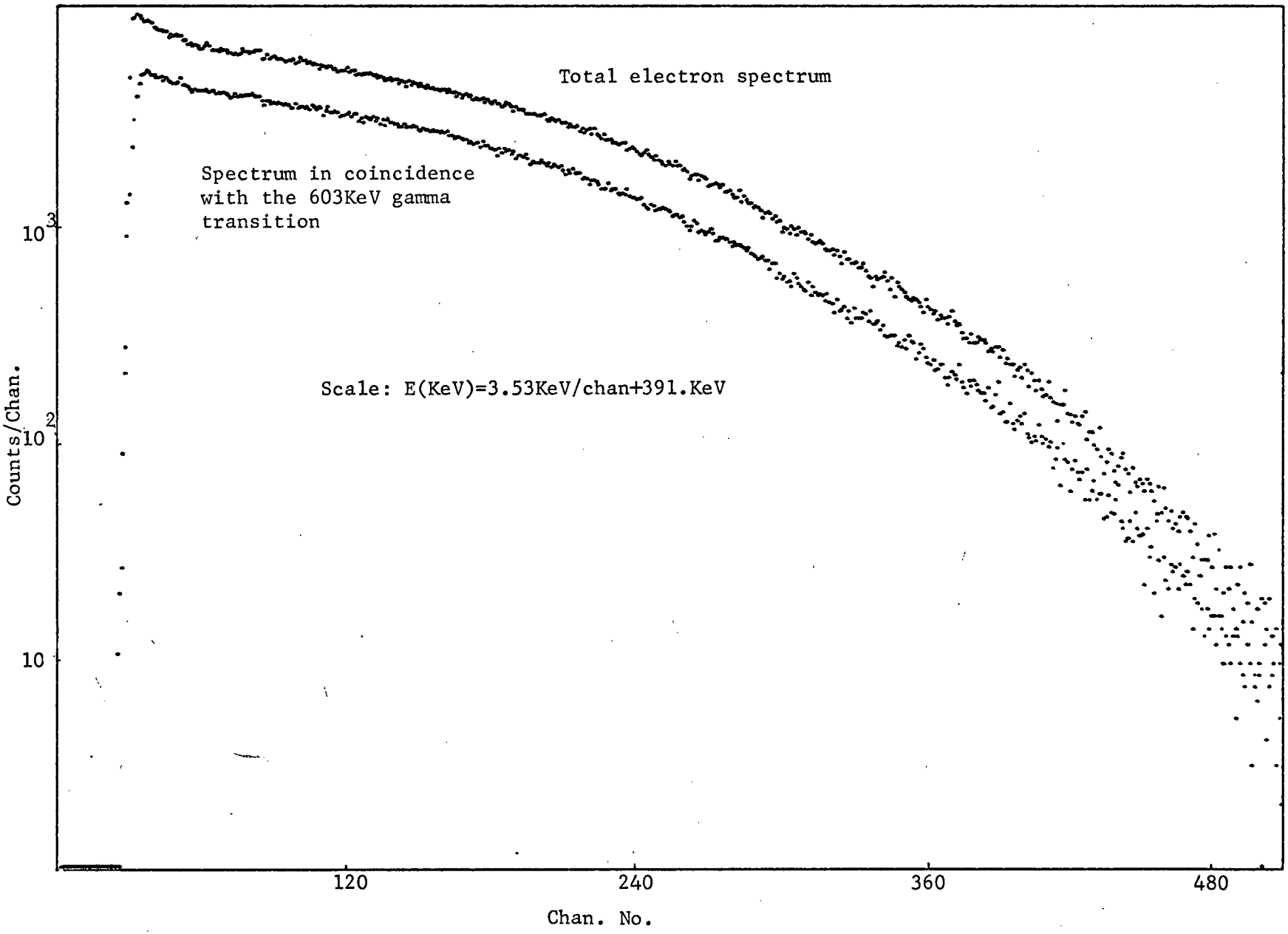

Fig. V-8

Electron Spectra of ^{124}Sb

603, 1691 and 2091 KeV gates were good enough that shape factors and end-point energies could be calculated. The β^- transitions found in coincidence with the 645, 709 + 714 and 723 KeV gates were weak, and only approximate end-point energies could be estimated.

The 30cc Ge(Li) detector was used as the gamma-ray gate detector. The 3mm Si(Li) detector was used as the analog detector for β^- spectra with end-point energies less than 1500 KeV. The 5mm Si(Li) detector was used for β^- spectra with end-point energies above 1500 KeV as the 3mm detector is not thick enough to stop completely all electrons with energies above 1500 KeV.[50]

Figure V-8 is the total singles electron spectrum of ^{124}Sb, along with the spectrum found in coincidence with the 603 KeV gate. The coincidence spectrum was corrected using equations V-6 and the shape factor and end-point energy calculated from the corrected data for the energy region 1500-2000 KeV. The results are shown in figure V-11(a)

Because of the similarity of the two spectra shown in figure V-8, it is immediately apparent that the β^- group feeding the level depopulated by the 603 KeV gamma transition is the highest energy β^- transition at measurable intensity in the ^{124}Sb decay. It is also apparent that all the electrons, at least down to approximately 500 KeV, are in coincidence with the 603 KeV gamma transiton. This fact implies that all the excited nuclear states populated by the beta transitions from ^{124}Sb, with end-point energies above 500 KeV, decay mainly via the 603 KeV transition. This implication is confirmed by the large number of gamma transitions found in coincidence with the 603 KeV gate in the gamma-gamma coincidence measurements. Figure V-9 shows the total coincidence spectrum and the coincidence spec-

Fig. V-9

Total (electron+gamma) and gamma spectra in coincidence with the 1691KeV gamma transition

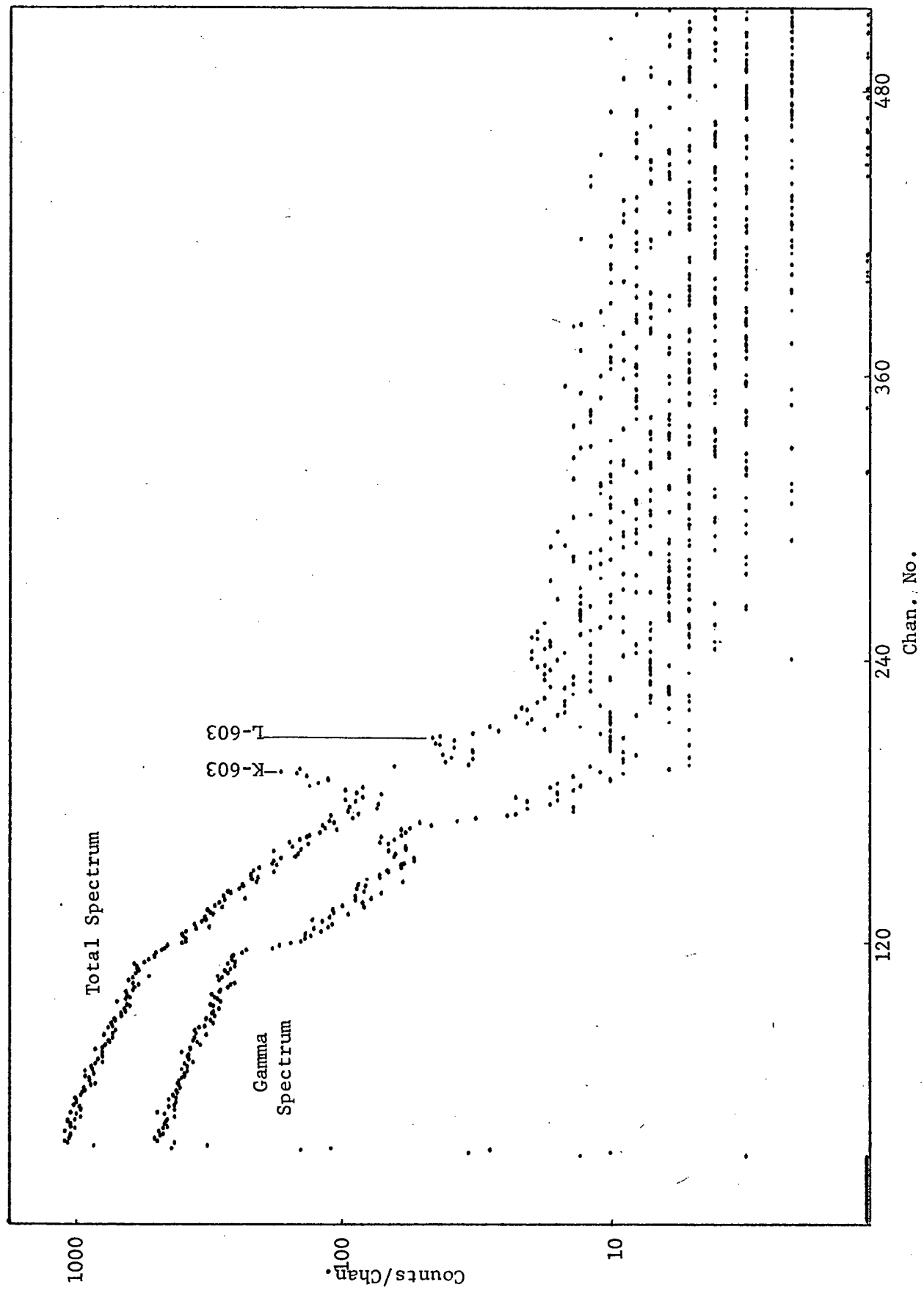

Fig. V-10

Residue after subtraction of the two spectra in Fig.V-9

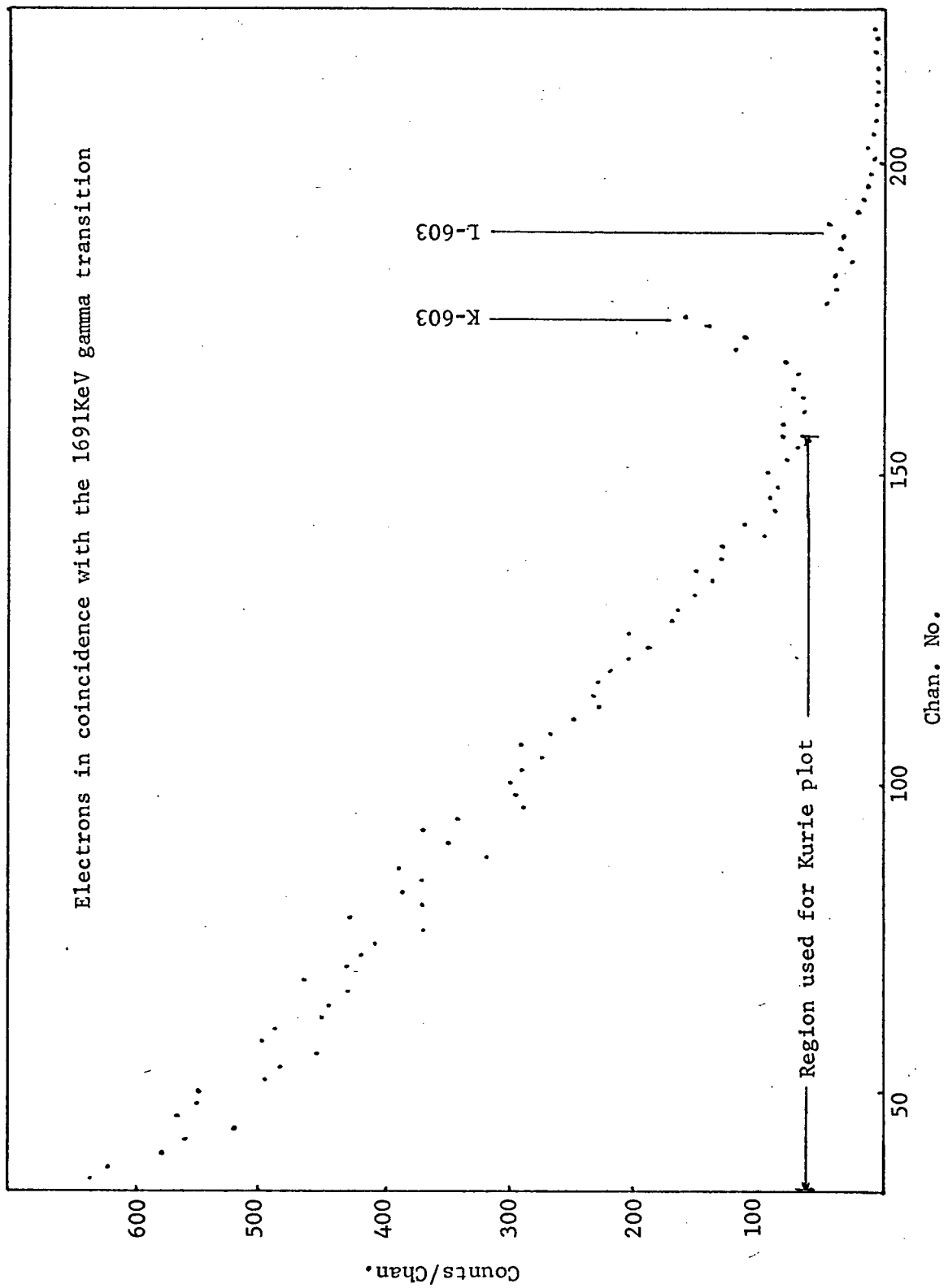

Fig.V-11(a)

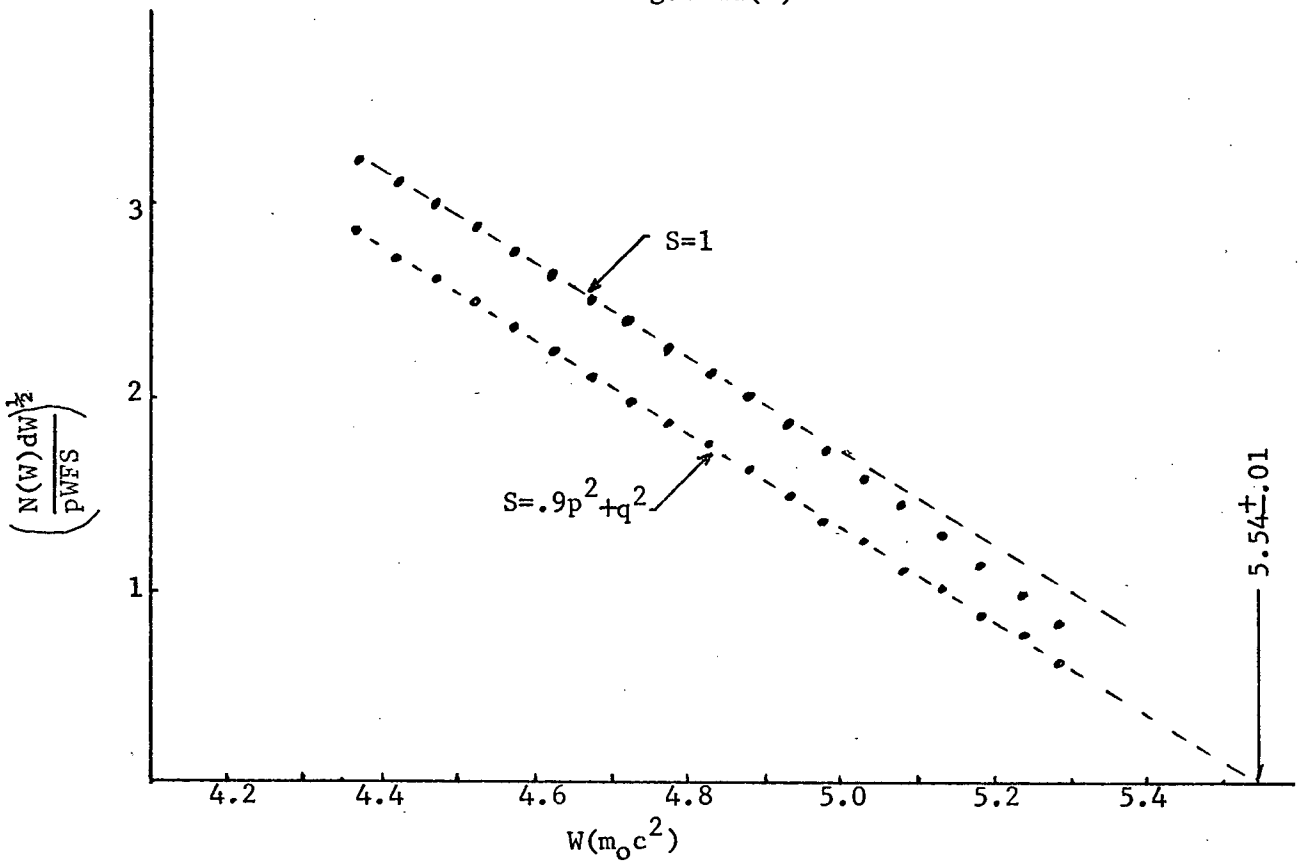

Fig. V-11(b)

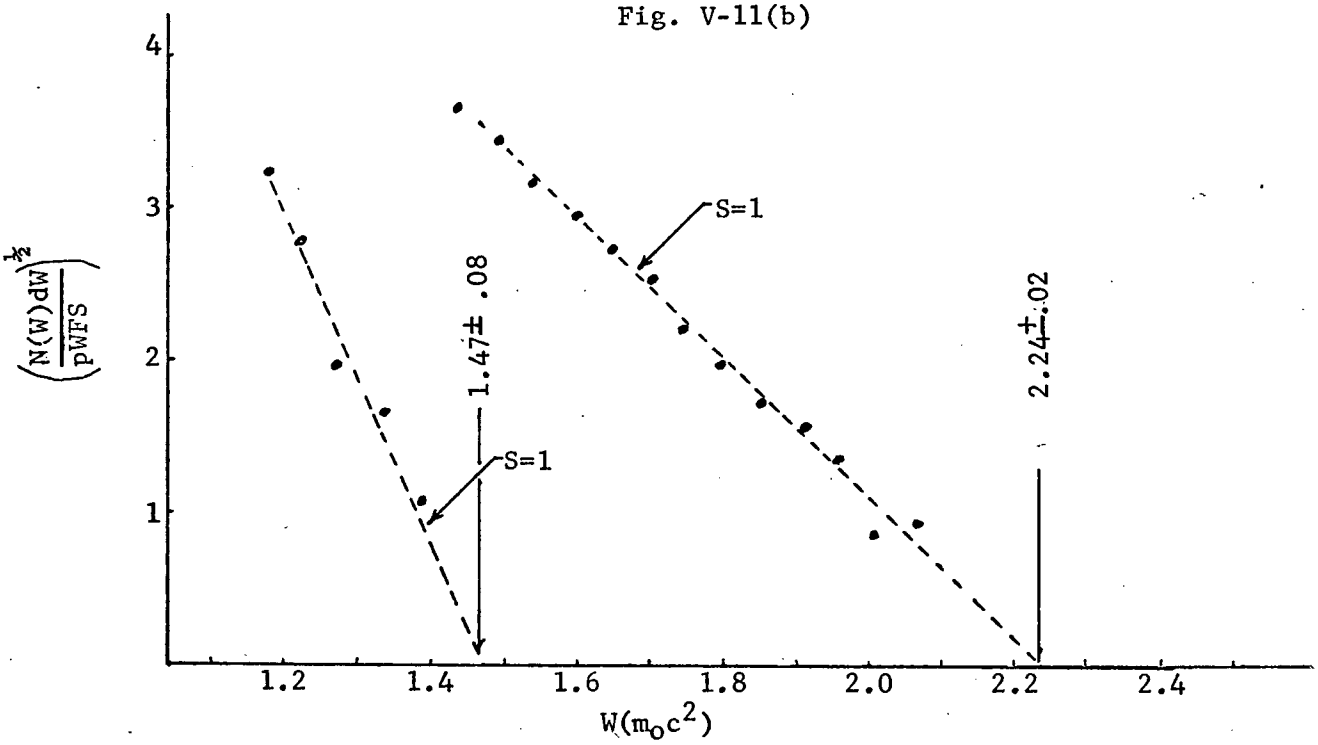

trum taken with a 50 mg/cm^2 absorber between the source and detector for the 1691 KeV gate. The difference between these two spectra is plotted in figure V-10. The spectrum of figure 10 was corrected for scattering, and the shape factor and end-point energy calculated. Similar spectra were obtained and analysed using the 2091 KeV gate. The results of these calculations are plotted in figure V-11(b).

The results of the coincidence measurements are tabulated in table V-2 along with the approximate end-point energies found using the other gates. Approximate log ft values, which are the logarithms of the comparative halflives of the transitions,[41] are also given in table V-2. The log ft values were calculated from the estimated relative intensities of the transitions. The relative intensities were estimated to be 20 %, 50 %, and 10 % for the β^- transitions found in coincidence with the 603, 1691 and 2091 KeV gamma transitions respectively. The intensities of the transitions found in coincidence with the 645, 709 + 714 and 723 KeV gates were each estimated to be approximately 5 %.

V-2 Internal Conversion Electrons

a) Internal Conversion Coefficients

An excited state of a nucleus may lose its energy by transferring it to a bound atomic electron, a process called internal conversion. The electron will then be emitted with energy $E_\gamma - E_B$, where E_B is the binding energy of the electron before emission. The energy transfer is by a direct interaction between the bound electron and the same multipole field which otherwise would have resulted in the emission of a gamma ray. The transition probability for internal conversion therefore contains the same nuclear wave functions as the transition probability for gamma emission.[52]

Table V-2

Beta Transitions from ^{124}Sb

Gate	End Point Energy(KeV)	Shape Factor	Forbiddeness	ΔJ	$\Delta\pi$	Log ft
603	2320±5	$.9p^2+q^2$	1^{st}	0,1	Yes	~10
646	~1600	-	1^{st} or 2^{nd}	-	-	~10
709+714	~1000	-	1^{st} or 2^{nd}	-	-	~10
723	~1600	-	1^{st} or 2^{nd}	-	-	~10
1691	634±15	1	Allowed	0,1	No	~7
2091	240±40	1	Allowed	0,1	No	~6

The internal conversion coefficients (I.C.C.), defined by $\alpha = W_e/W_\gamma$, where W_e and W_γ are the transition probabilities for internal conversion and gamma emission respectively, are almost independent of the nuclear wave functions.[52] The ICC's then depend only on the energy difference between the initial and final states, on the spin and parity change of the transition, and on the angular momentum, parity and binding energy of the electron being converted. Theoretical conversion coefficients have been calculated by Sliv and Band[53] for the K(α_k), L_I(α_{L_I}), L_{II}($\alpha_{L_{II}}$) and L_{III}($\alpha_{L_{III}}$) atomic states. Similar calculations have been done by Rose.[54]

Once the intensities of the conversion electrons and gamma rays for a given transition have been measured, the experimental conversion coefficients can be calculated. They are

$$\alpha_K = I_K/I_\gamma \quad , \quad \alpha_{L_I} = I_{L_I}/I_\gamma \quad \text{etc.}$$

where I_K, I_{L_I}, ... , and I_γ are the normalized intensities for the K, L_I, ... , conversion electrons, and gamma rays, respectively. A comparison of experimental ICC's to the theoretical ones for different spin and parity changes can be used to deduce the spin and parity changes of nuclear transitions.

b) K-Conversion Electrons in Coincidence with K-X-rays

The spectrum of ^{124}Sb taken with a Si(Li) detector has a very large background due to β^- transitions, Compton scattered gamma rays, etc. The conversion electron peaks, which are superimposed on this background, could not be identified except for those due to the transitions of 603, 646, 709, 714 and 723 KeV. This large background can be reduced by analysing only those events that are in coincidence with the K-X-rays. Of course, some of the β^- particles and gamma rays will be in coincidence with the K-X-rays, but the K-conversion electron intensities will be enhanced over

all others.

The relationship between the K-conversion electrons in coincidence with the K-X-rays and the total K-conversion electrons can be found by considering the decay scheme

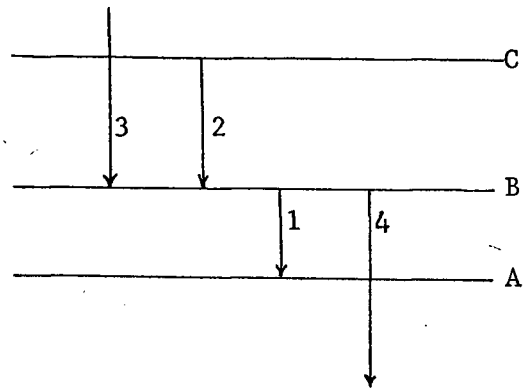

in which the transitions can take place by either the internal conversion or gamma process. Then if the gate detector is set on the K-X-ray peak, the rate of coincidences for K-conversion electrons from transition 1 will be

$$N^{1}_{K\text{-}X} = n_v \epsilon_X \epsilon_{K_1} F^{1}_{v} \omega_K$$

n_v is the total rate the K- shell vacancies are produced (equal to the sum of all K- conversion electrons emitted). ϵ_X and ϵ_{K_1} are the total efficiencies for the K-X-rays in the gate detector and the K_1 conversion electrons in the analog detector respectively. ω_K is the K- fluorescent yield[55] which is the probability that a K- shell vacancy will result in the emission of a K-X-ray, rather than Auger electrons. F^{1}_{v} is the fraction of the K- shell vacancies that could result in a K-X-ray in coincidence with the K_1- conversion electrons. For this simple decay scheme

$$F_K^1 = \frac{1}{n_v}\left(I_{K_1} + I_{K_2}\left(\frac{I_{K_1}}{I_1 + I_2} + \frac{I_{K_3}}{I_1 + I_2}\right)\right)$$

$$= \frac{1}{n_v} I_{K_1}\left(1 + \frac{\alpha_{K_2} f_B^2}{1 + \alpha_2} + \frac{\alpha_{K_3} f_B^3}{1 + \alpha_3}\right)$$

$$= \frac{I_{K_1}}{n_v} D_1$$

In these equations, the I_K's are the intensities of the K-conversion electrons, the I's are the total transition rates, and the α's and the α_K's are the total and K-conversion coefficients. f_B^2 and f_B^3 are the feeding ratios defined in chapter IV (equation IV-5). Similarly, the coincidence rate for the K_2-conversion electrons is

$$N_{K\text{-}X}^2 = n_v \epsilon_x \epsilon_{K_2} \omega_K F_K^2$$

with

$$F_K^2 = \frac{I_{K_2}}{n_v}\left(1 + \frac{\alpha_{K_1}}{1 + \alpha_1} b_B^1 + \frac{\alpha_{K_4}}{1 + \alpha_4} b_B^4\right)$$

$$= \frac{I_{K_2}}{n_v} D_2$$

and the b's are also defined in chapter IV (equation IV-5).

If the efficiency of the analog detector is independent of electron energy, the ratio of the coincidence rates is just

$$\frac{N_{K\text{-}X}^1}{N_{K\text{-}X}^2} = \frac{I_{K_1} D_1}{I_{K_2} D_2}$$

and, if the products $\alpha_{K_1} b_B^1$, $\alpha_{K_2} f_B^2$, etc., are small compared to unity the ratio is equal to the ratio of the true intensities,

$$I_{K_1} / I_{K_2}$$

The same type of equations can be written for a general decay scheme. The D factors will, in general, contain many more terms, but they will always be of the form

$D = 1 + \sum_i \alpha_{K_i} g_i$ with the g_i's all less than one. For ^{124}Sb, it can be shown that

$$\sum_i \alpha_{K_i} g_i \leq 1$$

for all transitions, and therefore the relative intensities of the K-conversion peaks found in coincidence with the K-X-rays and the relative intensities of the total K-conversion peaks are essentially equal.

c) K-Conversion Electrons of ^{124}Te

A spectrum of ^{124}Sb taken in coincidence with the K-X-rays is shown in figure V-12(a+b), along with the total spectrum. The enhancement of the K-conversion peaks is immediately apparent. The 3mm Si(Li) detector was used as the analog detector and the 5mm Si(Li) detector as the gate detector. The electronics used were those shown in figure IV-1.

The peak identified as K-427 is due to a ^{125}Sb contamination in the source material. This contamination was not noticed when the gamma spectra were taken because the amount of ^{124}Sb radiation was much greater than the ^{125}Sb radiation at that time (^{125}Sb has a 2.7 year lifetime, compared to 60 days for ^{124}Sb).[40]

The peak at 1386 KeV has not been identified. It may be due to

Fig. V-12(a)

K-Conversion Electrons of ^{124}Sb

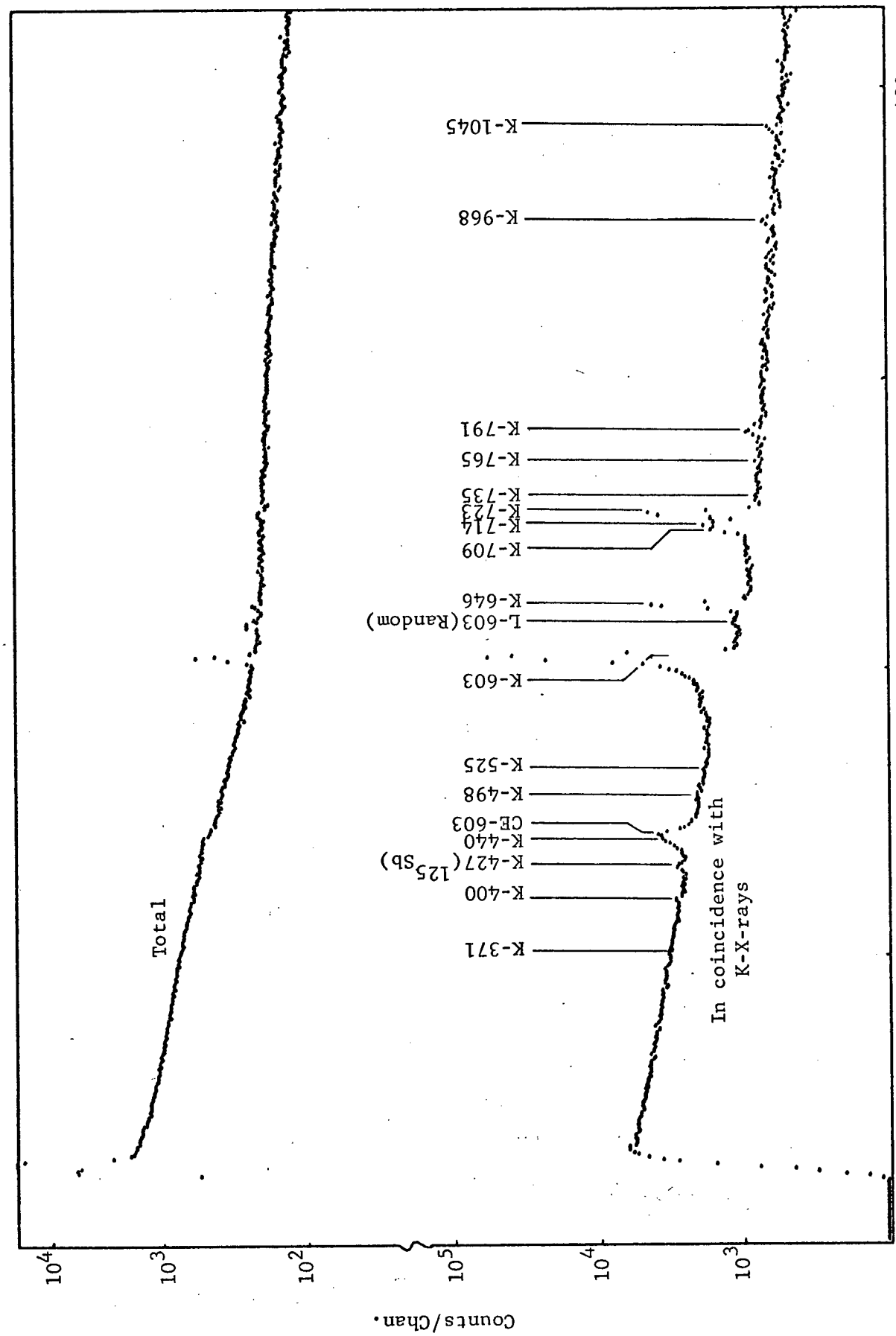

Fig. V-12(b)

K-Conversion Electrons of ^{124}Sb

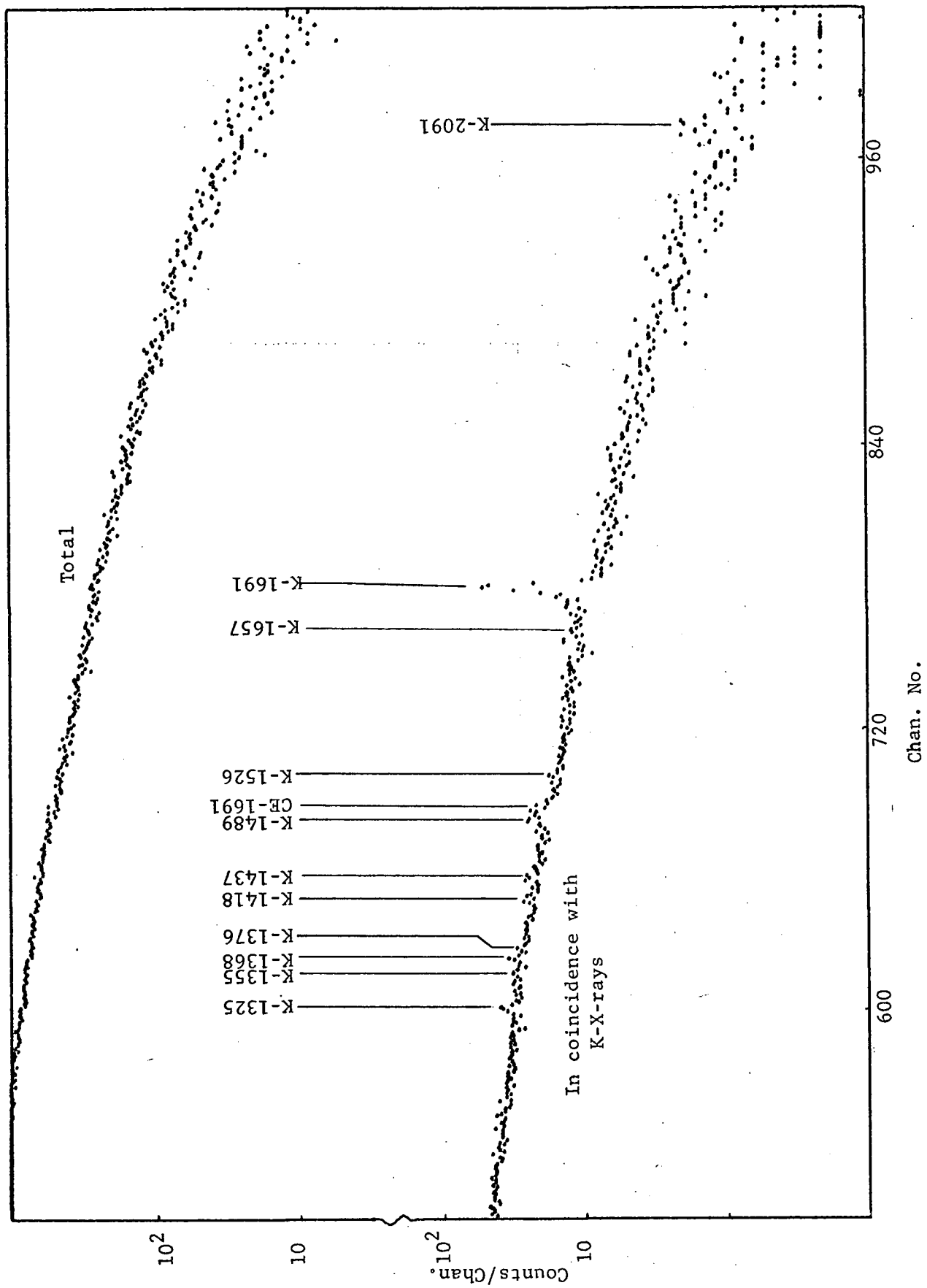

K-conversion electrons from a transition of 1418 KeV that was not found in the gamma spectra, either because the gamma intensity was too weak or the transition was between two J=0 states, in which case there would be no gamma radiation.

The low energy region (60 - 600 KeV) of the ^{124}Sb electron spectrum was re-taken four months after the spectrum in figure V-12. The coincidence spectrum is shown in figure V-13. The expected increase in the relative amount of ^{125}Sb contamination was calculated from the lifetimes of the two isotopes and found to agree with the increase in the relative intensity of the K-427 peak. Other K-conversion electron peaks from the ^{125}Sb contamination were identified using its known decay scheme. The relevant transitions are shown below.

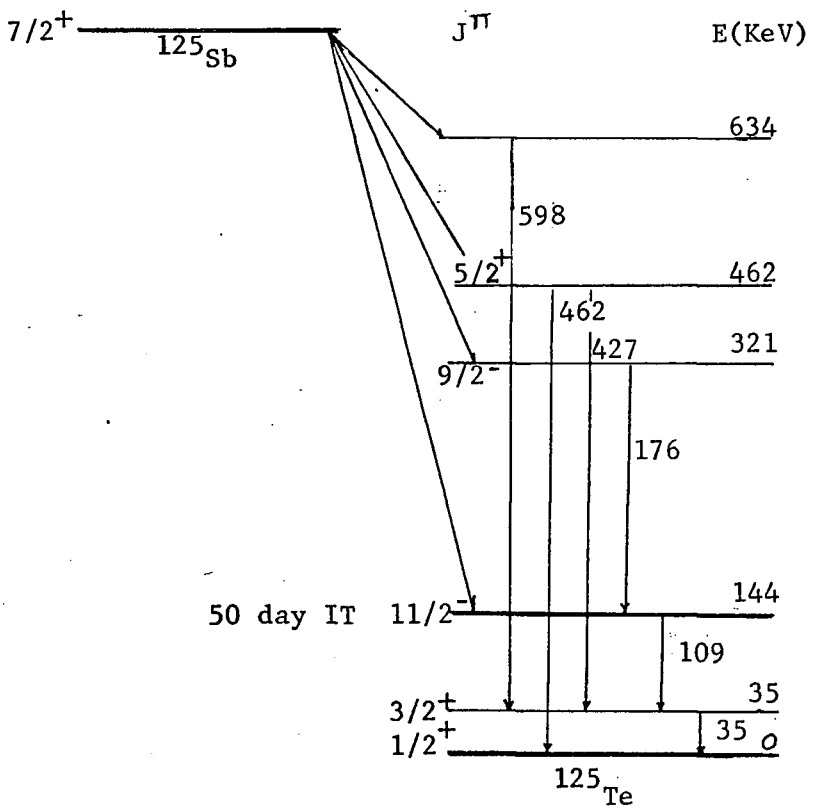

Fig. V-13

Low Energy K-Conversion Electrons of ^{124}Sb In Coincidence with the K-X-rays

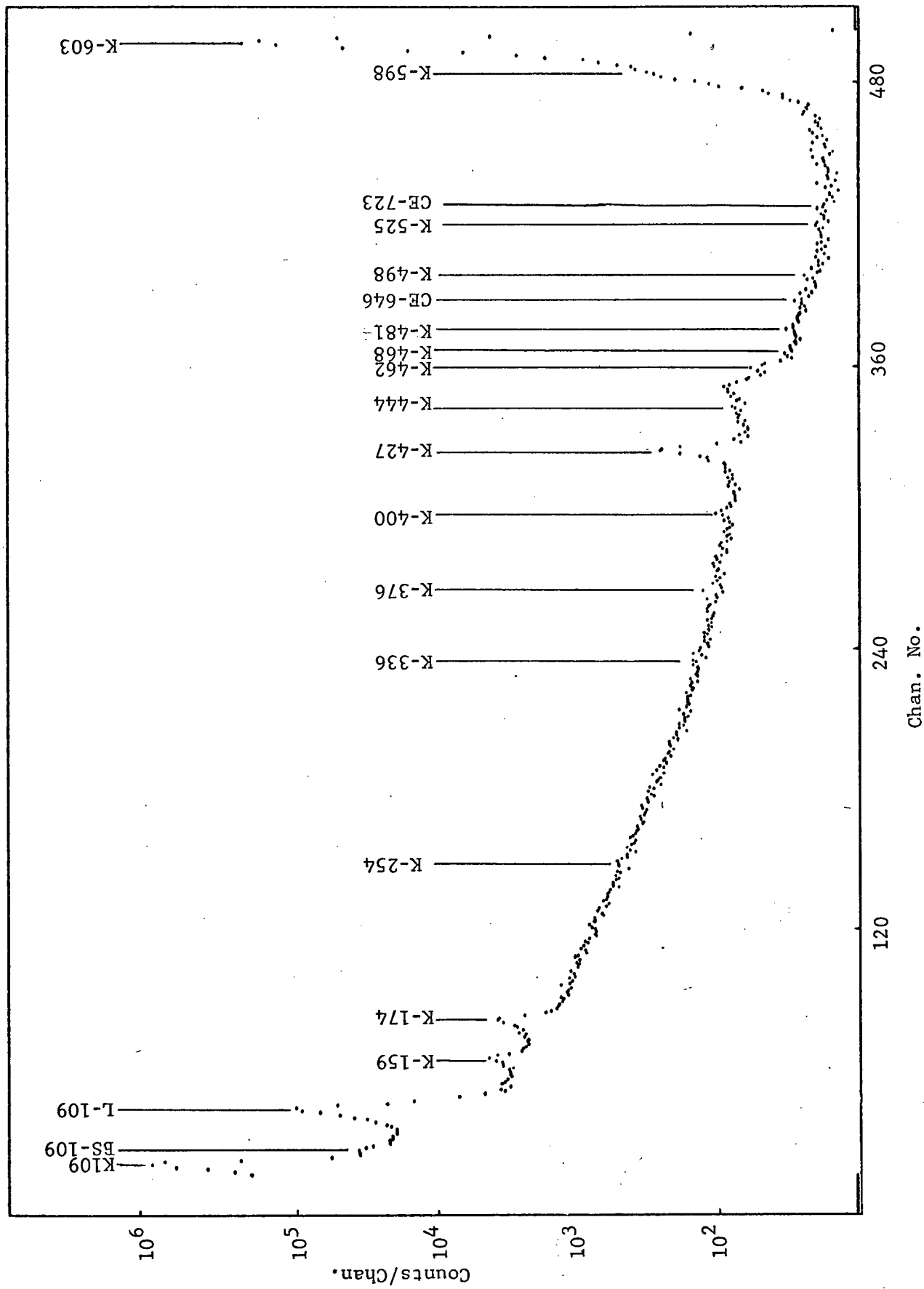

The reason that the L-109 conversion electron peak of ^{125}Sb appears in the coincidence spectrum is that a portion of the gammas from the 35 KeV transition would also lie in the region of the gate set on the K-X-rays (K-X-ray energies of Te range from 27.2 - 31.8 KeV).

The Compton edges (CE) and Compton backscatter (BS) peaks were identified by inserting an absorber between the source and detector and re-taking the coincidence spectrum.

It should be noted that the efficiency of the 3mm detector for electrons decreases rapidly above 1500 KeV electron energy. The high energy (1400 - 2100 KeV) portion of the electron spectrum was re-taken using the 5mm detector as the analog detector and the 3mm detector as the gate. The efficiency of the 5mm detector should be constant up to approximately 2300 KeV.[50]

The intensities of the K-conversion peaks of ^{124}Sb were calculated from the coincidence spectra and their relative intensities given in table V-3. The results of a recent study, using a magnetic spectrometer, by Grigor'ev et al[56] is included for comparison.

Table V-4 lists the experimental K-conversion coefficients, calculated using the gamma intensities listed in table III-4 and the electron intensities of table V-3. The 603 and 646 KeV transitions were used to normalize the electron intensities to the gamma intensities by assuming these transitions were pure E2.[57]

The theoretical conversion coefficients for the different multipolarities were taken from tables compiled by Sliv and Band.[53] Multipolarities were assigned to the different transitions by comparing these coefficients to the experimental ones. Many of the transitions could not be unambiguously assigned because of the large uncertainty in the experi-

Table V-3

Conversion Electrons of ^{124}Sb

Peak	Intensity		Peak	Intensity	
	This Work	Gregor'ev[56]		This Work	Gregor'ev[56]
K-159	2.3(.2)	-	K-765	.035(.02)	.06(.02)
K-254	.10(.08)	-	K-791	.44(.08)	.44(.03)
K-336	..12(.08)	-	K-968	.24(.08)	.33(.03)
K-371	.10(.08)	-	K-1045	.18(.08)	.25(.03)
K-400	.45(.08)	-	K-1325	.35(.1)	.30(.03)
K-444	.35(.15)	-	K-1355	.17(.1)	.20(.02)
K-468	<.14	-	K-1368	.14(.05)	.22(.03)
K-481	<.07	-	K-1376	.035(.03)	-
K-525	.14(.08)		K-1418	.25(.1)	-
K-603	100.	100.	K-1437	.28(.1)	.17(.03)
K-646	5.4(.5)	6.6(.3)	K-1489	.14(.1)	.13(.02)
K-709	1.4(.5)	1.2(.1)	K-1526	.035(.03)	<.04
K-714	1.6(.5)	1.6(.2)	K-1657	.2(.1)	-
K-723	5.7(.5)	6.5(.3)	K-1691	2.7(.4)	2.5(.2)
K-735	.04(.02)	-	K-2091	.24(.06)	.2(.04)

Table V-4

Conversion Coefficients

Transition Energy(KeV)	Exper. $\alpha_K X10^3$	Theoretical $\alpha_K X10^3$ E1	E2	M1	M2	Assumed Polarity
159	500±250	51	300	178	1210	M1,E2
254	39±30	10.3	55	45	220	M1,E2
336	10±6	6.5	24	23	90	E1
371	16±12	5.0	17	17	66	Not M2
400	16±4	4.1	14	15	52	M1,E2
444	8±2	3.1	10	11	37	M1,E2
468	< 20	2.8	8.6	9.8	33	Not M2
481	<16	2.6	7.8	9.2	30	Not M2
498	18±14	2.4	7.2	8.3	28	?
525	4.8±3.5	2.0	5.9	7.0	22	M1,E2
603	4.2	1.6	4.2	5.2	15	E2
646	3.5	1.3	3.5	4.4	13	E2
709	4.7±2.0	1.1	2.7	3.5	9.4	M1,E2
714	3.1±2.0	1.0	2.7	3.5	9.4	M1,E2
723	2.4±.5	1.0	2.6	3.4	9.3	E2
736	.9±.7	1.0	2.6	3.3	9.2	E1
765	15±12	.90	2.3	2.9	7.8	?
791	2.6±.6	.86	2.0	2.5	6.6	M1,E2
968	.53±.2	.57	1.4	1.7	4.3	E1
1045	.43±.2	.49	1.2	1.5	3.4	E1
1325	.9±.3	.31	.70	.84	1.9	M1,E2
1355	.67±.4	.30	.67	.80	1.8	M1,E2
1368	.23±.2	.3	.67	.80	1.8	E1
1376	.3±.3	.3	.66	.79	1.8	E1
1437	.92±.4	.27	.60	.72	1.6	M1,E2

Table V-4(cont.)

1489	.9±.7	.26	.55	.66	1.5	M1,E2
1526	.35±.3	.25	.52	.62	1.4	(E1)
1657	-	-	-	-	-	E0
1691	.24±.08	.21	.42	.49	1.1	E1
2091	.19±.08	.15	.28	.32	.66	E1

mental coefficients. A further complication at low energies arises because the theoretical M1 and E2 coefficients are almost identical.

The different types of transitions (M1, E2, etc.), along with the allowed changes in spin and parity for each type, are discussed in Appendix B.

Chapter VI

Results of the ^{124}Sb Investigation

VI-1 Decay Scheme of $^{124}Sb \rightarrow ^{124}Te$

The decay scheme of $^{124}Sb \rightarrow ^{124}Te$ was constructed using the gamma-ray energies and intensities from the singles spectra (table III-4), the gamma-gamma coincidence results (tables IV-2,3 and 4), and the beta-gamma coincidence results (table V-2). In addition, the results of other investigations provided useful evidence or confirmation in the assignments of a few levels and transitions. In particular use was made of the results of recent studies of the decay $^{124}I \rightarrow ^{124}Te$ by Ragaini et al[72] and by LaGrange;[73] of the reactions $^{123}Sb(^{3}He,d)^{124}Te$ and $^{126}Te(p,t)^{124}Te$ by Auble and Ball,[74] $^{123}Te(n,\gamma)^{124}Te$ by Bushnell et al,[75] $^{124}Te(p,p')^{124}Te$ by Rao et al[76] and $^{124}Te(d,d')^{124}Te$ by Christensen et al.[77]

Figure VI(a) and (b) shows the decay scheme of $^{124}Sb \rightarrow ^{124}Te$ deduced in this investigation. The values of the spin J, and parity π, quoted for the levels are derived in section VI-3. Table VI-1 summarizes the evidence that supports the placing of the levels. Only seven of the twenty-two levels could not be unambiguously placed using the coincidence results alone. These levels were positioned by energy and intensities fits of the gamma transitions found in the decay and the results of the ^{124}I decay and reaction studies. Only the placement of levels at 1657, 2335 and 2484 KeV remain in some doubt.

VI-2 Log ft Values

The relative intensites of the beta transitions from the 3^- ground state of ^{124}Sb to all the levels of ^{124}Te populated in this decay were calculated, along with their log ft values, from the gamma-ray intensities

Fig. VI-1(a)

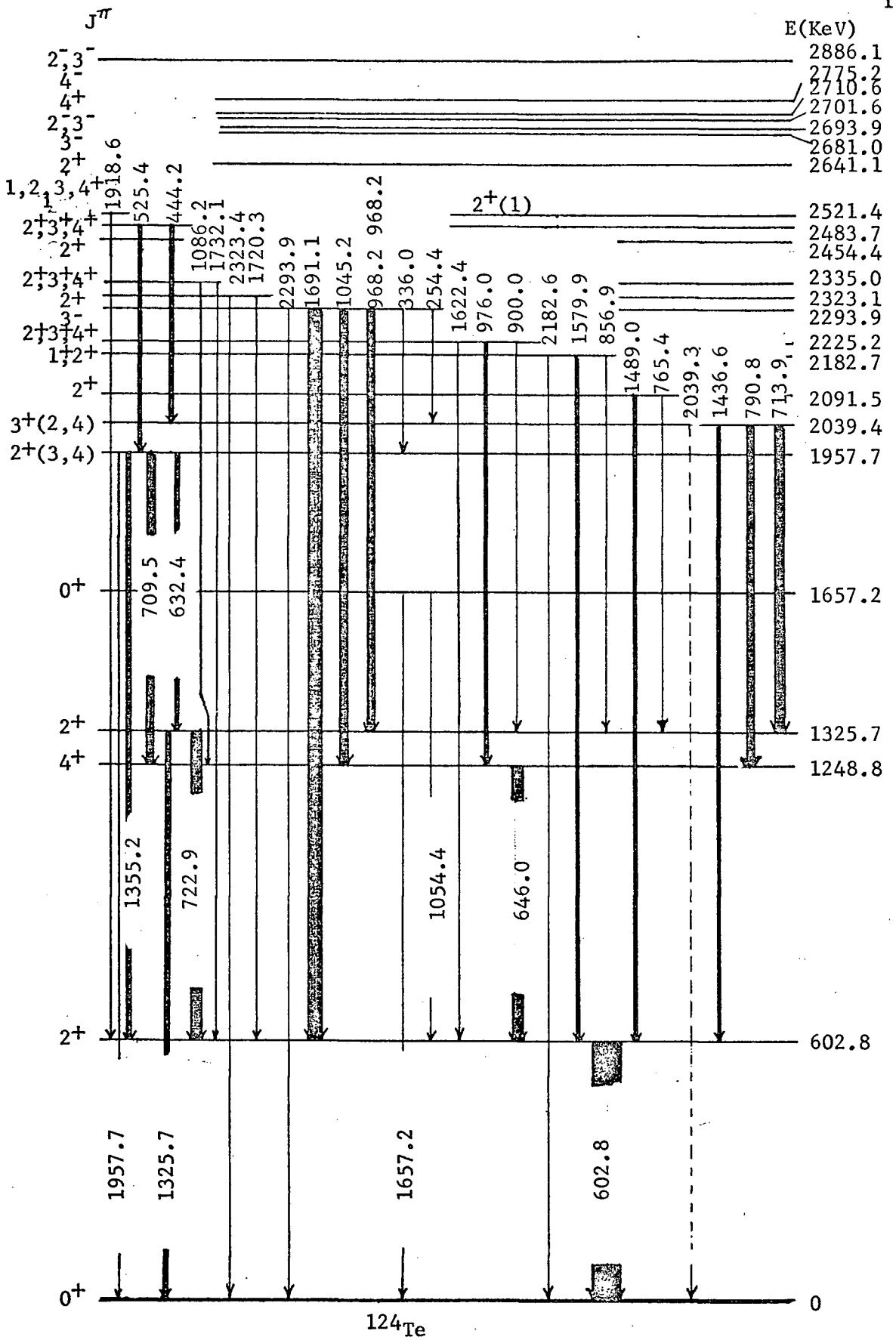

Decay Scheme of $^{124}Sb \rightarrow ^{124}Te$

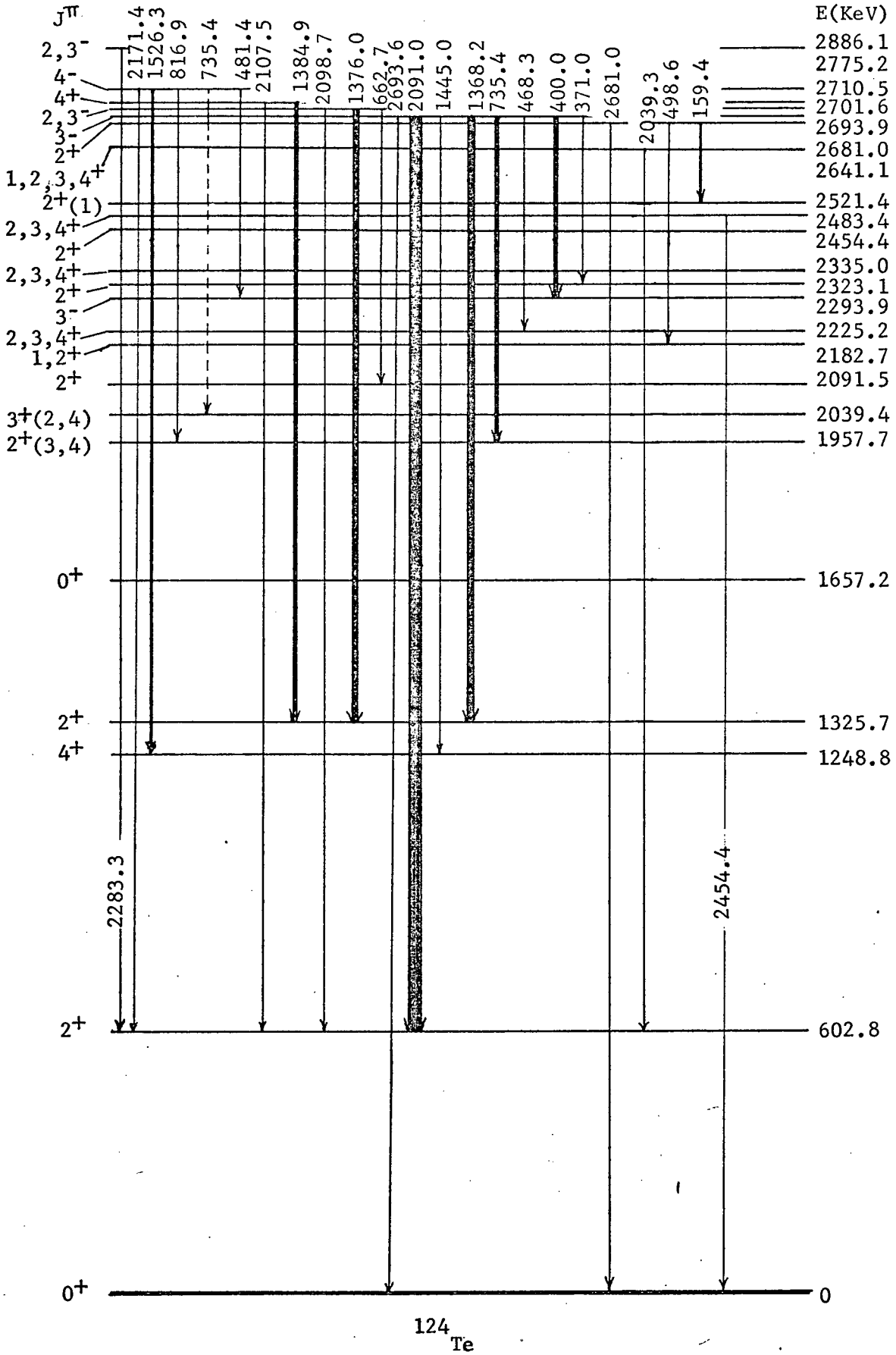

Decay Scheme of $^{124}Sb \rightarrow {}^{124}Te$

Evidence for the levels of ^{124}Te populated in the ^{124}Sb decay

Level (KeV)	This Investigation			Others	
	Coin.		Energy and Inten. Fit	^{124}I	Reactions
	γ-γ	γ-β			
602.8	x	x	x	x	x
1248.8	x	x	x	x	x
1325.7	x	x	x	x	x
1657.2			x	x	x
1957.7	x	(x)	x	x	x
2039.4	x	(x)	x	x	x
2091.5	x		x	x	x
2182.7	x		x		x
2225.2	x		x	x	x
2293.9	x	x	x	x	x
2323.1	(x)		x	x	x
2335.0			x	(x)	x
2454.4			x	x	x
2483.7			x	x	
2521.4	(x)		x	x	x
2641,1	x		x	x	x
2681.0	x		x	x	x
2693.9	x	x	x	x	x
2701.6	x		x	x	
2710.5	x		x		x
2775.2	x		x	x	(x)
2886.1			x	x	(x)

given in table III-4. They are listed in table VI-2. Included for comparison are beta intensities calculated from the beta-gamma coincidence measurements. The log ft values found by Ragaini et al[72] for the decay from the 2^- ground state of ^{124}I are also listed. The allowed values of J and π of the levels that are consistent with these log ft values are listed in column 6.

The log ft values listed in table VI-2 are about 3 larger than the usual log ft values quoted for different degrees of forbiddenness. That is

			Usual[41] log ft	From ^{124}Sb
Allowed	0,1	No	3-6	6-9
1st forbidden	0,1,2	Yes	6-10	9
2nd forbidden	2,3	No	10	?

The fact that the ^{124}Sb beta transitions are hindered by about a factor of 1000 and the ^{124}I beta transitions by about a factor of 100 can possibly be explained by considering the single particle configurations[78] of the initial and final nuclei.

^{124}Sb has one proton and 23 neutrons outside the doubly closed shell of 50 protons and 50 neutrons. These "extra core" nucleons couple together to give a ground state J^π value of 3^-. The simplest shell model description of this configuration is the coupling of a $d_{5/2}$ proton to an unpaired $h_{11/2}$ neutron produces a 3^- state, and the other 22 neutrons couple to form a 0^+ core. ^{124}I has 3 protons and 21 neutrons outside the doubly closed shell. These extra core nucleons couple to produce a 2^- ground state. In this case a $g_{7/2}$ unpaired proton couples to a $h_{11/2}$ unpaired neutron to give a 2^- state and the other 2 protons and 20 neutrons form a 0^+ core. The ground state

Table VI-2

Log ft values and most likely J^{π} assignments for levels in ^{124}Te

Level (KeV)	Beta feed from ^{124}Sb %		Log ft		J^{π}
	from γ inten.	from β^- inten.	^{124}Sb	^{124}I	
0	0	0	-	8.1	0^+
602.8	22.6	20	10.1	7.6	$1,2,3,4^+$
1248.8	2.5	5	9.4	9.8	$1,2,3,4^+$
1325.7	3.6	5	9.5	7.8	$1,2,3,4^+$
1657.2	.01	-	12.3	9.4	0^+
1957.7	1.7	5	9.7	9.7	$1,2,3,4^+$
2039.4	4.2		9.2	9.6	$1,2,3,4^+$
2091.5	.7		9.8	8.9	$1,2,3,4^+$
2182.7	.2		10.3	-	$1,2,3,4^+$
2225.2	.1		10.5	8.8	$1,2,3,4^+$
2293.9	54.0	50	7.7	6.9	$2,3^-$
2323.1	.06		10.5	8.6	$1,2,3,4^+$
2335.0	.04		10.6	10*	$1,2,3,4^+$
2454.4	.001		9-11	8.2	$1,2,3,4^+$
2483.7	.3		9.5	8.8	$1,2,3,4^+$
2521.4	.03		10,3	8.3	$1,2,3,4^+$
2641.1	.1		9.3	7.9	$1,2,3,4^+$
2681.0	1.0		8.2	7.8	$1,2,3,4^+$
2693.9	9.0	10	7.2	7.4	$2,3^-$
2701.6	.6		8.4	7.1	*
2710.5	.08		9.3	-	4^+
2775.2	.5		7.8	-	4^-
2886.1	.007		7.4	6.7	$2,3^-$

*See discussion in Section VI-3

particle configuration of ^{124}Te has no unpaired protons or neutrons and its 0^+ ground state particle configuration consists of 2 $g_{7/2}$ protons and 8 $g_{7/2}$, 6 $d_{5/2}$, and 8 $h_{11/2}$ neutrons.

A beta transition from ^{124}Sb to the ground state particle configuration of ^{124}Te requires that an ℓ=5 ($h_{11/2}$) neutron decays to an ℓ=4 ($g_{7/2}$) proton and and ℓ=3 ($d_{5/2}$) proton change to an ℓ=4 ($g_{7/2}$) proton. Both of these transitions are called ℓ-hindered and can produced hindrance factors as large as 1000.[79] On the other hand, a beta transition from ^{124}I to the ground state particle configuration of ^{124}Te only requires that an ℓ=4 ($g_{7/2}$) proton decay to an ℓ=5 ($h_{11/2}$) neutron and these transitions will not be hindered as much as the ^{124}Sb beta transitions.

VI-3 Spin and Parity Assignments

The allowed spin and parity (J^{π}) of the levels populated in the ^{124}Sb decay were deduced from the gamma transition intensities, conversion coefficients (table V-4), log ft values, and the results of references 72 to 77. The justification for each assignment is explained below. The identifying abbreviations $T(E)^{\sigma L}$ for an EL or ML transition of energy E, and $L(E)^{J\pi}$ for a level with spin J and parity π at excitation energy E are used in this discussion.

The levels are also discussed in terms of the simple vibrational model. The relative reduced branching ratios from the positive parity levels, and the relative transition probabilities from the negative parity levels, used in this section are derived in section VI-4 and are listed in tables VI-3 and VI-4 respectively.

602.8 KeV Level $J^{\pi} = 2^+$

This level is a well established 2^+ collective state.[74,76,77] It is interpreted to be the one quadrupole phonon state.

1248.8 KeV Level $J^{\pi} = 4^+$

The E2 transition [$T(646)^{E2}$] to the 2^+ 603 KeV level [$L(603)^{2+}$] limits J^{π} to 0^+, 1^+, 2^+, 3^+ or 4^+. The log ft=9.4 forbids the 0^+ assignment. Since there is no transition to ground the 1^+ and 2^+ assignments are ruled out. (α, α') measurements[80] give a 4^+ assignment and a large reduced transition rate. This level is therefore interpreted to be the 4^+ member of the 0^+, 2^+, 4^+ two quadrupole phonon triplet.

1325.7 KeV Level $J^{\pi} = 2^+$

The $T(723)^{E2}$ and $T(1325)^{E2}$ to $L(603)^{2+}$ and $L(0)^{0+}$ respectively restrict J^{π} to 1^+, 2^+. (α, α') experiments[80] require the 2^+ assignment. This level is interpreted as the 2^+ member of the two quadrupole phonon triplet as it decays preferentially to the one quadrupole phonon (603 KeV) state. That is, from table VI-3

$$\frac{B(E2;\ 2_2^+ \rightarrow 2_1^+)}{B(E2;\ 2_2^+ \rightarrow 0_0^+)} = 138$$

where J_j refers to a J^{π} state with j phonons. The single particle value for this ratio is close to one, while the simple vibrational model forbids transitions that change the phonon number by more than one.

1657.2 KeV Level $J^{\pi} = 0^+$

The evidence for this level is the weak T(1054) to $L(603)^{2+}$, $T(1657)^{E0}$ to $L(0)^{0+}$, and the results of the reaction measurements of Bushnell[75] and Auble and Ball.[74] Assuming that these transitions are

not misplaced, then the only J^{π} assignment consistent with these transitions and the log ft value is 0^+.

The log ft = 12.3 for the ^{124}Sb decay to this state was calculated by assuming that there were no weak gamma transitions populating this level that were not observed.

We interpret this level to be the 0^+ member of the two quadrupole phonon triplet, although it could be the 0^+ member of the three quadrupole phonon states. The two phonon assignment is more likely if the splitting of these two phonon states is the result of the coupling of the two extra core protons to the coherent vibrations of the 22 extra core neutrons, as is assumed by Lopac (see section II-4).

1957.7 KeV Level $J^{\pi} = 2^+(3^+, 4^+)$

The $T(1355)^{M1,E2}$ to $L(603)^{2+}$, $T(709)^{M1,E2}$ to $L(1248)^{4+}$, and $T(735)^{E1}$ from $L(2693)^{3-}$ restrict J^{π} to 2^+, 3^+, or 4^+. The weak $T(1957)$ to $L(0)^+$ would rule out all but the 2^+ assignment if this transition has not been misplaced.

This level is assumed to be a three quadrupole phonon state as it decays preferentially to the two phonon states (see table VI-3).

The reduced branching ratio to the two phonon states is

$$\frac{B(E2;J_3^+ \rightarrow 2_2^+)}{B(E2;J_3^+ \rightarrow 4_2^+)} = .16$$

The simple vibration model reduced transition rates from the three to two quadrupole phonon states (see A ppendix B, table 1).

$$\frac{B(E2;2_3^+ \rightarrow 2_2^+}{B(E2;2_3^+ \rightarrow 4_2^+)} = \frac{4/7\ K_2^2}{36/35\ K_2^2} = .55$$

$$\frac{B(E2;3_3^+ \rightarrow 2_2^+)}{B(E2;3_3^+ \rightarrow 4_2^+)} = \frac{15/7\ K_2^2}{6/7\ K_2^2} = 2.5$$

$$\frac{B(E2;4_3^+ \rightarrow 2_2^+)}{B(E2;4_3^+ \rightarrow 4_2^+)} = \frac{11/7\ K_2^2}{10/7\ K_2^2} = 1.1$$

The best description of the 1957 KeV level in terms of the simple vibrational model is that it is the 2^+ member of the 0^+, 2^+, 3^+, 4^+ and 6^+ three quadrupole phonon states.

2039.4 KeV Level $J^\pi = 3^+ (2^+, 4^+)$

The M1 or E2 transitions, T(1436), T(790) and T(714), to $L(603)^{2+}$, $L(1248)^{4+}$ and $L(1325)^{2+}$ restrict J^π to 2^+, 3^+, or 4^+. A weak transition to ground cannot be ruled out as, although the 2039 KeV transition was found in coincidence with the 603 KeV transition, the error in the intensity was large.

The experimental relative reduced branching ratios to $L(603)^{2+}$, $L(1248)^{4+}$ and $L(1325)^{2+}$ are 1:10.9:57.8. (See table VI-3.) The 2039 level is therefore assumed to be a three quadrupole phonon state. The best spin assignment from the viewpoint of simple vibrational model is 3^+ as indicated by the reduced branching ratios to the two phonon states. That is

Experimental	Theory		
	$J_3^+ = 2^+$	$J_3^+ = 3^+$	$J_3^+ = 4^+$
$\frac{57.8}{10.9} = 5.3$	.55	2.5	1.1

2091.5 KeV Level $J^\pi = 2^+(1^+)$

The $T(1489)^{M1,E2}$ to $L(603)^{2+}$ restricts J to 0^+, 1^+, 2^+, 3^+, or 4^+. The log ft of 9.2 from the 3^- ^{124}Sb ground state rules out 0^+.

The (n, γ) results of Bushnell[75] gives $J^{\pi} = 0^+, 1^+, 2^+$. A weak transition to ground from this level cannot be ruled out as it would be masked by the intense T(2091) from L(2693).

The radically different nature of this state compared to the three phonon states at 1957 and 2039 KeV is apparent from the relative reduced branching ratios from these three states as shown in table VI-3. As this level does not preferentially decay to the two phonon states it is assumed to be a two particle state. It could possibly be the $(g_{7/2})^2$ proton state, where the two protons have total spin 2, rather than 0, as is the case for the ground state.

2182.7 KeV Level $J^{\pi} = 1^+, 2^+$

The T(2182) to L(0)$^{0+}$ limits J^{π} to $1^{\pm}$ 2^+ 3^- (E3 transitions cannot be excluded). The log ft = 10.5 for the decay from the ^{124}Sb ground state indicates that the parity is positive. This limits the choice to 1^+ or 2^+.

A comparison of the reduced branching ratios from this level (see table VI-3) reveals its collective nature. Since the transitions to the two phonon states are enhanced over those to the one phonon and ground states, this level is probably mainly a three, or possibly a four quadrupole phonon state.

2225.1 KeV Level $J^{\pi} = 2^+, 3^+, 4^+$

The T(1622) to L(603)$^{2+}$, and T(976) to L(1248)$^{4+}$ implies that $2 \leq J \leq 4$. The log ft value of 10.5 requires a positive parity assignment to this level. The T(468), which is not M2 (from its conversion coefficient), from the well established L(2693)$^{3-}$ is consistent with the $J^{\pi} = 2^+, 3^+$, or 4^+ assignment.

This level is another multi quadrupole phonon state as it decays preferentially to the two phonon states. That is, the relative reduced branching ratios to the $L(603)^{2+}$, $L(1248)^{4+}$ and $L(1325)^{2+}$ are 1:42:7. It could be the 4^+ member of the three quadrupole phonon quintet.

2293.9 KeV Level $J^\pi = 3^-$

The $T(1691)^{E1}$, $T(1045)^{E1}$, and $T(968)^{E1}$ to the $L(603)^{2+}$, $L(1248)^{4+}$ and $L(1325)^{2+}$ respectively uniquely determine J^π to be 3-. This assignment is consistent with the log ft values and reaction studies.

This level is taken to be the one octupole phonon state. The reason for this assumption is that the $T(2293)^{E3}$ is enhanced over the $T(1691)^{E1}$, compared to the single particle estimates, by a factor of 3.5×10^4. [Table VI-4 lists the relative (not reduced) branching ratios of all the negative parity states populated in the ^{124}Sb decay in terms of single particle units normalized to the value one for transitions to the 603 KeV level.]

2323.1 KeV Level $J^\pi = 2^+$

T(2323) to $L(0)^{0^+}$ and the log ft for the ^{124}Sb decay of 10.5 set practical limits to J^π of 1^+ and 2^+. The T(371), which is not M2, from the $L(2693)^{3-}$ requires that T(371) is E1, as M1 or E2 transitions require $\Delta\pi = +1$. Therefore $J^\pi \neq 1^+$ and the 2^+ assignment is the only remaining choice.

It would seem likely, on the basis of the reduced branching ratios, that this level is a multi-quadrupole phonon state.

2335.0 KeV Level $J = 2^+, 3^+, 4^+$

This level is placed by T(1086) and T(1732) to the $L(1248)^{4+}$ and $L(603)^{2+}$, respectively. Ragaini, Walters and Meyer[72] find T(1086) in the ^{124}I decay but place it between a supposed level at 2412 KeV and

L(1325), as do Meyer, Walters and Ragaini[36] in their study of the ^{124}Sb decay. A level at 2.335 MeV is found in (p,p') scattering by Rao,[76] and a level at 2.34 MeV in the (^{3}He,d) reaction by Auble and Ball.[74] There is no evidence for a level at 2412 KeV in either of these experiments, or in the (n, γ) reaction studied by Bushnell.[75]

The possible J^π values are restricted to π = + from the log ft values and J=2,3 or 4 from T(1086) to L(1248)$^{4^+}$ and T(1732) to L(603)$^{2^+}$.

The relative reduced branching ratios (see table VI-3) indicate that L(2335) is a multi quadrupole phonon state because of its preferential decay to two phonon states over the one phonon state.

2454.4 KeV Level $J^\pi = 2^+ (1^+)$

The T(2454) to L(0)$^{0^+}$ and log ft = 10.6 are consistent with a J^π assignment of 1^+ or 2^+. The (^{3}He,d) reaction[74] populates a level at 2.45 MeV with J = 2^+ or 6^+. If these levels are the same the 1^+ assignment is ruled out.

No comment can be made about the nature of this level as weak transitions to the one and two quadrupole phonon states might exist but they were not found in this investigation. An upper limit on the intensities of these transitions of 50 (on the normalized scale of table II-4) would make the reduced branching ratios to the one and two phonon states greater than the reduced branching ratio to ground.

2483.7 KeV Level $J^\pi = 2^+, 3^+, 4^+$

The T(525)^{M1,E2} and T(444)^{M1,E2} to the positive parity L(1957) and L(2039) respectively, together with the log ft of 9.5 and 8.8 for the ^{124}Sb and ^{124}I beta decays limit the J^π possibilities to 1^+, 2^+, 3^+, or 4^+.

This level decays only to the three qudrupole phonon states at 1957

and 2039 KeV. A possible explanation is that this level is an almost pure four quadrupole phonon state. Since there is no 1^+ four phonon state the J^π value is 2^+, 3^+, or 4^+.

2521.4 KeV Level $J^\pi = 1^+, 2^+$

The log ft values of 10.3 and 8.3 for the ^{124}Sb and ^{124}I beta decay limit J^π to 1^+, 2^+, 3^+ or 4^+. The (n,γ) reactions[75] populates a level at 2522.7 with $J^\pi = 0^+$, 1^+ or 2^+. Assuming that these are the same levels, the assignment 1^+ or 2^+ would be correct.

The nature of this level will be discussed along with the L(2681)$^{2+}$.

2641.1 KeV Level $J^\pi = 3^+, 4^+ (1^+, 2^+)$

The position of this level is determined by the coincidence found between T(2039) and T(603). The log ft values limit J^π to 1^+, 2^+, 3^+ or 4^+. As no transition to L(0)$^{0+}$ was observed the 1^+ or 2^+ assignments seem unlikely, although they cannot be ruled out if this is a collective state that decays preferentially to the 2^+ one quadrupole phonon state. Transitions to the two quadrupole phonon states were not found but they could easily exist and be masked by large background in that energy region of the singles gamma spectrum (figure III-7).

2681.0 KeV Level $J^\pi = 2^+$

The T(2681) to L(0)$^{0+}$ and T(159)^{M1,E2} to L(2521)$^{J+}$, along with a log ft value of 8.2 for the ^{124}Sb beta decay require that J^π is 1^+ or 2^+. The (n,γ) reaction[75] populates a level at 2681.1 KeV with $J^\pi = 0^+$ or 2^+. The 2^+ assignment is therefore assumed.

Transitions from this level to L(2182) and L(2521) were found, which suggests some coupling between these levels that does not exist for other levels in this energy region. The relative E2 reduced branching ratios to the L(0)$^{0+}$, L(2182)$^{(4)+}$ and L(2521)$^{2+}$ are $1:4.5\times10^4 : 1.4\times10^7$.

T(159) may have a large M1 component which would make the reduced branching ratio of that transition smaller than 1.4×10^{7}. However, this transition would still be enhanced over the T(2681) to $L(0)^{0+}$. It is possible that this level is a mixture of collective and particle excitations, with the collective motion similar to that of L(2182) and the particle configuration similar to that of L(2521).

2693.9 KeV Level $J^{\pi} = 3^{-}$

The T(2693) to $L(0)^{0+}$, the $T(2091)^{E1}$ to $L(603)^{2+}$, and the log ft = 7.2 require that this level is 3^{-}.

In table VI-4, we see that the enhancement of the E3 transition to ground over the E1 transition to the one quadrupole state, $L(603)^{2+}$, is 2.0×10^{4}. This value is close to the enhancement of 3.6×10^{4} found for the E3 transition from $L(2293)^{3-}$, the one octupole phonon state. The $T(400)^{E2}$ that connects these two 3^{-} states is enhanced over the $T(2091)^{E1}$ by a factor of 1.1×10^{6}. The two enhanced transitions, $T(2693)^{E3}$ and $T(400)^{E2}$, are the only ones allowed by the simple vibrational model if $L(2693)^{3-}$ is the 3^{-} member of the one quadrupole-one octupole phonon quintet (1^{-}, 2^{-}, 3^{-}, 4^{-}, 5^{-}). We therefore assume that $L(2693)^{3-}$ has this character.

2701.6 KeV Level $J^{\pi} = 2^{-}, 3^{-}$

The $T(1376)^{E1}$ to $L(1325)^{2+}$ restricts J^{π} to 1^{-}, 2^{-}, or 3^{-}. The log ft of 8.4 for the ^{124}Sb decay to this level eliminates the 1^{-} assignment.

This level decays preferentially to the two quadrupole phonon states rather than the one quadrupole phonon state as is shown by the data in table VI-4. The enhancement of the $T(1376)^{E1}$ to $L(1325)^{2+}$ over $T(2098)^{E1}$ to $L(603)^{2+}$ suggests that L(2071) is possibly a two quadrupole-one

octupole state.

2710.5 KeV Level $J^{\pi} = 4^+$

The T(2107) and T(1384) to L(603)$^{2+}$ and L(1325)$^{2+}$, along with the log ft of 9.3 for the ^{124}Sb decay restrict J^{π} to 1^+, 2^+, 3^+, or 4^+. A level at 2.71 MeV with $J^{\pi} = 3^+$ or 4^+ is found in the (^{3}He,d) reaction.[74] The 4^+ assignment is assumed as this level is not populated by the beta decay from the 2^- ^{124}I ground state.

The T(1384) to the two phonon L(1325)$^{2+}$ is slightly favored over the T(2107) to the one phonon L(603)$^{2+}$ as shown in table VI-3. The possibility of a weak transition to L(1248)$^{4+}$ can not be excluded since a relatively large background peak occurs at this energy (1462 KeV). There is not enough information to attempt to interpret the character of this state.

2886.3 KeV Level $J^{\pi} = 2^-, 3^-$

The log ft of 7.4 for the ^{124}Sb decay and 6.7 for the ^{124}I decay exclude all J^{π} values except 2^-, 3^-. The only transition found from this level in the ^{124}Sb beta decay is the T(2283). Transitions to the two phonon levels from this level are found in the ^{124}I decay where the relative number of beta transitions to L(2886) is greater than in the ^{124}Sb decay.

VI-4 Summary of the Levels Populated in the ^{124}Sb → ^{124}Te Decay

a) Positive Parity Levels

The relative reduced branching ratios of all the positive parity states populated in the ^{124}Sb decay were calculated from the measured transition intensities by assuming that the transitions to other positive parity levels were pure E2. The only other transition multipolarity that is expected to be of any importance is M1 (see Appendix B).

M1 transitions are not allowed by the vibrational model, but may result from vibrational states mixing with particle states for high energy levels.[81] Because the reduced branching ratios have energy dependence E^{2L+1}, any M1 component is expected to be small except for low energy transitions.[82]

The relative reduced branching ratios were calculated using formula B-5, i.e.

$$R_1^2 = \frac{E_2^5 \, I_1}{E_1^5 \, I_2}$$

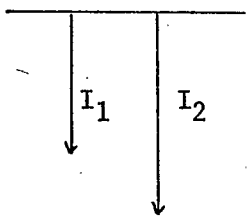

and the R's normalized to the transition to the 603 KeV level whenever it existed. The energies and intensities of the transitions were taken from table III-4. Table VI-3 lists the results of these calculations, which are shown schematically in figure VI-2.

The broad lines in figure VI-2 represent transitions whose reduced branching ratios are greater than 10% of the total for that level. These broad lines do not necessarily correspond to intense transitions. The dominant feature of this "reduced branching ratio decay scheme" is that most levels do not decay with approximately equal probability by all transitions that are allowed by spin and parity selection rules. These levels decay preferentially by lower energy transitions, supposedly to levels that differ by the fewest number of quadrupole phonons. The best examples of this feature are the enhanced transitions from the levels at 1325 KeV, 1957, 2039, and 2225 KeV and 2483 KeV, which are

Table VI-3

E2 Relative Reduced Branching Ratios

From Level (KeV)	To Level (KeV)	Reduced Branching Ratio	Phonon Assignment of Initial State
603(2+)	$0(0)^+$	1	one quadrupole phonon
1248(4^+)	603(2^+)	1	two quadrupole phonons
1325(2^+)	0(0^+)	1	two quadrupole phonons
	603(2^+)	138	
1657(0^+)	603(2^+)	1	two quadrupole phonons
1957(2^+)	0(0^+)	6.3×10^{-4}	three quadrupole phonons
	603(2^+)	1	
	1248(4^+)	30.0	
	1325(2^+)	4.7	
2039(3^+)	0(0^+)	*	three quadrupole phonons
	603(2^+)	1	
	1248(4^+)	10.9	
	1325(2^+)	57.8	
2091(2^+)	0(0^+)	*	(no phonons)
	603(2^+)	1	
	1248(4^+)	<.2	
	1325(2^+)	.4	
2182(1^+,2^+)	0(0^+)	.053	three quadrupole phonons and particle
	603(2^+)	1	
	1325(2^+)	3.1	
2225(2,3,4^+)	603(2^+)	1	three quadrupole phonons
	1248(4^+)	42.3	

Table VI-3 (Cont.)

	$1325(2^+)$	6.3	
$2323(2^+)$	$0(0^+)$	2.3×10^{-4}	four quadrupole phonons and particles
	$603(2^+)$	1	
	$1248(4^+)$	<.5	
	$1325(2^+)$	<.5	
$2335(2^+,3^+,4^+)$	$603(2^+)$	1	multi-quadrupole phonons
	$1248(4^+)$	31	
	$1325(2^+)$	<5	
$2454(2^+)$	0(0+)	1	particle state
$2483(2^+,3^+,4^+)$	$1957(2^+)$	1	four quadrupole phonons
	$2039(3^+)$	3.0	
$2521(1^+,2^+)$	$603(2^+)$	1	?
$2641(3^+,4^+)$	$603(2^+)$	1	?
$2681(2^+)$	$0(0^+)$	1	multi-quadrupole phonons and particles
	$603(2^+)$	*	
	$2\ 82(1^+,2^+)$	4.5×10^4	
	$2521(1^+,2^+,3^+,4^+)$	1.4×10^7	
$2710(4^+)$	$603(2^+)$	1	multi-quadrupole phonons
	$1248(4^+)$	<2	
	$1325(2^+)$	4.6	

* See discussion

Fig. VI-2

E2 Relative Reduced Branching Ratios

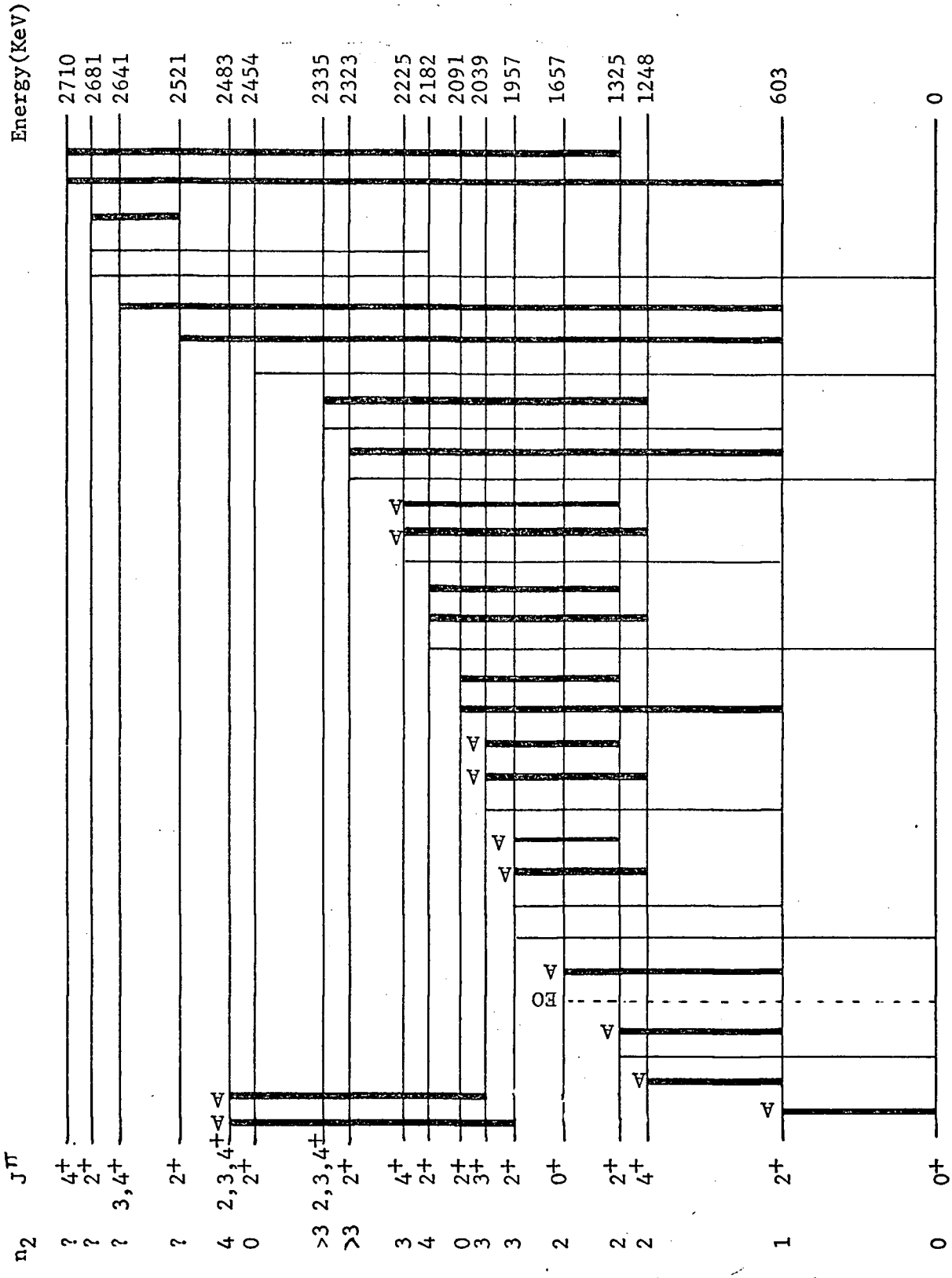

identified as 2, 3, and 4 quadrupole phonon states respectively. These transitions all have $\Delta n_2=1$ and are therefore allowed by the simple vibrational model described in Appendix A. They are labelled with an A (for allowed) in figure VI-2.

Other levels that are assumed to be mainly multi-quadrupole vibrational states of the ground state particle configeration are the 2182, 2323, 2335, and 2710 KeV levels. The selection rule, $\Delta n_2=1$, is not expected to be obeyed as well for transitions from these levels as it is for the lower phonon number levels because anharmonic terms are expected to be important.[5,6] One should also expect mixing of the ground state particle configuration with excited particle state configurations at these energies, and this would induce transitions between levels that differ by more than one quadrupole phonon.[14]

Levels that are not assumed to be quadrupole vibrations of the ground state particle configuration are the 2091, 2454, 2641, and 2681 KeV levels. These levels are assumed to be excited particle or "particle-hole" configurations. The 2681 KeV level is interesting in that it decays preferentially to the 2521 KeV level. It may be that it is a quadrupole phonon state of the 2521 KeV particle configuration, although there is no theoretical justification for this statement.

b) Negative Parity Levels

The intensities of transitions from the negative parity levels found in this investigation have been compared to the single particle estimates given in reference 83 by assuming that the transitions have the lowest allowed electric multipolarities. The transition intensities from each level were normalized so that the ratio of the experimental value to the single particle estimate for the transition

Table VI-4

Relative Rates of Transitions from Negative Parity States Compared to Single Particle Estimates

Level	Transition Multipolarity	To Level	Ratio
2293(3^-)	E3	0(0^+)	3.5×10^4
	E1	603(2^+)	1
	E1	1248(4^+)	.16
	E1	1325(2^+)	.21
	E1	1957(2^+)	.14
	E1	2039(3^+)	.07
2693(3^-)	E3	0(0^+)	2.0×10^4
	E1	603(2^+)	1
	E1	1248(4^+)	.15
	E1	1325(2^+)	1.7
	E1	1957(2^+)	.56
	E1	2225($2^+,3^+,4^+$)	.46
	E2	2293(3^-)	1.1×10^6
	E1	2323(2^+)	.90
2701($2^-,3^-$)	E1	603(2^+)	1
	E1	1325(2^+)	37
	E1	2039(3^+)	9.5
2775(4^-)	E3	603(2^+)	1
	E1	1248(4^+)	4.8×10^{-4}
	E3	1957(2^+)	5.6×10^6
2886($2^-,3^-$)	E1	603(2^+)	1

Fig. VI-3

Enhancement Factors for Transitions from Negative Parity States

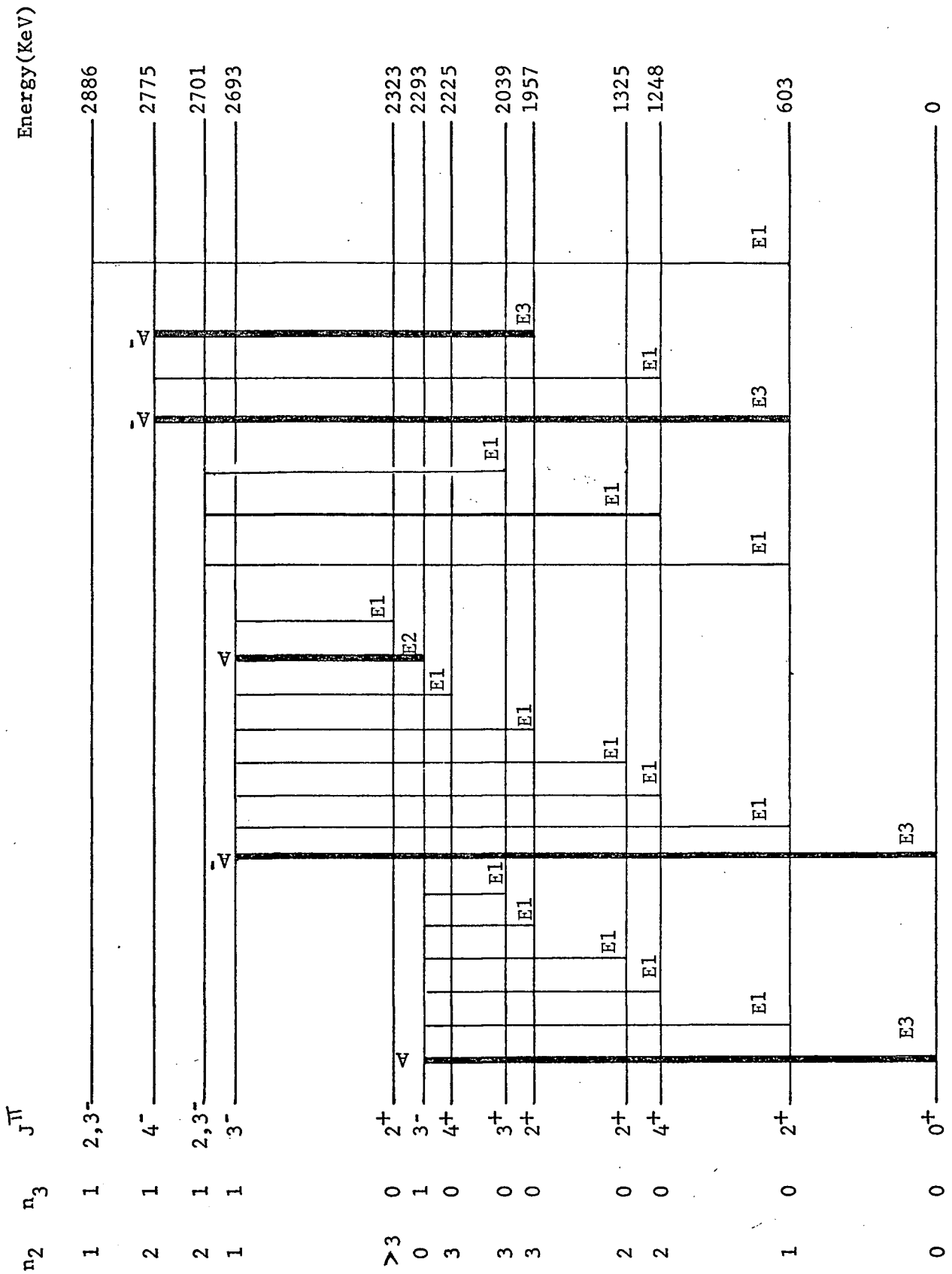

to the 603 KeV level was unity. The enhancement factor for the other transitions from a given level over the transition to the 603 KeV level is then compared to the single particle estimate

$$EH = \frac{I(E_B)_{exp}}{I(EL_B;E_B)_{sp}} \times N_{603}$$

The $I(E_B)_{exp}$ are the transition intensities listed in table III-4, $I(EL_B;E_B)_{sp}$ are the single particle estimates for EL_B transitions of energy E_B, and N_{603} is the normalizing factor. These enhancement factors are listed in table VI-4 and are displayed schematically in figure VI-3.

The broad lines connecting levels in figure VI-3 represent transitions that are enhanced over the single particle estimates by at least a factor of 100. The semi-broad lines represent transitions that are enhanced by factors of 10 to 100. Transitions allowed by the simple vibrational model with the phonon numbers given in the figure, are labelled A; i.e., $\Delta n_2=1$ or $\Delta n_3=1$. Transitions that are allowed when coupling between the quadrupole and octupole vibrations are taken into account, as described in Chapter II, are labelled A'. The selection rules in this case as $\Delta n_2=1$ and/or $\Delta n_3=1$. The 3^- level at 2293 is assumed to be the one-octupole vibrational state. The next 3^- level, at 2693, is assumed to be the 3^- member of the one quadrupole-one octupole states. The E3 transition to ground from this level is not allowed in the simple vibrational model without coupling but is allowed in the coupling model. It also has an enhanced E2 transition to the one-octupole state, which is allowed by the simple model.

The level at 2701 is assumed to be a two quadrupole-one octupole

state. The only evidence to support this assignment is its negative parity and slightly enhanced transition rates to the 2^+ quadrupole phonon state at 1325 KeV and the 3^- quadrupole phonon state at 2039 KeV.

The 4^- level at 2775 is also assumed to be a two quadrupole-one octupole state as the supposed E3 transitions to the 1 quadrupole level at 603 KeV and the three quadrupole level at 1957 are greatly enhanced.

The level at 2886 KeV may be a one quadrupole-one octupole state. It may also be a negative parity particle configuration.

VI-5 Comparison to the Semi-Microscopic Model

Figure VI-4 gives the comparison of the energies of the low energy positive parity states found in this investigation to those derived by Lopac using the semi-microscopic theory, as explained in section II-4. The 6^+ experimental level was not found in the ^{124}Sb decay but has been identified in (α, α') scattering[80] and $(\alpha, 2n)$ reactions.[84]

It is also possible to compare some reducing branching ratios to those calculated by Lopac. These are given in table VI-5. The experimental ratios were calculated from the ratios given in table VI-3. The theoretical ratios were calculated from the reduced transition probabilities given in table 4 of reference 14. These ratios are all infinite in the simple vibrational model theory.

It appears, from the energy levels of figure VI-4, and also from the reduced branching ratios in table VI-5, that this semi-microscopic theory gets progressively less accurate as the number of quadrupole phonons is increased. This trend is to be expected as Lopac has assumed that the excitations of the 22 extra-core neutrons can be ade-

Fig. VI-4

Comparison of experimental results to the semi-microscopic theory

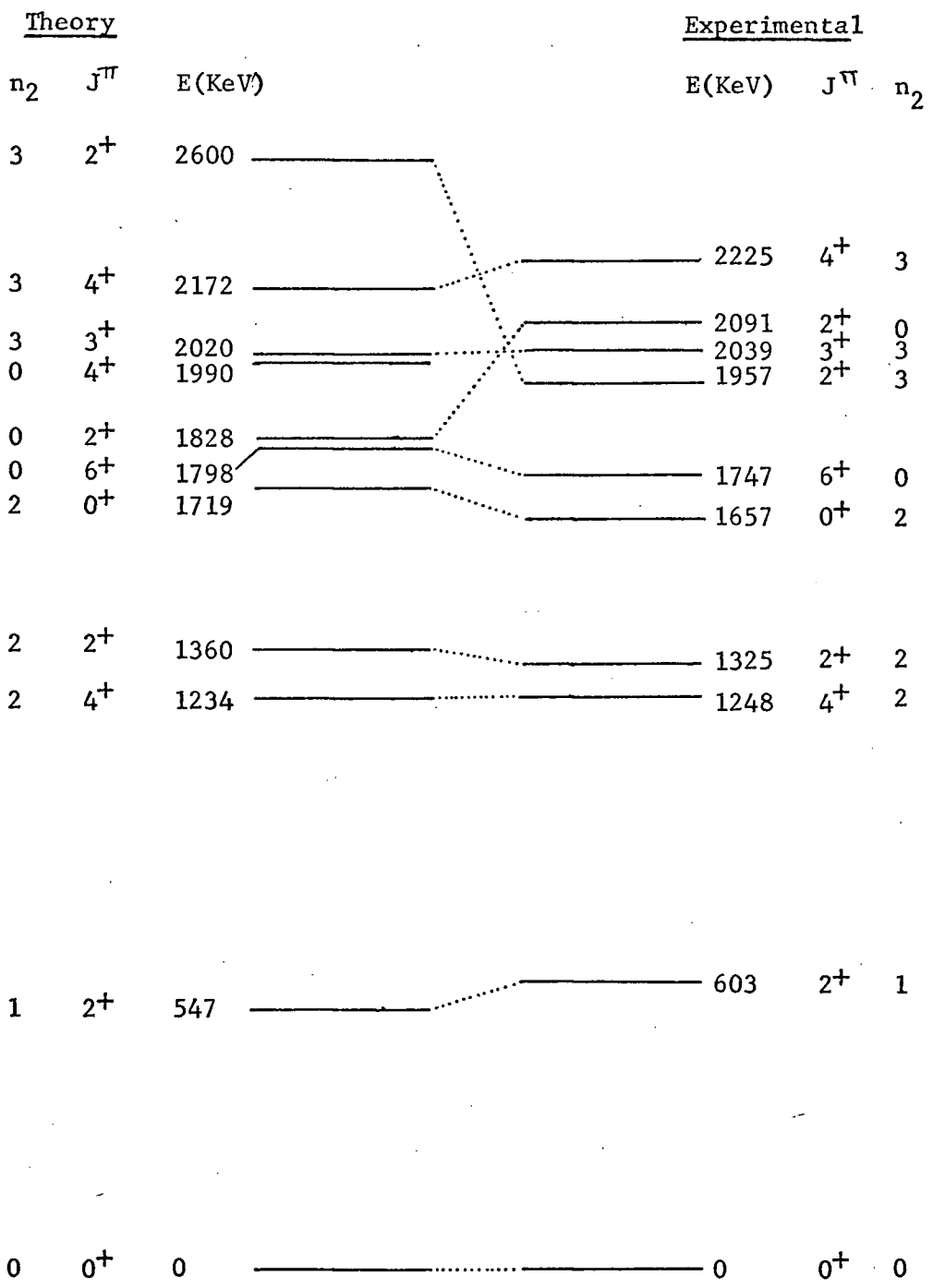

Table VI-5

Initial State(Kev)	Final States(Kev)		Ratios Experiment	Theory
1325(n_2=2)	603(n_2=1) 0(n_2=0)	$\frac{2_2^+ \rightarrow 2_1^+}{2_2^+ \rightarrow 0_0^+}$	138	290
2039(n_2=3)	1325(n_2=2) 603(n_2=1)	$\frac{3_3^+ \rightarrow 2_2^+}{3_3^+ \rightarrow 2_1^+}$	59.8	800
2225(n_2=3)	1325(n_2=2) 603(n_2=1)	$\frac{4_3^+ \rightarrow 2_2^+}{4_3^+ \rightarrow 2_1^+}$	6.3	∞
2091(n_2=0)	603(n_2=1) 1325(n_2=2)	$\frac{2_0^+ \rightarrow 2_1^+}{2_0^+ \rightarrow 2_2^+}$	2.5	2

quately described by simple harmonic quadrupole vibrations involving only the quadrupole states up to $n_2=3$. The interaction Hamiltonian he used coupled states that differ by one quadrupole phonon. Since he was only trying to reproduce the splitting of the $n_2=2$ (two quadrupole phonon) states, this assumption is valid. However, to reproduce the splitting of the three quadrupole phonon states, and to calculate their transition rates, one must include, at the very least, the four quadrupole phonon states.

VI-6 Conclusions

The levels populated in the beta decay of ^{124}Sb to ^{124}Te have all been assigned parity values on the basis of log ft values, conversion coefficients, and decay scheme considerations. In addition, many of the levels have been assigned definite spin values, and, for those that could not be assigned unambiguously, the choice has been narrowed to, at most, three different values.

The excited states of ^{124}Te populated in this decay have been discussed in terms of the vibrational model, which, as shown in sections VI-3 and VI-4, is adequate in describing the general features of this nucleus in a semiquantitative way. Quadrupole and octupole phonon numbers have been assigned to many of the excited states of ^{124}Te. Some of the assignments are fairly speculative. However, in spite of the fact that current theory for spherical "vibrational" nuclei such as ^{124}Sb is not by any means in such satisfactory shape as that for deformed "rotational" nuclei, it is possible to use it, as has been done in this thesis, to recognize and categorize, with some reasonable assurance, the types of excitations that exist. It is to be hoped that

in the near future, improvements in theory will lead to our further understanding of these interesting nuclei.

Appendix A

Phonon Number Representation for Vibrational States

A-1 Creation and Destruction Operators

Introduce the operators

$$a_{\lambda\mu} = A\,\alpha_{\lambda\mu} + iB\,\pi^{+}_{\lambda\mu} \qquad \text{A-1}$$

$$a^{+}_{\lambda\mu} = A\,\alpha^{+}_{\lambda\mu} - iB\,\pi_{\lambda\mu}$$

and require that

$$a^{+}_{\lambda\mu}\,a_{\lambda\mu}\,\Psi = n_{\lambda\mu}\,\Psi \qquad \text{A-2}$$

In these equations, $\alpha_{\lambda\mu}$ and $\pi_{\lambda\mu}$ are the generalized coordinates and conjugate momenta, respectively,[58] that describe the motion of the nuclear surface R, where

$$R = R_0\left(1 + \sum_{\lambda=2}^{\infty}\sum_{\mu=-\lambda}^{\lambda}\alpha_{\lambda\mu}\,Y_{\lambda\mu}(\theta,\phi)\right) \qquad \text{A-3}$$

$n_{\lambda\mu}$ is the number of 2^{λ}-pole phonons with orientation μ that are described by the state function Ψ.

The number of 2^{λ}-pole phonons is

$$N_{\lambda} = \sum_{\mu=-\lambda}^{\lambda} n_{\lambda\mu} \qquad \text{A-4}$$

that is,

$$\sum_{\mu} a^{+}_{\lambda\mu}\,a_{\lambda\mu}\,\Psi = N_{\lambda}\,\Psi \qquad \text{A-5}$$

With the proper choice of A and B in equation A-1, $a_{\lambda\mu}$ will destroy, and $a^{+}_{\lambda\mu}$ will create a $\lambda\,\mu$ type phonon when operating on Ψ.[58]

A-2 Energy Levels

By substituting equations A-1 into equation A-5 one gets

$$\sum_{\mu} [A^2 |\alpha_{\lambda\mu}|^2 + B^2 |\pi_{\lambda\mu}|^2 + iAB(\alpha^{\dagger}_{\lambda\mu}\pi^{\dagger}_{\lambda\mu} - \pi_{\lambda\mu}\alpha_{\lambda\mu})] = N_\lambda \qquad \text{A-6}$$

Now, using the relationships (given in chapter II)

$$\alpha^{\dagger}_{\lambda\mu} = (-1)^{\mu}\alpha_{\lambda-\mu} \; ; \; \pi^{\dagger}_{\lambda\mu} = (-1)^{\mu}\pi_{\lambda\mu} \qquad \text{A-7}$$

and the commutation relationship

$$[\alpha_{\lambda\mu}, \pi_{\lambda'\mu'}] = i\hbar\,\delta_{\lambda\lambda'}\,\delta_{\mu'\mu} \qquad \text{A-8}$$

equation A-6 becomes

$$\sum_{\mu} [A^2 |\alpha_{\lambda\mu}|^2 + B^2 |\pi_{\lambda\mu}|^2] - \hbar AB(2\lambda + 1) = N_\lambda$$

Multiplying by $\hbar\omega_\lambda$

$$\sum_{\mu} \hbar\omega_\lambda A^2 |\alpha_{\lambda\mu}|^2 + B^2 \sum_{\mu} \hbar\omega_\lambda |\pi_{\lambda\mu}|^2 = \omega_\lambda \hbar (N_\lambda + \hbar A B(2\lambda+1)) \qquad \text{A-9}$$

If equation A-7 is compared to the Hamiltonian of equation II-3

$$H_\lambda = \sum_{\mu} \frac{1}{2B_\lambda} |\pi_{\lambda\mu}|^2 + \sum_{\mu} \frac{C_\lambda}{2} |\alpha_{\lambda\mu}|^2 = \epsilon_\lambda \,,$$

one can make the identifications

$$\frac{1}{2B_\lambda} = \hbar\omega_\lambda B^2 \; ; \; \frac{C_\lambda}{2} = \hbar\omega_\lambda A^2 \qquad \text{A-10}$$

and using $\omega_\lambda = \frac{C_\lambda}{B_\lambda}$, one gets

$$\epsilon_\lambda = \omega_\lambda \hbar (N_\lambda + \frac{2\lambda + 1}{2}) \qquad \text{A-11}$$

which is the excitation energy of a state containing N_λ, 2^λ-pole phonons.

A-3 Commutation Relations for $a^{\dagger}_{\lambda\mu}$ and $a_{\lambda\mu}$.

From equation A-1, the commutation relationship is

$$\begin{aligned}[a_{\lambda\mu}, a^{\dagger}_{\lambda'\mu'}] = {} & A^2 (\alpha_{\lambda\mu}\alpha^{\dagger}_{\lambda'\mu'} - \alpha^{\dagger}_{\lambda'\mu'}\alpha_{\lambda\mu}) \\ & + B^2 (\pi^{\dagger}_{\lambda\mu}\pi_{\lambda'\mu'} - \pi_{\lambda'\mu'}\pi^{\dagger}_{\lambda\mu}) \\ & + iAB (\pi^{\dagger}_{\lambda\mu}\alpha^{\dagger}_{\lambda'\mu'} - \alpha^{\dagger}_{\lambda'\mu'}\pi^{\dagger}_{\lambda\mu} \\ & - \alpha_{\lambda\mu}\pi_{\lambda'\mu'} + \pi_{\lambda'\mu'}\alpha_{\lambda\mu})\end{aligned}$$

The first two terms are zero as $[\alpha_{\lambda\mu}, \alpha^{+}_{\lambda'\mu'}] = [\pi_{\lambda\mu}, \pi^{+}_{\lambda'\mu'}] = 0$. The third term can be written, with the aid of equations A-7 and A-8 as

$$[\, a_{\lambda\mu} \,,\, a^{+}_{\lambda'\mu'} \,] = iAB(\, [\, \pi_{\lambda-\mu}, \alpha_{\lambda'-\mu'}] + [\, \pi_{\lambda'\mu'}, \alpha_{\lambda\mu}])$$

$$= iAB(\, -i2\hbar\, \delta_{\lambda\lambda'}\, \delta_{\mu\mu'})$$

which, using equations A-10, reduces to

$$[\, a_{\lambda\mu} \,,\, a^{+}_{\lambda'\mu'} \,] = \delta_{\lambda\lambda'}\, \delta_{\mu\mu'} \qquad \text{A-12(a)}$$

It can be shown, in a similar manner, that

$$[a^{+}_{\lambda\mu}, a^{+}_{\lambda'\mu'} \,] = [a_{\lambda\mu} \,,\, a_{\lambda'\mu'} \,] = 0 \qquad \text{A-12(b)}$$

A-4 The Hamiltonian

The Hamiltonian of equation II-3 can be written as a function of the creation and destruction operators by solving euqations A-1 for $\alpha_{\lambda\mu}$ and $\pi_{\lambda\mu}$ and using A and B from equations A-10. That is, substituting

$$\alpha_{\lambda\mu} = \left(\frac{\hbar}{2\omega_\lambda B_\lambda}\right)^{1/2} (\, a_{\lambda\mu} + (-1)^{\mu} a^{+}_{\lambda-\mu}) \qquad \text{A-13}$$

and

$$\pi_{\lambda\mu} = i\left(\frac{B_\lambda \hbar\omega_\lambda}{2}\right)^{1/2} (\, a^{+}_{\lambda\mu} - (-1)^{\mu} a_{\lambda-\mu}) \qquad \text{A-14}$$

into

$$H_\lambda = \sum_{\mu} \frac{1}{2B_\lambda} |\pi_{\lambda\mu}|^2 + \sum_{\mu} \frac{C_\lambda}{2} |\alpha_{\lambda\mu}|^2$$

gives

$$H_\lambda = \frac{\omega_\lambda \hbar}{2} \sum_{\mu} (\, a^{+}_{\lambda\mu} a_{\lambda\mu} + a^{+}_{\lambda-\mu} a_{\lambda-\mu} + 1) \qquad \text{A-15}$$

A-5 State Functions

The state functions, represented by Ψ in equation A-2, can be expressed in terms of the creation and destruction operators, $a^{+}_{\lambda\mu}$ and $a_{\lambda\mu}$, operating on the vacuum state, $|0\rangle$. The vacuum state is, of course, the ground state.

A state containing one $\lambda\mu$ type phonon can be written as

$$a^{+}_{\lambda\mu}|0\rangle$$

The spin of this state[59] will be $J = \lambda$ and the parity, $\pi = (-1)^{\lambda}$.

A state containing two phonons can be written as[60]

$$C_{12}\, a^{+}_{\lambda_1 \mu_1}\, a^{+}_{\lambda_2 \mu_2} |0\rangle$$

where C_{12} represents the sum over the appropriate vector addition coefficients. The allowed values of angular momentum (J) and parity (π) of these states are

$$|\lambda_1 - \lambda_2| \leq J \leq \lambda_1 + \lambda_2$$

$$\pi = (-1)^{\lambda_1}(-1)^{\lambda_2}$$

States with three phonons will be

$$C_{123}\, a^{+}_{\lambda_1 \mu_1}\, a^{+}_{\lambda_2 \mu_2}\, a^{+}_{\lambda_3 \mu_3} |0\rangle$$

with the restrictions on J given by

$$|J' - \lambda_3| \leq J \leq J' + \lambda_3$$

where J' is the intermediate angular momentum[60] of the coupling of λ_1 and λ_2 with restrictions

$$|\lambda_1 - \lambda_2| \leq J' \leq \lambda_1 + \lambda_2$$

The parity of the three phonon state is given by

$$\pi = (-1)^{\lambda_1}\ (-1)^{\lambda_2}\ (-1)^{\lambda_3}$$

The allowed values of J for states with two or more phonons will be reduced by symmetry considerations if any two phonons are indistinguishable. That is, since the phonons have integer spin and therefore must obey Bose-Einstein statistics,[61] the state functions must remain the same if the two indistinguishable phonons are exchanged.

The state functions describing the lower energy states, which involve only quadrupole and octupole phonons, are written explicitly below. The notation used is $|j_2 n_2 j_3 n_3 JM\rangle$, which is a state containing n_2 quadrupole phonons coupled to give a spin j_2, n_3 octupole phonons coupled to give a spin j_3, and j_2 and j_3 coupled to give a total spin of J, with projection

onto the quantization axis, M.

$n_2 = 1 \quad n_3 = 0$

$$|2_1\ 002M\rangle = a^{\dagger}_{2M}\,|0\rangle$$

$n_2 = 2 \quad n_3 = 0$

$$|J200JM\rangle = \frac{1}{\sqrt{2}} \sum_m C(22J;\ m\ M\text{-}m) \times a^{\dagger}_{2m}\, a^{\dagger}_{2M-m}\,|0\rangle$$

The convention used to write the Clebsch-Gordon coefficients

$$C(22J;\ m\ M\text{-}m) = C(\lambda_1\ \lambda_2\ J;\ \mu_1\ M\text{-}\mu_1) \qquad M = \mu_1 + \mu_2$$

is that of Rose.[60]

The restrictions on J from the symmetry requirements can be deduced from the following considerations.

The interchange of phonons does not affect $a^{\dagger}_{2m}$ $a^{\dagger}_{2M-m}$, as they commute for all m and M-m (see equation A-12(b)). The Clebsch-Gordon coefficients have the symmetry property[60]

$$C(j_1 j_2 J;\ m_1\ M\text{-}m_1) = C\ (j_1 j_2 J;\ m_1 m_2 M) = (-1)^{j_1 + j_2 - J}\ C\ (j_2\ j_1\ J;\ m_2\ m_1\ M)$$

The interchange of phonons will therefore have the effect of multiplying $|J200JM\rangle$ by $(-1)^{j1\ +\ j2-J}$, and J must be even for the function to be symmetric. The allowed values of J are 0, 2, and 4. The parities of these 3 degenerate states will be positive.

$n_2 = 3 \quad n_3 = 0$

$$|J300JM\rangle = [\ 2+4\ (2J'+1) \begin{Bmatrix} 22J \\ J'2J \end{Bmatrix}]^{-\frac{1}{2}} \times \sum_{\nu} \sum_{\sigma} [\ C\ (2J'J;\ \sigma\ M\text{-}\sigma\ )\ C\ (22J;\ \nu\ \sigma\text{-}\nu\ )\ ] \times a^{\dagger}_{2M-\sigma}\, a^{\dagger}_{2\sigma-\nu}\, a^{\dagger}_{2\nu}\,|0\rangle$$

The $\begin{Bmatrix} \ \end{Bmatrix}$ is a six-j symbol[62] (Racah coefficient).

Fig. A-1

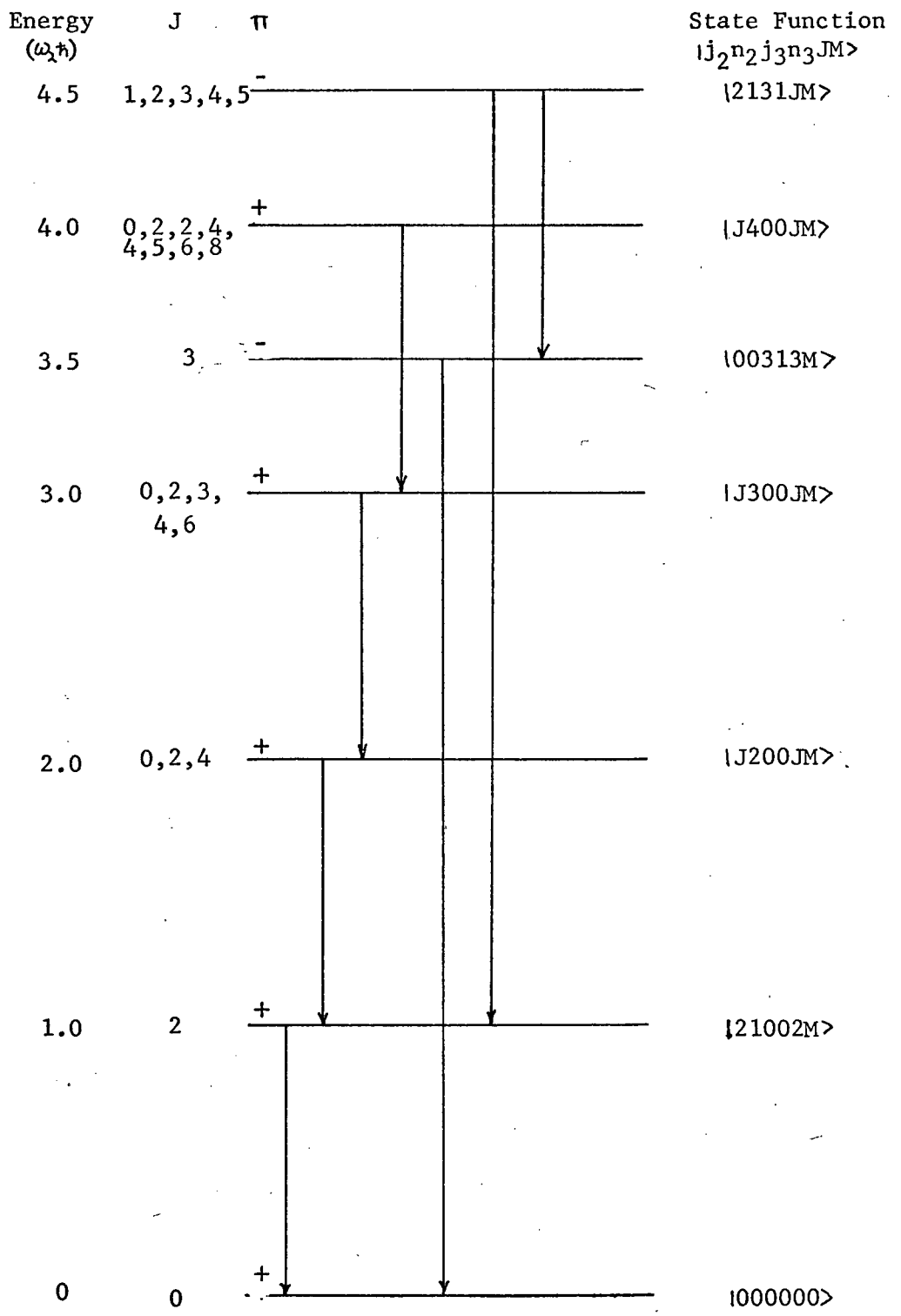
Energy
(ω₁ħ)
J
π
State Function
|j₂n₂j₃n₃JM>
4.5
1,2,3,4,5
-
|2131JM>
4.0
0,2,2,4,
4,5,6,8
+
|J400JM>
3.5
3
-
|00313M>
3.0
0,2,3,
4,6
+
|J300JM>
2.0
0,2,4
+
|J200JM>
1.0
2
+
|21002M>
0
0
+
|000000>

It has been shown[63] that the values of J not allowed by symmetry considerations are 1 and 5. The allowed values of J for this state are 0, 2, 3, 4 and 6. The parity is, of course, positive.

$n_2 = 0 \quad n_3 = 1$

$$|00313M\rangle = a^{\dagger}_{3M}|0\rangle$$

The spin is 3 and parity is negative.

$n_2 = 1 \quad n_3 = 1$

$$|2131\,J\,M\rangle = \frac{1}{\sqrt{2}} \sum_{m} C\,(23J;\, m\; M\text{-}m)\; a^{\dagger}_{2m}\; a^{\dagger}_{3M-m}\; |0\rangle$$

The allowed values of J in this case are 1, 2, 3, 4 and 5, and the parity is negative.

$n_2 = 4 \quad n_3 = 0$

The allowed values of J for this case are[64] 0, 2,2, 4,4, 5, 6, 8 and the parity is positive.

A spectrum of these states is shown in figure A-1. The ratio $\omega_3/\omega_2 = 3.5$ was chosen as this is approximately the ratio of the energies of the first 3- state to the first 2+ state found in ^{124}Te. The transitions between these states that are allowed by the simple vibrational model, which will be determined in Appendix B, are also shown.

Appendix B

Electromagnetic Transitions

B-1 General Considerations

The probability for a transition from a state $|J_i\ M_i \pi_i>$ to a state $|J_f\ M_f\ \pi_f>$ with the emission of a photon with angular momentum L is, for the long wavelength approximation[65]

$$T^{\sigma}_{LM} = \frac{8\ \ (L+1)}{L\ [(2L+1)!!]^2}\ \ \frac{k^{2L+1}}{\hbar}\ |<J_f M_f \pi_f|\ \mathcal{M}^{\sigma}_{LM}\ |J_i M_i \pi_i>|^2 \qquad \text{B-1}$$

$|J_i M_i \pi_i>$ and $|J_f M_f \pi_f>$ refer to the spin, spin projection, and parity of the initial and final states respectively. k is the wave number, related to the energy difference (E) between the initial and final states by $E=\hbar ck$.

The long wavelength approximation requires that $kR \ll 1$, where R is the radius of the radiating body; for example, the radius of the nucleus for nuclear transitions. The approximation is valid whenever the spherical Bessel functions, $j_L(k,r)$, which are contained in the multipole operators, $\mathcal{M}^{\sigma}_{LM}$, can be adequately represented by[66]

$$j_L(kr) = \frac{(kr)^L}{(2L+1)!!}$$

for all r such that the reduced transition probabilities

$$B(\sigma L;\ J_i M_i \rightarrow J_f M_f) = |<J_f M_f \pi_f|\ \mathcal{M}^{\sigma}_{LM}\ |J_i M_i \pi_i>|^2 \qquad \text{B-2}$$

are non-vanishing.

This expression described the reduced transition probability for a transition from a given substate M_i of J_i to a given substate M_f of J_f. A more useful quantity, for most cases, is the reduced transition probability for transitions from all the substates of J_i to all the substates of J_f.

This probability is the sum over the final states and the average over the initial states.[67] That is

$$B(\sigma L;\ J_i \rightarrow J_f) = \frac{1}{2J_i+1} \sum_{M_i=-J_i}^{J_i} \sum_{M_f=-J_f}^{J_f} B(\sigma L;\ J_i M_i \rightarrow J_f M_f) \qquad \text{B-3}$$

The values of L and M of the multipole operator for which the $B(\sigma L;\ J_i \rightarrow J_f)$ will be non-zero can be deduced from angular momentum conservation to be

$$|J_f - J_i| \leq L \leq J_f + J_i \qquad \text{B-4}$$

$$M_i + M = M_f$$

Parity must also be conserved, and therefore terms in $\mathcal{M}^{\sigma}_{LM}$ that do not have parity $\pi = \pi_i \times \pi_f$ will not contribute in the calculation of $B(\sigma L;\ J_f \rightarrow J_i)$. $\mathcal{M}^{\sigma}_{LM}$ can be divided into two parts[67] for each value of allowed L, one with parity $(-1)^L$ and the other with parity $(-1)^{L+1}$. If $\pi_i \pi_f = (-1)^L$, then only the part of $\mathcal{M}^{\sigma}_{LM}$ with this parity will contribute. In this case, $\mathcal{M}^{\sigma}_{LM}$ is called an electric 2^L-pole operator and written as $\mathcal{M}^{E}_{LM}$. The transition is called an electric 2^L-pole transition and is given the identification, EL. For instance, if L=2, π =1, the $\mathcal{M}^{E}_{2M}$ is an electric quadrupole operator and the transition is E2. Similarly, if $\pi_i \times \pi_f = (-1)^{L+1}$, only the part of $\mathcal{M}^{\sigma}_{LM}$ with this parity will contribute. These terms are called magnetic; that is, for L=2, π = -1, $\mathcal{M}^{M}_{2M}$ is a magnetic quadrupole operator and the transition is M2.

The total transition probability from a state with spin J_i to one with spin J_f, with the emission of a photon with any of the allowed values of L is

$$T(J_i \rightarrow J_f) = \sum_L T^{\sigma}_{LM}$$

$$= \sum_L \frac{8\pi(L+1)}{L[(2L+1)!!]^2} \frac{k^{2L+1}}{(2J_i+1)} \sum_{M_i} \sum_{M_f} |\langle J_f M_f \pi_f | \mathcal{M}^{\sigma}_{LM} | J_i M_i \pi_i \rangle|^2$$

The individual T_{LM} will alternate between electric and magnetic terms as $\mathcal{M}^{E}_{LM}$ and $\mathcal{M}^{M}_{LM}$ have opposite parity. The relative sizes of the T_{LM}'s can be shown, quite generally, to depend on k and R as[67]

$$T^{E}_{LM} \propto (kR)^{2L}$$

for electric transitions and

$$T^{M}_{LM} \propto (kR)^{2L+2}$$

for magnetic transitions. Therefore, since $kR \ll 1$ in this approximation, only the first term in the sum need be considered if it is electric and only the first two need be considered if the first is magnetic.

The multipolarities of transitions between states $|J_i M_i \pi_i\rangle$ and $|J_f M_f \pi_f\rangle$ with the emission of a photon with angular momentum L are tabulated below for spin changes up to $|J_f - J_i| = 3$.

$\lvert J_f - J_i \rvert$	$\pi_i \pi_f$	Multipolarity (σ L)
0	1	(E0) M 1 + E 2
	-1	(M0) E 1
1	1	M 1 + E 2
	-1	E 1
2	1	E 2
	-1	M 2 + E 3
3	1	M 3 + E 4
	-1	E 3

E0 and M0 electromagnetic transitions cannot take place with the emission of a photon as the minimum allowed photon angular momentum is $\hbar$[68]. Also, as the maximum allowed L is $J_f + J_i$, no photons can be emitted in $J_i=0 \rightarrow J_f=0$ transitions. These transitions may take place only with the emission of conversion electrons, or if the energy difference is large enough ($\geq 2M_o c^2$), electron-positron pairs.

Experimental transition rates are usually compared to theoretical transition probabilities by comparing ratios of reduced branching ratios to ratios of reduced transitions probabilities. That is, for transitions 1 and 2 in the decay scheme

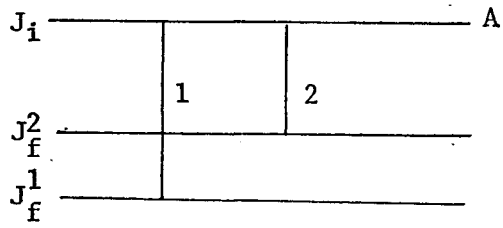

the ratio

$$\frac{b_A^1}{b_A^2} \propto \frac{(k_2)^{2L_2+1}}{(k_1)^{2L_1+1}} \qquad \text{B-5}$$

is compared to the ratio

$$\frac{B(\sigma L_1;\ J_i \rightarrow J_f^1)}{B(\sigma L_2;\ J_i \rightarrow J_f^2)} \qquad \text{B-6}$$

The b_A's are the branching ratios defined in Chapter IV and the B's and the reduced transition probabilities given in equation B-3. These comparisons are often a critical test of the model used to calculate the reduced transition probabilities.[69]

B-2 Simple Vibration Model Transitions

The multipole operators for transitions between collective states can be written as[70]

$$\mathcal{M}^{\epsilon}_{LM} = \int \rho(\underline{r})\ r^L\ Y^*_{LM}(\theta,\phi)\ d\underline{r} \qquad \text{B-7}$$

$$\mathcal{M}^{M}_{LM} = \frac{-i}{L+1}\left(\frac{4\pi}{2L+1}\right)^{\frac{1}{2}} \int \underline{L}\, r^{L}\, Y^{*}_{LM}(\theta,\phi) \cdot \underline{j}(\underline{r})\, d\underline{r} \qquad \text{B-8}$$

$\rho(\underline{r})$ is the charge density, $\underline{j}(\underline{r})$ is the current density, and $\underline{L}$ is the photon angular momentum operator ($= -i\, \underline{r} \times \underline{\nabla}$).

With the assumptions of the simple vibrational model given in Chapter II,

$$\rho(\underline{r}) = \frac{3\,Ze}{4\pi R_o^3}$$

and

$$\underline{j}(\underline{r}) = \frac{\rho(\underline{r})}{c}\ \underline{V}(\underline{r})$$

where $\underline{V}(\underline{r})$ is the velocity density given by[71]

$$\underline{V}(\underline{r}) = \tfrac{1}{2} \sum_{\lambda} \sum_{\mu} \dot{\alpha}_{\lambda\mu}\, \underline{\nabla}\, r^{\lambda} Y_{\lambda\mu}(\theta,\phi)$$

The electric multipole operators can easily be evaluated.

$$\mathcal{M}^{E}_{LM} = \frac{3\,Ze}{4\pi R_o^3} \int_{\Omega}\int_{0}^{R} r^{L+2}\, Y^{*}_{LM}(\theta,\phi)\, d\Omega$$

where R is the nuclear radius defined in equation A-3. Therefore

$$\mathcal{M}^{E}_{LM} = \frac{3\,Ze}{4\pi}\ \frac{R_o^L}{L+3} \int_{\Omega} \left(1 + \sum_{\lambda}\sum_{\mu} \alpha_{\lambda\mu} Y_{\lambda\mu}\right)^{L+3} Y^{*}_{LM}\, d\Omega$$

which, to first order in $\alpha_{\lambda\mu}$, becomes

$$\mathcal{M}^{E}_{LM} = \frac{3\,Ze\,R_o^L}{4\pi}\, \alpha_{\lambda\mu}$$

using the transformation of equation A-13 this becomes

$$\mathcal{M}^{E}_{LM} = K_L\,(a_{LM} + (-1)^{M}\, a_{L-M}) \qquad \text{B-9}$$

with

$$K_L = \frac{3\,Ze\,R_o^L}{4\pi}\left(\frac{\hbar}{2\omega_L B_L}\right)^{\frac{1}{2}}$$

The magnetic operators are much more difficult to evaluate. The results of reference 71 quoted by Davidson[70] for λ-type surfaces is

$$\mathcal{M}^{M}_{LM} = \frac{-3\,Ze\,i}{8\pi c}\, k\, R_o^{L+1} \left[\frac{L(L+2\lambda+1)(2\lambda-1)}{L+1}\right]^{\frac{1}{2}} C(L\ \lambda-1\ \lambda;\ 000) \times \sum_{\nu} (-1)^{\nu}\, \dot{\alpha}_{\lambda\mu}\, \dot{\alpha}^{+}_{\lambda\, M-\nu}\, C(L\,\lambda\,\lambda;\ M\ -\nu\ M-\nu) \qquad \text{B-10}$$

The $\dot{\alpha}^{+}_{\lambda M-\nu}$ (and the $\dot{\alpha}_{\lambda\mu}$) can again be expressed in terms of the creation and destruction operators given in Appendix A.

$\mathcal{M}^{E}_{LM}$ will only connect states that differ by one phonon. That is, transitions will only occur between $|j_2 n_2 j_3 n_3 JM\rangle$ states (see Appendix A) for which $\Delta n_2 = 1$ or $\Delta n_3 = 1$, but not both. These allowed transitions are shown in figure A-1. Furthermore, since $\mathcal{M}^{M}_{LM}$ depends on $C\ (L\ \lambda-1\ \lambda;000)$ which is non-zero only if $L + \lambda - 1 + \lambda$ is even, and since $\lambda \geq 2$, the lowest order magnetic multipole transitions are octupole.

The reduced transition probabilities between the states given in Appendix A using the electric multipole operators of equation B-9 were calculated. The results are tabulated in table B-1. Two sample calculations are given below.

a) Transitions from one-phonon states to the ground state

$|21002M\rangle \xrightarrow{E2} 0$ or $|00313M\rangle \xrightarrow{E3} 0$

$$B(EL;J\to 0) = \frac{1}{2J+1} \sum_{m} |\langle 0|\mathcal{M}^{E}_{LM_L}\, a^{+}_{JM_J}|\ 0\rangle|^2$$

$$= \frac{K_L^2}{2J+1} \sum_{m} |\langle 0|\, a_{LM_L}\, a^{+}_{JM}|0\rangle|^2$$

from equation A-12

$$a_{LM_L}\, a^{+}_{JM_J} = \delta_{JM}\delta_{M_L M_J} + a^{+}_{JM_J}\, a_{LM_L}$$

therefore

$$B(EL;J\to 0) = K_L^2 \qquad \text{B-11}$$

b) Transitions from two phonon states to one phonon states

$$|2200 J_i M_i\rangle \longrightarrow |21002M\rangle$$

Only E2 transitions are allowed.

$$B(E2; J_i \to 2) = \frac{1}{2J_i+1} \sum_{M_i} \sum_{M_f} |\langle 0 | a_2 \, m^E_{LM}$$

$$\times \frac{1}{\sqrt{2}} \sum_{\mu} C(22J_i; \mu M_i - \mu) \, a_2^+ \, a^+_{2M_i - \mu} |0\rangle|^2 \qquad \text{B-12}$$

The matrix element can be reduced with the aid of the Wigner-Eckhart theorem,[60] which states that

$$\langle J_f M_f | T_{LM_L} | J_i M_i \rangle = C(J_i L J_f; M_i M_L M_f) \times \langle J_f | T_L | J_i \rangle$$

Therefore equation B-12 becomes

$$B(E2; J_i \to 2) = \frac{K_2^2}{2(2J_i+1)} \sum_{M_i M_f} |C(J_i 22; M_i M_L M_f)|^2$$

$$\times |\langle 0 \, a_2 a_2 a^+ a_2^+ |0\rangle|^2 \qquad \text{B-13}$$

The Clebsch-Gordon coefficients have the symmetry property[60]

$$C(j_1 j_2 j_3; m_1 m_2 m_3) = (-1)^{j_1 - m_1} \left(\frac{2j_3+1}{2j_2+1}\right)^{\frac{1}{2}}$$

$$\times C(j_3 j_1 j_2; m_3, -m_1 m_2)$$

and orthogonality

$$\sum_{m_1} |C(j_1 j_2 j_3; m_1 m_2 m_3)|^2 = 1$$

Therefore the sum over M_f in B-13 is one. [The symmetry condition is used because the number of final substates is always the same for these transitions, whereas the number of initial states varies with J_i.]

The commutation relations (equations A-12) for the creation and destruction operators can be used to achieve the result

Table B-1

Initial State			Final State			Multipolarity	Reduced Transition Rate
n_2	n_3	J^π	n_2	n_3	J^π		
1	0	2^+	0	0	0^+	E2	K_2^2
2	0	$0^+,2^+,4^+$	1	0	2^+	E2	$2K_2^2$
3	0	0^+	2	0	2^+	E2	$3K_2^2$
3	0	2^+	2	0	0^+	E2	$7/5K_2^2$
3	0	2^+	2	0	2^+	E2	$4/7K_2^2$
3	0	2^+	2	0	4^+	E2	$36/35K_2^2$
3	0	3^+	2	0	2^+	E2	$15/7\ K_2^2$
3	0	3^+	2	0	4^+	E2	$6/7\ K_2^2$
3	0	4^+	2	0	2^+	E2	$11/7\ K_2^2$
3	0	4^+	2	0	4^+	E2	$10/7\ K_2^2$
0	1	3^-	0	0	0^+	E3	K_3^2
1	1	$1^-,2^-,3^-,4^-,5^-$	0	1	3^-	E2	K_2^2
1	1	$1^-,2^-,3^-,4^-,5^-$	1	0	2^+	E3	K_3^2

that

$$a_2 a_2 a_2^+ a_2^+ = a_2 a_2^+ + a_2 a_2^+ a_2 a_2^+$$

$$= 2 + 3a_2^+ a_2 + a_2^+ a_2 a_2^+ a_2$$

Therefore equation B-13 reduces to

$$B(E2;J_i \quad 2) = \frac{K_2^2}{2(2J_i+1)} \sum_{M_i} |2|^2$$

$$= 2K_2^2 \qquad \text{B-14}$$

This simple result could have deduced from the fact that there are two phonons in the $n_2=2$ state, and either one of them could cause the transitions to the $n_2=1$ state; whereas there is only one phonon to cause transitions between the $n_2=1$ and $n_2=0$ states. Therefore a transition from a two phonon state to a one phonon state is twice as probable as a transition from the one phonon state to the ground state.

Appendix C

Beta Spectra of ^{152}Eu

^{152}Eu decays by electron emission (β^-) to ^{152}Gd and by positron emission (β^+) and electron capture to ^{152}Sm with a lifetime of 12 years.[40] The gamma transitions following these decays have been studied in this laboratory to T.G. Walton.[48] The β^+ spectra have been measured by C.R. Brown,[49] also in this laboratory, using a magnetic spectrometer. It was felt that an analysis of the β^- spectra using a Si(Li) detector would be useful for completeness, and also as a check on the usefulness and accuracy of this type of β^- analysis. A short summary of the procedure used and the results obtained follows.

The β^- transitions that populate the different excited states of ^{152}Gd were identified by obtaining coincidence spectra of electrons (using the 3mm Si(Li) detector as the gate detector) in coincidence with gamma transitions selected with the 30cc Ge(Li) detector (used as the gate detector). The gamma transitions used as gates are shown in figure C-1. The electronics used were those shown in figure IV-1.

Coincidence spectra were taken for each gate with and without an absorber between the Si(Li) detector and source so that the Compton background could be subtracted. The difference spectrum between the two spectra for each gate was corrected for scattering and the shape factors and end-point energies found as described in Chapter V. The Kurie plots of the five β^- transitions found are shown in figure C-2(a) and (b). The results are listed in table C-1.

The relative intensities of the five β^- transitions was difficult to calculate from the coincidence spectra as different intensity sources and source-detector geometry was used to minimize the random rates for each gate.

Fig. C-1

Partial Decay Scheme of ^{152}Eu(Ref.48)

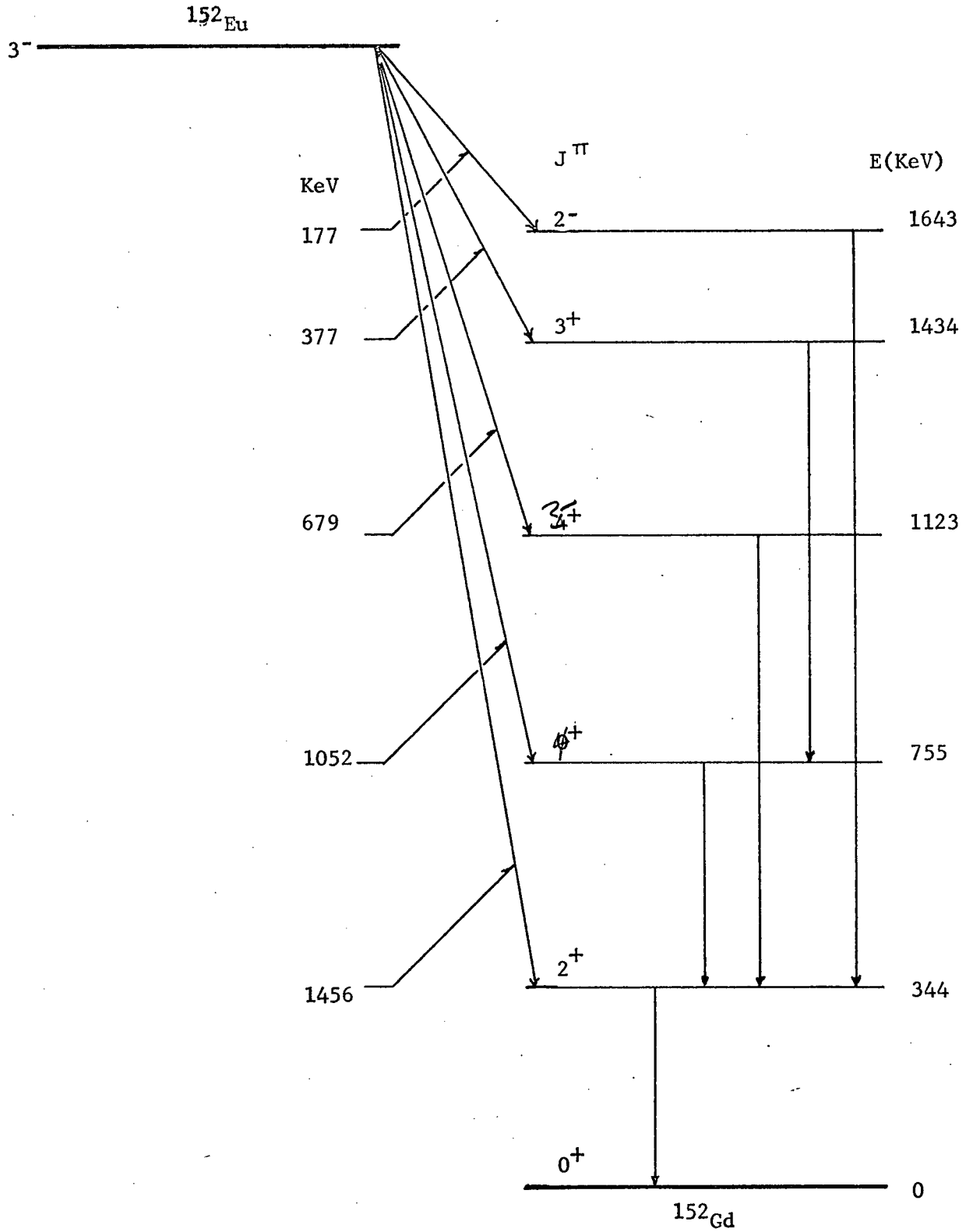

Fig. C-2(a)

Kurie Plots of $^{152}Eu\,\beta^-$ Spectra

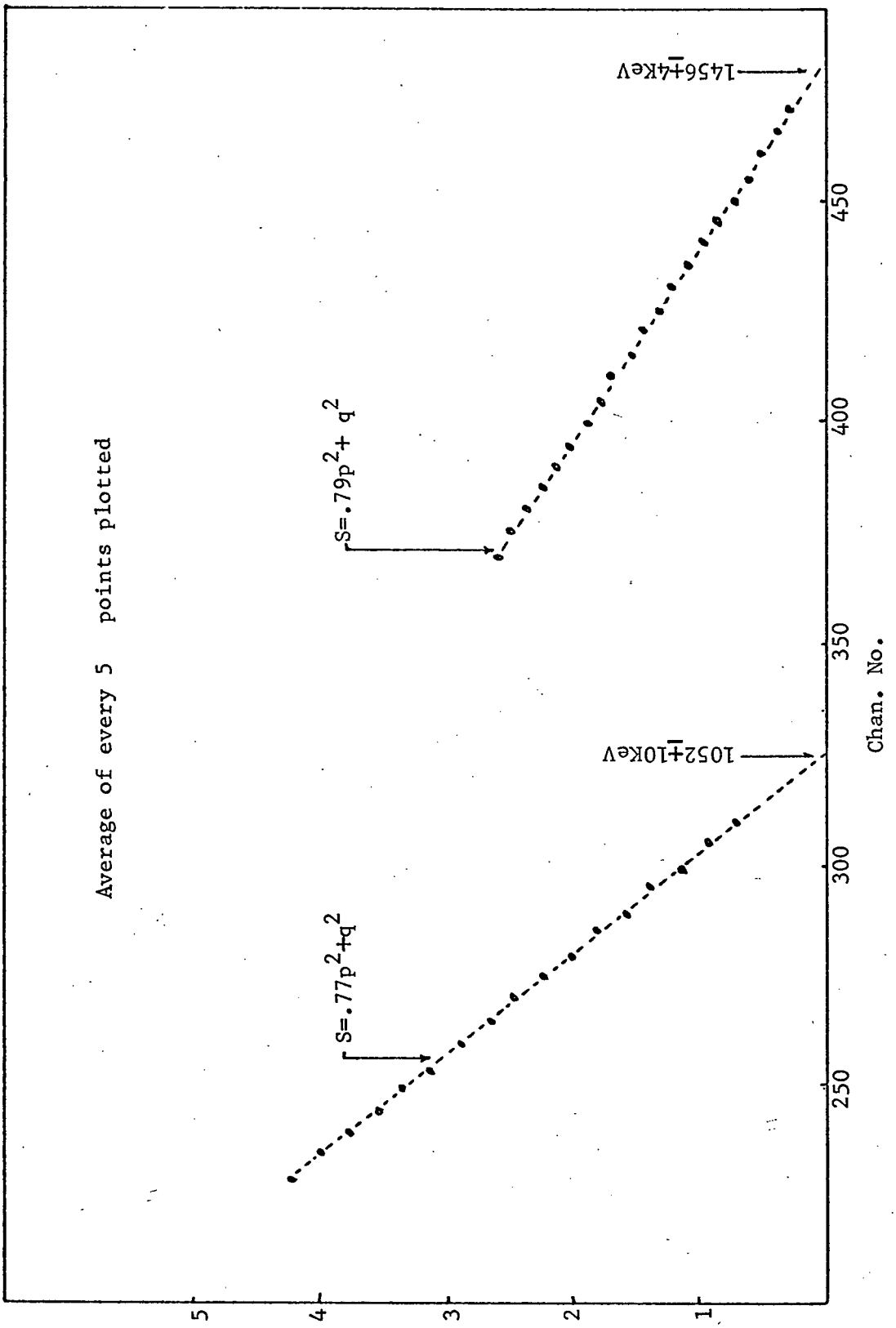

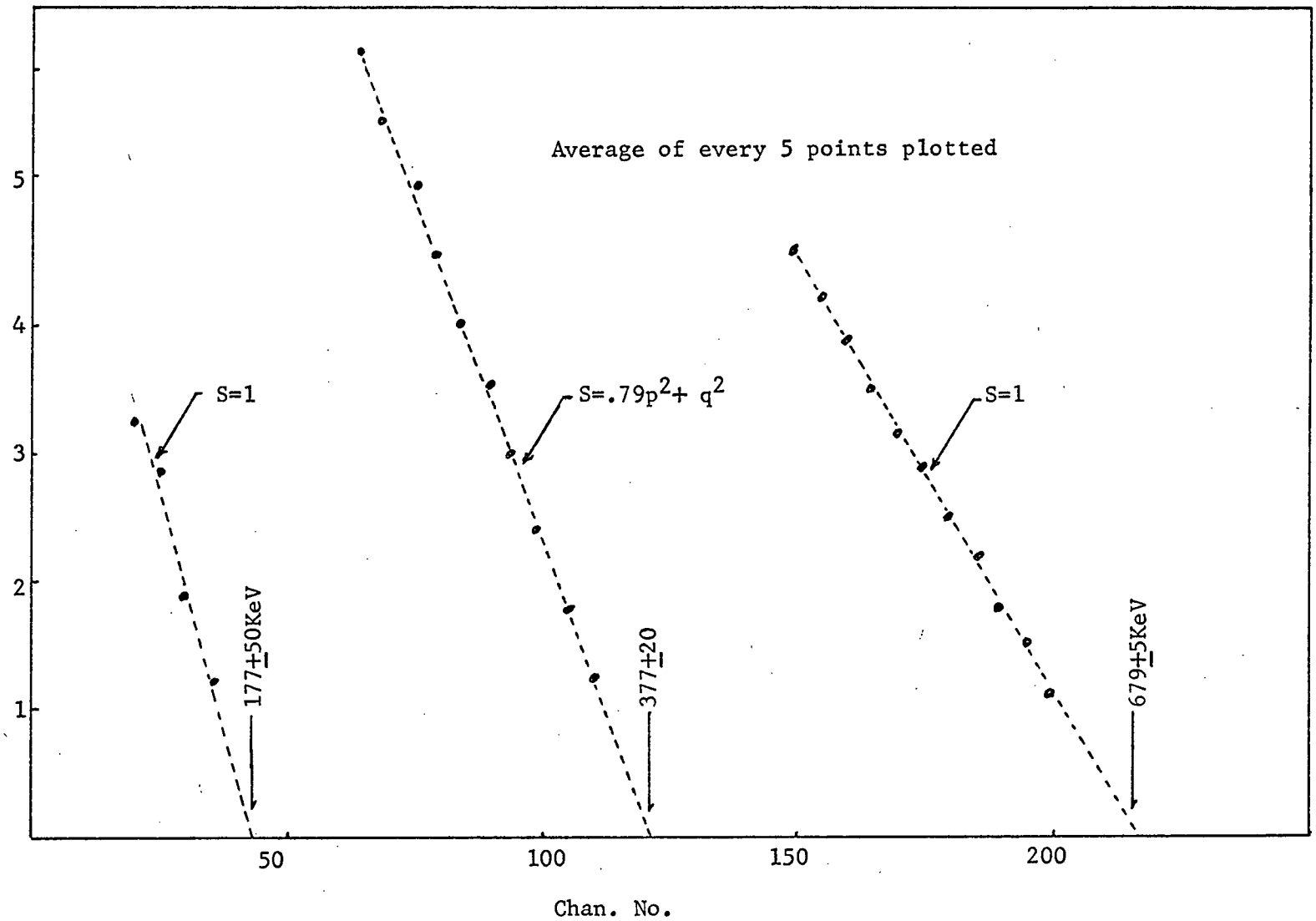
Average of every 5 points plotted
S=1
S=.79p2+ q2
S=1
177±50KeV
377±20
679±5KeV
5
4
3
2
1
50
100
150
200
Chan. No.

Fig. C-2(b)

Table C-1

β^- Transitions in $^{152}Eu \rightarrow {}^{152}Gd$

Gate Transition (KeV)	Shape Factor	End-Point Energy (KeV)
344	$.79p^2 + q^2$	1456 ± 2
411	$.77p^2 + q^2$	1052 ± 10
779	1	679 ± 5
678	$.79p^2 + q^2$	377 ± 20
1299	1	177 ± 50

Table C-2

End-Point Energy (KeV)	Relative Intensity(%)	Forbiddenness*
1456	30 ± 2	1^{st}
1052	5 ± 2	1^{st}
679	45 ± 5	allowed
377	10 ± 3	1^{st}
177	10 ± 5	allowed

* The degree of forbiddenness was assumed from the form of the shape factor.

Therefore the coincidence spectrum gated with the 344 KeV gamma transition was used, since most of the transitions from higher excited states in ^{152}Gd decay via the 344 KeV level.[48] This coincidence spectrum was analysed by subtracting the β^- group that feeds the 344 KeV level using the calculated shape for this group. The remainder was then used to find the contribution of the next highest energy group, and this subtracted. This procedure was repeated until only the lowest energy group remained. The end-point energies and shape factors found from the individual coincidence spectra were used in this subtraction procedure. The relative intensities found from these calculations are listed in table C-2. These results are in good agreement with those found by other investigations[40].

References

1. N. Bohr and F. Kalckar, Dan. Mat. Fys. Medd, 14 No. 10 (1937)
2. A. Bohr, Dan. Mat. Fys. Medd 26 No. 14 (1952)
3. A. Bohr and B.R. Mottelson, Dan. Mat. Fys. Medd 27 No. 16 (1953)
4. O. Hansen and O. Nathan, Nucl. Phys. 42 (1963) 197
5. A.K. Kerman and C.M. Shakin, Phys. Lett. 1 (1962) 151
6. F.K. McGowan et al, Nucl. Phys. 66 (1965) 97
7. S.T. Belyeav, Dan. Mat. Fys. Medd. 31 No. 11 (1959)

   S.T. Belyeav and V.G. Zelevinsky, Nucl. Phys. 39 (1962) 582
8. L.S. Kisslinger and R.A. Sorenson, Dan. Mat.Fys. Medd. 32 No.9 (1960)
9. O. Nathan and S.G. Nilsson in Alpha-, Beta-, and Gamma-Ray Spectroscopy. Edited by K. Siegbahn. North-Holland Publishing Co.(1965).
10. M. Baranger, Phys. Rev. 120 (1960) 957
11. L.S. Kisslinger and R.A. Sorensen, Rev. of Mod. Phys. 35 (1963) 853
12. D. Mitra and M.K. Pal, Phys. Rev. 133 (1964) B257
13. G. Alaga et al, Nucl. Phys. A97 (1967) 600
14. V. Lopac, Nucl. Phys. A155 (1970) 513
15. K.C. Mann and R.M. Pearce, Proc. Roy. Soc. Canada 47 (1953) 130A
16. L.M. Langer and D.R. Smith, Phys. Rev. 119 (1960) 1308
17. D.H. Stelson, Phys. Rev. 157 (1966) 1098
18. I.P. Auer et al, Nucl. Phys. A124 (1969) 199
19. Data Sheet, supplied with the ^{124}Sb sample.
20. J.P. Davidson, Collective Models of the Nucleus. Academic Press, (1968).
21. E. Merzbacher, Quantum Mechanics. John Wiley and Sons (1961)
22. A. Messiah, Quantum Mechanics John Wiley and Sons, Inc. (1966)
23. P.O. Lipas, Nucl. Phys. 82 (1966) 91
24. B. Sorensen, Phys. Lett. 21 (1966) 683

25. A. deShalit and I. Talmi, Nuclear Shell Theory Academic Press(1963)

26. B.R. Mottelson and S.G. Nilsson, Mat. Fys. Skr. Dan. Vid. Selsk 1 No. 8 (1959)

J. P. Davidson, Rev. Mod. Phys. 37 (1965) 105

27. C.A. Heras et al, Phenomenological and Microscopic Properties of Even-Even Nuclei . United States Atomic Energy Commission, Report NP-17506

28. V. Lopac, Nucl. Phys. A138 (1969) 600

29. K. Hyde et al, Nucl. Phys A104 (1967) 81 and A.G. DePinho et al, Nucl. Phys. A116 (1968) 408

30. D.C. Robinson, Nucl. Instr. and Meth. 78 (1970) 120

31. System/360 Scientific Subroutine Package, IBM Programmer's Manual

32. I.A.E.A. calibration sheets supplied with calibration sources.

33. W.R. Kane et al, Nucl. Instr. and Meth. 56 (1967) 189

34. D. Paatero et al, Nucl. Instr. and Meth. 44 (1966) 357

35. J.E. Freund, Mathematical Statistics. Prentice-Hall(1962)

36. R.A. Meyer et al, Nucl. Phys. A127 (1969) 595

37. J.L. Putman, in Alpha-and Beta- Ray Spectroscopy, edited by K. Siegbahn. North-Holland Publishing Co.(1965)

38. R. Van Lieshout et al, in Alpha- Beta- and Gamma- Ray S pectroscopy, edited by K. Siegbahn. North-Holland Publishing Co. (1965)

39. Ortec Application Note AN31 (1970)

40. C.M. Lederer et al, Table of Isotopes. John Wiley and Sons (1967)

41. H.F. Schopper, Weak Interactions and Nuclear Beta Decay. North-Holland Publishing Co. (1966)

42. T. Kotani et al, Phys. Rev. 113 (1953) 622

43. C.S. Wu and S.A. Moszkowski, Beta Decay. John Wiley and Sons (1966)

44. J.R. Johnson, M.Sc. Thesis, University of British Columbia.

45. G. Malmsten et al, Arkiv Fysik 33 (1966) 361
and J.S. Larsen et al, Nucl. Phys. A100 (1967) 248

46. P. Charoenkwan, N.I.M. 34 (1965) 93

47. L.M. Langer et al, Phys. Rev. 82 (1951) 635

48. T.G. Walton, Ph.D. Thesis, University of British Columbia.

49. C.G. Brown, M.Sc. Thesis, University of British Columbia.

50. Ortec, Application Note. in Cat. Number 1001

51. M.E. Rose, in Nuclear Spectroscopy, edited by F. Ajzenberg-Selove, Academic Press (1960) p. 834.

52. Ibid., p. 840

53. L.A. Sliv and I. M. Band, Coefficients of Internal Conversion of Gamma Radiation. Leningrad Physics-Technical Institute (1956)

54. M.E. Rose, Internal Conversion Coefficients. North-Holland pub. Co. (1958)

55. A.H. Wapstra et al, Nuclear Spectroscopy Tables. North-Holland Publishing Co. (1959)

56. E.P. Grigor'ev et al, English Translation in Bull. Acad. Sci. USSR Phys. Ser.(USA) 32 (1968) 711

57. J.R. Sites et al, Nucl. Phys A156 (1970) 19

58. P.A.M. Dirac, The Principles of Quantum Mechanics. Fourth Edition, Oxford Press (1958)

59. E.M. Henley and W. Thirring, Elementary Quantum Field Theory . McGraw Hill (1962)

60. M.E. Rose, Elementary Theory of Angular Momentum. John Wiley and Sons (1957)

61. R.F. Streater and A.S. Wightman, PCT, Spin and Statistics, and All That. W.A. Benjamin, Inc. (1964)

62. G. Racah, Phys. Rev. 62 (1942) 438

63. K.T. Hecht, in Selected Topics in Nuclear Spectroscopy, edited by B.J. Verhaar, North-Holland Pub. Co. (1964), p. 58.

64. P.O. Lipas, Nucl Phys. 82 (1966) 91

65. S. DeBeneditti, Nuclear Interactions. John Wiley and Sons (1967)

66. M. Abramowitz and I.A. Stegum, Handbook of Mathematical Functions. Dover Publishing (1965)

67. S. DeBenedetti, Nuclear Interactions. John Wiley and Sons (1967)p.253.

68. E. Fermi, Nuclear Physics. University of Chicago Press (1949)

69. S.A. Moszkowski, in Alpha- and Beta- Ray Spectroscopy, edited by K. Siegbahn. North-Holland Pub. Co. (1955) p.375.

70. J.P. Davidson, Collective Models of the Nucleus. Academic Press (1965)p.94.

71. S.W. Williams, Phys. Rev. 125 (1967) 340

72. R.C. Ragaini et al, Phys. Rev. 187 (1969) 1721

73. J. LaGrange, Le Journal de Physique 30 (1969) 893

74. R.A. Auble et al, Nucl. Phys. A179 (1972) 353

75. D.L. Bushnell et al, Phys. Rev. 179 (1969) 1113

76. M.N. Rao et al, Nucl. Phys. A147 (1970) 1

77. P.R. Christensen et al, Nucl. Phys. A149 (1970) 302

78. R.D. Evans, The Atomic Nucleus. McGraw Hill Book Co. (1955)

79. L.W. Nordhein, Rev. of Mod. Phys. 23 (1951) 332

80. F.R. Leonard et al, Phys. Rev. 162 (1967) 1125

81. P.O. Lipas, Phys. Lett. 8 (1964) 279

82. Y. Yoshizawa, Phys. Lett. 2 (1962) 261

83. S.A. Moszkowski, in Alpha-, Beta-, and Gamma- Ray S pectroscopy, edited by K. Siegbahn, North Holland Pub. Co.(1965) P.881.

84. A. Kerek, Nucl. Phys. A176 (1971) 466